Technische Universität München
Fakultät für Physik

Master's Thesis

Abschlussarbeit im Masterstudiengang Physik

2-Input-2-Output Quantum Feedback Amplification and Coherent PID Feedback Control

Quanten-Feedback-Verstärkung mit zwei Eingängen und zwei Ausgängen
und
Kohärenter PID-Feedback-Regler

Yuki Nojiri

July 18, 2018

Erstgutachter (Themensteller): Dr. Frank Deppe
Zweitgutachter: Prof. Dr. Naoki Yamamoto

Abstract

In almost all current technological devices, the feedback amplifiers are used for example in cell phones, DVD players, and wireless communication technologies. This important concept provides a robust transfer function and various interesting functionalities such as log amplifiers, active filters, and Lock-In amplifiers. Since in the quantum world quantum devices such as quantum computers, quantum sensors, and quantum communications are a hot topic between the researchers, the development of quantum feedback amplification theory and its application is highly demanded, as this feedback system is fundamental to electronic devices.

In this research we suggest a 2-input-2-output quantum feedback amplifier and investigate the feedback gain and quantum-noise limit with respect to added noises. We observe this scheme makes the controlled amplifier significantly robust, and furthermore it realizes the minimum-noise amplification even under realistic imperfections.

This feedback concept is then used to design a directional active differentiator and integrator for a quantum signal. We obtain the condition for achieving minimal added noise is exactly the same as the condition for achieving high feedback gain in both cases.

Further, by combining those with a proportional amplifier we suggest a basic construction method of a coherent PID controller and study its properties. Especially, the effect of added noises coming from the coherent PID controllers is investigated for coherent P, PI, and PD feedback control system through a concrete example, namely, through an optomechanical system. It appears for coherent P controller this can be used to further cool the sideband-cooled optomechanical system. In case of coherent PI controller, we notice the effect of the idler coming from coherent I controller is immense such that the steady state variance of the system operator spreads dramatically. Finally, for coherent PD controller the cold-damping method for the optomechanical system is studied and compared with the measurement-based feedback system. This results that if the detection efficiency is 1, then the coherent PD feedback system can never outperform the measurement-based one.

論旨

増幅器とコントローラーが組み込まれているフィードバック回路で構成されているフィードバック（FB）増幅器と呼ばれるものは,Black 氏が 1927 年に長距離通信のために初めて提案されたもので, 今現在でも電話などによる通信において欠かせない存在である．というのも、増幅器自体は環境変化を受けやすい機器で,FB を施さないと, 通話中に相手が言ったことが聞き取れなかったからである．しかし,FB 増幅器の応用先は通信技術に止まらず, 現在使われている全ての電子デバイスの基盤となっている．その背景には, フィードバック増幅が内包している多様で斬新な安定機能にある．その一部を例に挙げるのであれば, バンドパスフィルター, シュミットトリガ,PID 制御器などである。つまり, 日常的に使っているコンピューター, 携帯電話, 電車や自動車に至るまであらゆる電子回路で動いているものを FB 増幅器は我々の日常を支えているのである．そして近年, 量子通信, 量子コンピューター, 量子センサーなど様々な量子デバイスが盛んに研究されている．そして, 電子デバイスの発展の歴史に FB 増幅器の発展の歴史が必ずついて回っているように, 量子デバイスの発展には量子 FB 増幅器の発展が必要不可欠である．

本研究では,2 入力 2 出力量子フィードバック増幅器を提案し, フィードバックゲインと追加ノイズを視野に入れた量子雑音限界について研究する．このスキームは制御されている増幅器を非常にロバスト化し, 更に現実的な状況においても最小雑音を持った増幅が可能であることが示された．

このフィードバック構造を使い, 量子信号に対する指向性を持った能動的な微分器と積分器を構成することが出来る．最小追加雑音を得るための条件が最大フィードバックゲインを得る条件と一致することが判明した．

加えて, これと信号振幅を定数倍させる増幅器を合わせたコヒーレントな PID 制御器の構成法を提案し, その性質を探る．特に, コヒーレント P,PI,PD フィードバック制御システムにおけるコヒーレント PID 制御器から出てくる追加雑音の効果をオプトメカ系という例を通じて調べる．コヒーレント P 制御をしようするとサイドバンド冷却されたオプトメカを更に冷却できることが判明した．コヒーレント PI 制御の場合は, コヒーレント積分器から出てくるアイドラーの効果が非常に大きく, システム演算子の定常分散の拡大に大きく貢献することが分かった．最後に, コヒーレント PD 制御を粘性冷却法でオプトメカ冷やし, 測定フィードバク系とその冷却パフォーマンスを比較した．結果, 測定効率が 1 である場合, コヒーレント PD 制御が測定ベースの冷却より上回ることができないということが分かった．

Zusammenfassung

In vielen technologischen Geräten wie zum Beispiel in Smartphones, DVD-Spielern und drahtlosen Kommunikationstechnologien werden heutzutage sogenannte Feedback-Verstärker benutzt. Dieses wichtige Konzept garantiert eine robuste Übertragungsfunktion und verschiedenartige interessante Funktionalitäten wie Log-Verstärkung, aktive Filter, und Lock-In-Verstärker. Da nun Quantentechnologien wie Quantencomputer, Quantensensoren und Quantenkommunikationen weltweit von Wissenschaftlern aktiv erforscht werden, ist die Entwicklung einer Quanten-Feedback-Verstärkungstheorie und ihrer Anwendungen sehr erwünscht.

In dieser Masterarbeit schlagen wir in diesem Zusammenhang einen 2-Input-2-Output Quanten-Feedback-Verstärker vor. Wir untersuchen seinen Feedback-Gain und sein Quantenrauschlimit bezüglich zusätzlichem Rauschen. Wir sehen, dass das Feedback-Schema den Verstärker äußerst robust macht und dass es zudem das minimale Rauschlimit auch unter realistischen Bedingungen verwirklicht.

Dieses Feedback-Konzept wird dann benutzt, um einen direktionalen aktiven Differentiator und einen aktiven Integrator für ein Quantensignal zu gestalten. Wir erhalten, dass die Bedingung für das Erreichen des minimalen Rauschens genau mit der für hohen Feedback-Gain übereinstimmt.

Indem wir Integrator und Differentiator mit einem Proportionalitätsverstärker verbinden, schlagen wir zusätzlich eine grundlegende Konstruktionsmethode für ein kohärentes PID Feedback-Kontrollsystem vor und untersuchen dessen Eigenschaften. Insbesondere wird der Effekt des zusätzlichen durch den kohärenten PID-Regler hinzugefügten Rauschens für das kohärente P-, PI- und PD-Feedback-Kontrollsystem anhand eines konkreten Beispiels, nämlich eines optomechanischen Systems, bestimmt. Wir finden, dass der kohärente P-Regler für seitenbandgekühlte optomechanische Systeme zusätzliche Kühleffekte erzielt. Im Fall des kohärenten PI-Reglers erkennen wir, dass das Rauschen aus dem kohärenten I-Regler die stationäre Varianz der Systemoperatoren stark erhöht. Zuletzt wird ein Cold-Damping-Szenario im optomechanischen System für den kohärenten PD-Regler untersucht und mit einem messungsbasierten Feedbacksystem verglichen. Es stellt sich heraus, dass bei perfekter Quanteneffizienz das kohärente PD-Feedbacksystem das messungsbasierte nicht übertreffen kann.

Contents

1 Introduction

In our daily life, we are using electronic technologies such as cell phones, DVD players, and global positioning systems or in optics such as optical fiber systems and wireless communication technologies. All those inventions are supported by the so-called feedback amplification theory, which is a combination of the amplifier, controller, and feedback theory [1, 2, 3, 4]. An amplifier with feasible isolation between inputs and outputs in electronics was first invented by Lee DeForest in 1906, known as Audion tube [1, 2]. After the invention of transistors by Bardeen, Brattain, and Shockley and the impressive developments in solid-state technology, most microwave amplifiers are transistor amplifiers such as Si BJT, MOSFET or HEMT due to robust and low-cost properties. However, amplification itself is not enough to reach those technologies mentioned above. Only with the combination of feedback theory, first suggested by Harold S. Black in 1927 [5, 6], the electronic devices could be revolutionized as one found the feedback amplification is not only useful for stabilizing signals, but also for building-up new functionalities such as Differentiators and Lock-In Amplifiers by choosing proper controllers.

If we now look at the quantum world, some physicists have started not to research on fundamental quantum physics, but its application to the quantum devices such as quantum computers, quantum network and quantum sensors [7, 8, 9, 10]. As the feedback system composed of amplifier and controller is fundamental to the electronic devices, the quantum feedback amplifier based on quantum amplifiers and controllers will play an important role. Indeed, there are quantum amplifiers to amplify tiny quantum signals, which cannot be detected without the so-called phase-preserving quantum amplifiers. In quantum optics, this is achieved by utilizing a crystal with Kerr effect [11], and in superconducting circuits by Josephson Bifurcation Amplifier[12], Josephson Ring Modulator[13, 14] or just by SQUID[15]. Additionally, coherent controllers such as cavities and beam splitters exist, to design the so-called coherent feedback circuits. But there are no quantum feedback amplifiers with specific functionalities, which are urgently needed.

In this thesis, we present quantum feedback amplification concept for 2-input-2-output amplifiers for superconducting circuits (the Directional SQUID Amplifier [15]), and suggest for the first time a quantum feedback amplifier (QFA) with certain functionality, namely the coherent proportional-integral-derivative controller, and its applications to optomechanical system.
This thesis is largely organized into two parts. The preliminaries are from the second to fifth section, while the contents of this research start from the sixth to the eighth section. In the last section, we summarize and con-

clude this thesis. In the preliminary, we begin with the basics of operational amplifiers and feedback amplifiers in the second section. In the next section, the classical PID controller is explained: firstly introducing the three term controller, then secondly expressing the state space representation of PID feedback control system, and lastly discussing about the PID control performance. The fourth section is about the derivation of quantum electromagnetic circuit theory which enters with the classical transmission line theory and consequently to its quantization. The relation between the hybrid and scattering parameters is also shown. Finally, the function of directional microwave SQUID amplifier is discussed. The main research begins with 2-input-2-output quantum feedback amplifier with its modeling, feedback gain analysis, and quantum-noise limit and added noises. In the seventh section, the feedback scheme for coherent proportional, differentiator and integrator is suggested, and its added noises are also discussed. Finally, utilizing the previous results, the coherent PID feedback control is investigated. Beginning with the basic coherent PID feedback control system scheme, we discuss the steady-state covariance matrix for coherent P feedback control by applying this to the sideband-cooled optomechanical system. Having this application in mind, we then explore the added noise effect of the coherent PI controller and compare this effect with the previous coherent P controller. The coherent PD feedback control is then introduced and applied to the cold-damping of the optomechanical system. Its cooling performance is investigated by comparing it with the homodyne-detected controller. In the last subsection, we briefly discuss the coherent PID feedback control.

2 Amplifiers in Electronic Circuit

Amplifiers associated with feedback are one of the fundamental building blocks in an electronic circuit and are integrated into most of the electronic devices. As mentioned in the introduction, the first motivation of using feedback was providing gain stability of the signal, extending the bandwidth of an amplifier, or matching the input and output impedances. But its utility is not restricted in this small area, the potential of feedback amplifiers also opens the doors to active filters, PID controllers, Schmitt triggers, etc.. So the concept of amplifier and feedback is of enormous importance, and will be briefly explained in this section.

2.1 General Model of Operational Amplifier

In electronics, the so-called operational amplifiers (op amp) are the dominant circuit building block used as an amplifier. Speaking of op amps, often voltage amplifiers are intended, but there are four different types of amplifiers dependent on what kind of output should be increased as a function of the input: voltage amplifier, current amplifier, transconductance amplifier, and transresistance amplifier. For the signal analysis purposes, we can represent the op amps with amplifier gain A, input impedance Z_i, and output impedance Z_o, and thus with the network parameters Z, Y, G, and H in Eqs. (4.28) - (4.31). In case of voltage amplifier the input voltage is amplified as an output voltage (network parameter G), in case of current amplifier the input current as an output current (network parameter H), in case of transconductance amplifier the input voltage as an output current (network parameter Y), and in case of transresistance amplifier the input current as an output voltage (network parameter Z)(Fig. 4.3). The amplifier gain A is dependent on which amplifier we want to consider:

$$A = \begin{cases} G_{11} & \text{, voltage amplifier} \\ H_{22} & \text{, current amplifier} \\ Z_{21} & \text{, transresistance amplifier} \\ Y_{21} & \text{, transconductance amplifier} \end{cases} \tag{2.1}$$

which we can say is a connection between the signal analysis and electronic circuit point of view. Then some of the readers might ask, what the meaning of G_{22}, H_{11}, Z_{12}, and Y_{12} is, if G_{12}, H_{12}, Z_{11}, and Y_{11} correspond to input impedances and G_{21}, H_{21}, Z_{22}, and Y_{22} to output impedances. Physically, these imply reverse gain, which is often neglected in electronic circuits due to the consideration of an ideal case or due to the high performance of practical op amps [2, 4, 16].

As we will explain later, we will handle the input-output relation in scattering parameters (see also section 4.2 about scattering parameters and its merit in section 4). Hence, it is convenient to see the op amp in that representation. Surprisingly, the (reverse) gain in the scattering parameter, s_{21}, is proportional to the (reverse) gain of all four amplifiers (for confirmation see Appendix A):

$$s_{21} \propto A = \begin{cases} G_{11} & \text{, voltage amplifier} \\ H_{22} & \text{, current amplifier} \\ Z_{21} & \text{, transresistance amplifier} \\ Y_{21} & \text{, transconductance amplifier} \end{cases} \tag{2.2}$$

$$s_{12} \propto \lambda = \begin{cases} G_{22} & \text{, voltage amplifier} \\ H_{11} & \text{, current amplifier} \\ Z_{12} & \text{, transresistance amplifier} \\ Y_{12} & \text{, transconductance amplifier} \end{cases} \tag{2.3}$$

Hence, we do not have to consider every four cases, which input is amplified since we know any kind of inputs from the "left" side goes through the amplifier to the "right" side as an increased output.
From an electronic circuit point of view the op amp has three terminals: two input terminals v_+ and v_- and one output terminal v_o. Those three voltages including the power supplies V_{CC} and V_{EE} are referenced to the common (ground) terminals (Fig. 2.1 and Tab. 2.1).

2.2 Feedback Amplifier

Now introduced the four different kinds of amplifiers, we can move to the feedback amplifier. But before going directly to this concept for the electronic circuit, we briefly review the general abstract feedback amplifier model with its physical interpretation.

input\output	Voltage V_2	Current I_2
Voltage V_1	G (voltage amplifier)	Y (transconductance amplifier)
Current I_1	Z (transresistance amplifier)	H (current amplifier)

Table 2.1: The signal input-output relation of network parameters Z, Y, G, and H as *amplifiers*, which describes the input from "left" side (index 1) to the output at "right" side (index 2) based on the scheme in Fig. 2.1.

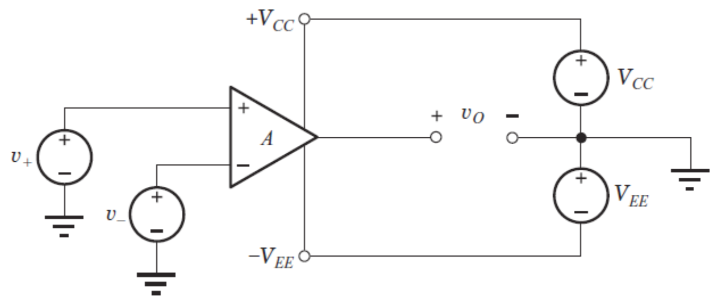

Figure 2.1: op amp with power supplies. Two input voltages v_+ and v_- and one output voltage v_o with the power supplies V_{CC} and V_{EE}. A is the amplifier gain. Normally, the depiction of power supplies are not shown, but they are implicitly supposed. Figure adapted from [2].

2.2.1 Abstract Feedback Amplifier Model

The block diagram for the feedback amplifier system is depicted in Fig. 2.2. If we want to solve it mathematically, we start with the equation

$$y[s] = G[s](u[s] + K[s]y[s]), \tag{2.4}$$

which can be solved easily as

$$y[s] = \frac{G[s]}{1 - G[s]K[s]}u[s], \tag{2.5}$$

where $G[s]$ is the gain in Laplace s-domain, $K[s]$ the controller gain, $u[s]$ the input signal and $y[s]$ the output signal. However, a problem arises if we want to interpret and solve the Eq. (2.4) physically. That is, if we view the feedback loop as an infinite circulation of the open loop gain $G[s]K[s]$, then we can write it as a series,

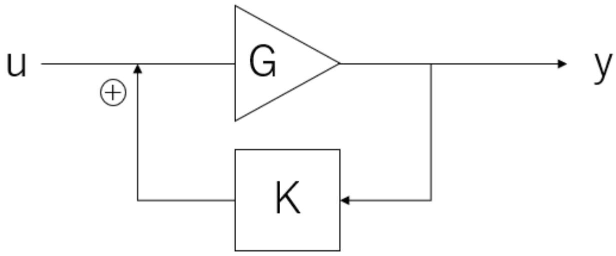

Figure 2.2: The input u travels through the amp G, part of the signal is fed back through the controller K and added to the input (positive feedback), and the other part leaves the feedback system as an output y.

$$
\begin{aligned}
y[s] &= G[s](u[s] + K[s]y[s]) && \text{(2.6a)}\\
&= G[s](u[s] + K[s](G[s](u[s] + K[s]y[s]))) && \text{(2.6b)}\\
&= G[s]\sum_{k=1}^{\infty}(G[s]K[s])^k u[s]. && \text{(2.6c)}
\end{aligned}
$$

In this case, the series converges if and only if (iff) $|G[s]K[s]| < 1$ is satisfied. But experiments show there are cases, where the output converges even for $|G[s]K[s]| > 1$.

This problem was first solved by Nyquist. He noted in his paper [17] [1] we should first consider the problem in the time domain and look for the steady state[2]. The important points to consider are the building-up process (transients) of the input signal, the causality and the exponential decay of the controller. The key point is the (convolution) integral over time. As depicted in Fig. 2.2, the input signal travels through G. When the signal arrives G, the outgoing signal at time t is also affected by the past because the effect of the past signal in the device can still remain, which we call as "memory effect". This is described by the convolution integral

$$\tilde{y}(t) = \int_{-\infty}^{\infty} d\tau G(t-\tau)u(\tau). \tag{2.7}$$

[1] The discussion of this convergence problem is very well discussed in his paper, and I personally suggest the readers to read it once because this leads in the end to the infamous Nyquist plot.

[2] This implies the stability condition of the whole system, where in Laplace domain all roots of the denominator of the transfer function has to lie on the left half of the complex plane.

But we have a problem since the above equation diverges. But since in the physical point of view the device can only react, if the signal has been built up at time t_0 (transients: $\Theta(\tau - t_0)$) and not if there is still no signal yet, and does not response to the signal in the future at time $t_1 > t$ (causality: $\Theta(t_1 - t)$), the integration region is therefore restricted, such that

$$\tilde{y}_0(t) = \int_{t_0}^{t} d\tau G(t-\tau)u(\tau). \tag{2.8}$$

Assuming $\int dt G(t)$ exists, which has mostly an exponential decay character, Eq. (2.8) is integrable. This convolution integral has a nice property that the integrand can be just expressed by a multiplication in Laplace s-domain

$$\tilde{y}_0[s] = G[s]u[s]. \tag{2.9}$$

In the feedback loop, we can just write every k-th round trip as

$$\tilde{y}_k[s] = (G[s]K[s])^k G[s]u[s]. \tag{2.10}$$

Since the total output y is just an infinite sum of the above round-trip-outputs, we can write it in the time domain as

$$\begin{aligned}
y(t) =& \lim_{n\to\infty} \frac{1}{2\pi i} \int ds \sum_{k=0}^{n} (G[s]K[s])^k e^{st} G[s]u[s] &\text{(2.11a)}\\
=& \lim_{n\to\infty} \frac{1}{2\pi i} \int ds \left(\frac{1}{1 - G[s]K[s]} - \frac{(G[s]K[s])^{n+1}}{1 - G[s]K[s]} \right) e^{st} G[s]u[s] &\text{(2.11b)}\\
=& \frac{1}{2\pi i} \int ds e^{st} \frac{G[s]u[s]}{1 - G[s]K[s]}\\
&- \lim_{n\to\infty} \frac{1}{2\pi i} \int d\tau ds' \frac{G[s']u[s']}{1 - G[s']K[s']} e^{s'(t-\tau)} \underbrace{\int ds (G[s]K[s])^{n+1} e^{s\tau}}_{\to 0}. &\text{(2.11c)}
\end{aligned}$$

One can then show the second term vanishes provided the first term exists, and the transient is assumed. This means all direct/normal outputs of the

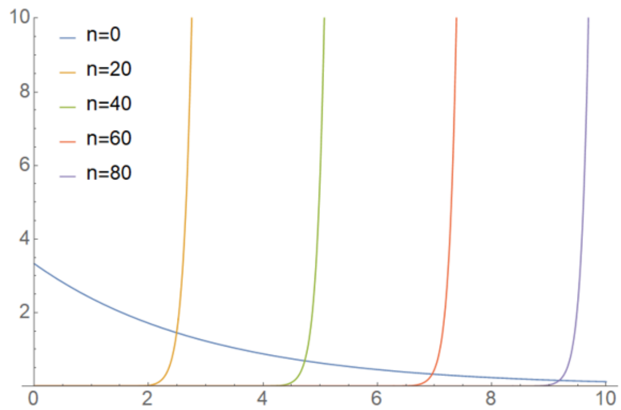

Figure 2.3: Physical interpretation of the second term in Eq. (2.11) which vanishes in the time domain for $n \to \infty$. As can be seen, infinite feedback loop generates infinite sum of outputs which are destructively interfering with each other in the time domain. This example is an active differentiator for an electronic device with the controller transfer function $K[s] = 1/(1+sCR)$ (see also Fig. 2.5).

devices (i.e., the transfer functions in the numerator) will not contribute to the total output. Nyquist then discovered that the system diverges iff $1 - G[s]K[s] = 0$ is satisfied.

Now in the limit $G[s] \longrightarrow \infty$, we read for Eq. (2.5) $G_{fb}[s] = 1/K[s]$. If for example $K[s] = \beta$ is a robust passive device, then feedback gain only depends on the robust feedback factor β, which is the reason for stability against gain fluctuations. This can be clearly seen by calculating the relative sensitivity

$$\frac{\Delta G_{fb}[s]}{G_{fb}[s]} = \frac{1}{1 - G[s]K[s]} \frac{\Delta G[s]}{G[s]}. \tag{2.12}$$

2.2.2 Feedback Amplifier in Electronic Circuit

Obviously, since there are four types of op amps, we obtain four different feedback amplifiers. While the op amps can be named as the voltage amplifier, current amplifier, transconductance amplifier, and transresistance amplifier, they can also be abstractly designated as $G, H, Y,$ and Z parameters, respectively. The same occurs in this feedback amplifier. While we can

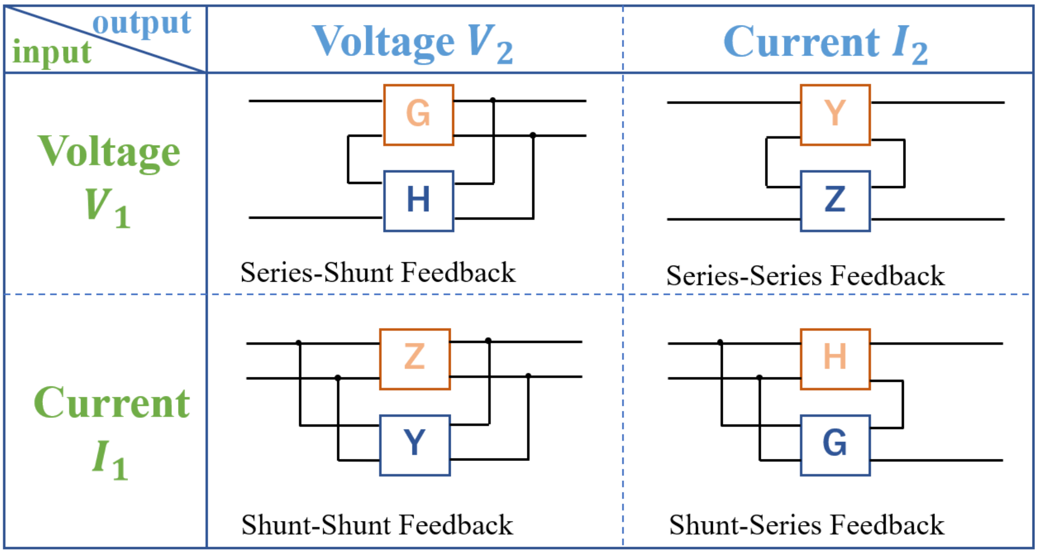

Figure 2.4: The signal input-output and schematic representation of feedback amplifiers which describes the input from "left" side (index 1) to the output at "right" side (index 2).

just add the word "feedback" behind the op amp names, in the abstract case we call them as Series-Shunt, Shunt-Series, Series-Series, and Shunt-Shunt Feedback amplifier, respectively (Fig. 2.4). The reason for such naming lies on the abstract representation of the electronic circuit. For example, if we look at series-shunt feedback amplifier of Fig. 2.4, we realize that the left side of G and H is connected in series, while their right side is connected in parallel - hence series-shunt.

The input-output relation of these feedback amplifiers are calculated as follows:

• feedback voltage amplifier (Series-Shunt Feedback Amplifier)

$$\begin{bmatrix} V_2 \\ I_1 \end{bmatrix} = \underbrace{\left(G^{-1} + H\right)^{-1}}_{G^{fb}} \begin{bmatrix} V_1 \\ I_2 \end{bmatrix}, \tag{2.13}$$

• feedback current amplifier (Shunt-Series Feedback Amplifier)

$$\begin{bmatrix} V_1 \\ I_2 \end{bmatrix} = \underbrace{\left(H^{-1} + G\right)^{-1}}_{H^{fb}} \begin{bmatrix} V_2 \\ I_1 \end{bmatrix}, \tag{2.14}$$

- feedback transconductance amplifier (Series-Series Feedback Amplifier)

$$\begin{bmatrix} I_1 \\ I_2 \end{bmatrix} = \underbrace{\left(Y^{-1} + Z\right)^{-1}}_{Y^{fb}} \begin{bmatrix} V_1 \\ V_2 \end{bmatrix}, \tag{2.15}$$

- feedback transresistance amplifier (Shunt-Shunt Feedback Amplifier)

$$\begin{bmatrix} V_1 \\ V_2 \end{bmatrix} = \underbrace{\left(Z^{-1} + Y\right)^{-1}}_{Z^{fb}} \begin{bmatrix} I_1 \\ I_2 \end{bmatrix}. \tag{2.16}$$

We can recognize the same structure of the feedback gain matrix (2.13) - (2.16) as in the general structure of feedback amplifier 2.5. Indeed in the ideal case, we can directly use Eq. (2.5) for calculating the feedback gain of feedback amplifiers [4].

2.2.3 Advantages of Active Filter over Passive Filter

In electronic and even in quantum electromagnetic circuits, the so-called filters are used, in order to suppress undesired frequencies. For instance, the low-pass filter (or integrator) let only signals pass with relatively low frequencies such that high frequencies are cut off. This is very useful since unwanted noises normally increase proportionally to the frequency. Thus, integrators are used for suppressing noises. For example, in electronic circuits, those filters are realized with resistance and capacitor as depicted in Fig. 2.5. But there is a problem that the gain and the cut-off frequency are fixed by 1 and by the parameters $1/RC$, respectively, as can be seen,

$$v_{out}[\omega] = \frac{1}{1 - i\omega RC} v_{in}[\omega]. \tag{2.17}$$

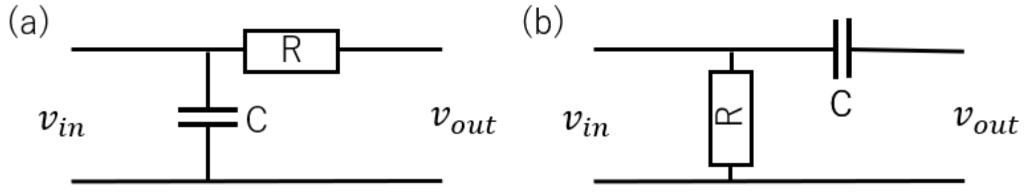

Figure 2.5: (a) A low-pass filter and (b) a high-pass filter realized by a circuit.

On the other hand, if we use a high-pass filter with the transfer function

$$v_{out}[\omega] = K_{HP}[w]v_{in}[\omega] \tag{2.18a}$$

$$= \frac{-i\omega RC}{-i\omega RC + 1} v_{in}[\omega] \tag{2.18b}$$

as a controller of a feedback amplifier system, due to the relation (2.5), we also obtain a low-pass filter.

$$v_{out}[\omega] = \frac{A}{1 - AK_{HP}[\omega]} v_{in}[\omega] \tag{2.19a}$$

$$= \frac{A(1 - i\omega RC)}{1 - (A+1)i\omega RC} v_{in} \tag{2.19b}$$

$$\overset{A\to\infty}{\to} (\frac{1}{-i\omega RC} + 1) v_{in}[\omega]. \tag{2.19c}$$

However, as we can also see from Fig. 2.6, the cut-off frequency $\omega_{co,LP} = 1/(A+1)RC$ can be arbitrarily set by choosing the amplifier gain properly, and the gain itself increases for low frequencies. Additionally, the region of $1/\omega$-dependence will be expanded.

Analogously, we can design a high-pass filter with the feedback amplifier using the passive low-pass filter as a controller (Eq. (2.17)) formulated as

$$v_{out}[\omega] = \frac{A}{1 - AK_{LP}[\omega]} v_{in}[\omega] \tag{2.20a}$$

$$= \frac{A(1 - i\omega RC)}{A + 1 - i\omega RC} v_{in} \tag{2.20b}$$

$$\overset{A\to\infty}{\to} (1 - i\omega RC) v_{in}[\omega]. \tag{2.20c}$$

In this case, the cut-off frequency $\omega_{co,HP} = (A+1)/RC$ widens the ω-dependent region, which is useful in terms of derivative control (see section 3).

To distinguish from the first low-pass filter, we call this filter as an active low-pass filter, since we are using amplifier which is putting energy into the system and hence actively modifying the transfer function, while the other one is called passive low-pass filter because it is only waiting for the incoming

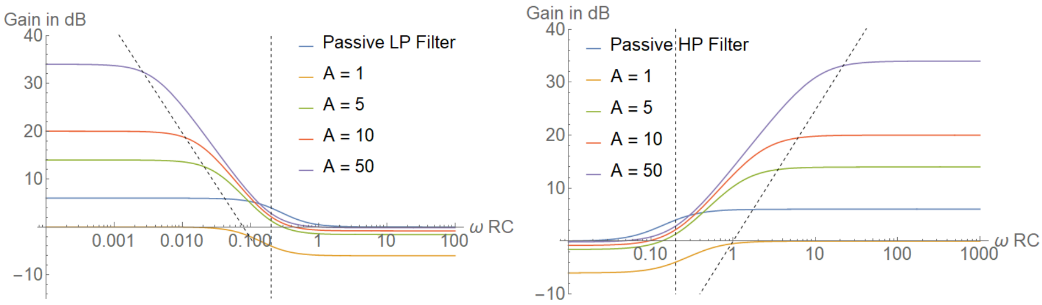

Figure 2.6: (left) A low-pass filter and (right) a high-pass filter realized by a passive and active filter. Time constant $RC = 5$ and gain $A = 1, 5, 10, 50$ are chosen. The vertical dotted line shows the frequency cut-off of a passive filter, and the tilted dotted line that of an active filter.

signal.

Generally, we call all filters using an energy supplier such as amplifier as an active filter, and the others as a passive filter.

3 Classical PID Controller

In industrial mass production, stable uniform quality of its products is highly demanded. But industrial control systems can be very complex such that detailed knowledge of those systems can be nearly impossible to control it precisely. However, the three-term proportional-integral-derivative controller (PID controller) modifies the controller input in such a way that the output of the plant tracks the reference value/signal, independent of the precise knowledge of the system. Thus, the PID controller is the most widely used control technique in the process industries.

In this section, we want to show how this controller is mathematically described as a transfer function and in a state space representation. The latter is introduced to connect this description with the application of the coherent PID controller to the optomechanical system in section 8. The PID control performance is also briefly discussed for the section 8.

3.1 Three Term Controller

The basic PID control feedback structure is shown in Fig. 3.1. What the PID controller precisely does is, it tries to make the error between the reference (setpoint) and the output of the plant zero. So, if the difference is zero, no control is needed, since we have achieved the desired output. The output of the PID controller calculates from the error, how much input is needed for the desired output (control input). We explain the function of each controller P, I, and D by taking a robotic motor arm operated by a current, which is affected under gravity, inertial mass or other forces. The setpoint is set to be in a certain position regardless of the weight of a thing the robotic arm is holding.

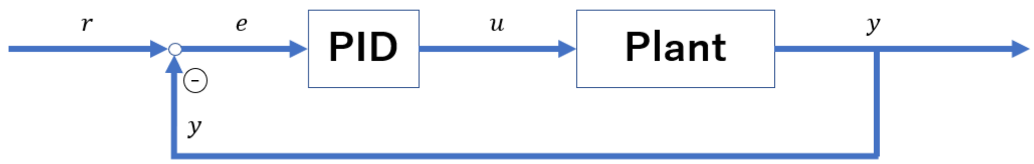

Figure 3.1: Block diagram of a basic PID control feedback structure. The reference signal r is subtracted by a current output value y, and its error e is put in into a PID controller to manipulate it into a control input u such that the output y of the plant tracks the reference signal.

The P controller multiplies the error by a proportional gain K_P

$$y_P(t) = K_P e(t) \tag{3.1a}$$
$$y_P[s] = K_P e[s], \tag{3.1b}$$

which works as a simple "energy" supplier. So, usually the factor K_P is set such that the robotic arm is supplied by a sufficient current to maintain its position. But this control fails if the robotic arm has to grab a light or heavy thing. If e.g. the proportional gain is set for a light one, the motor does not have enough current to keep. Hence, the integrator I is additionally required.

The integrator I changes its energy supply based on the past behavior of the error to cover the non-sufficient proportional gain K_P

$$y_I(t) = K_I \int_0^t d\tau e(\tau) \tag{3.2a}$$
$$y_I[s] = K_I e[s]/s. \tag{3.2b}$$

Therefore, the I controller brings the error to zero, however, the convergence is slow. Moreover, in case of too large K_I, the so-called integral wind-up occurs. Hence, we need a derivative control to speed down the error change for fast convergence.

The function of the derivative control is not to react on the error itself, but to its temporal change

$$y_D(t) = K_D \frac{d}{dt} e(t) \tag{3.3a}$$
$$y_D[s] = K_D s e[s]. \tag{3.3b}$$

So, if the error changes rapidly, the D controller tries to let it slow down such that the difference does not get too large. Thus, fast convergence is achieved because it calculates the futuristic behavior[3]. But in the physical system, there is no system which can predict the future. Hence, we use an approximation[18]. If we have the following transfer function

[3]If we remember the definition of the derivative, we find that the derivative predicts the future.

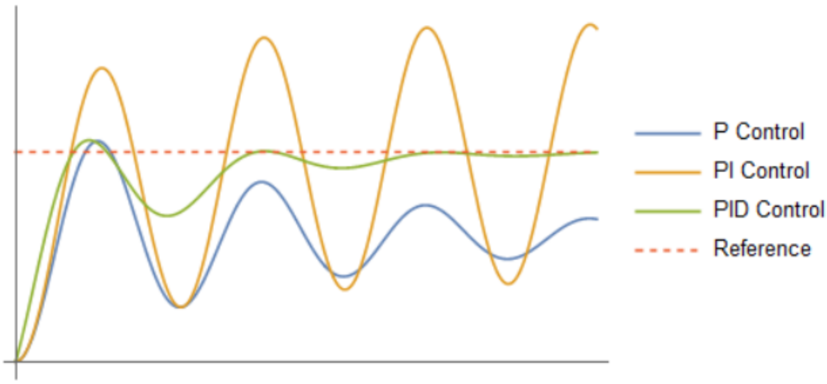

Figure 3.2: Comparison of convergence performance between three controllers: P controller, PI controller, and PID controller. The transfer function of the plant is a standard second order process (damped oscillator) $G_{osc}[s] = 1/(s^2 + \gamma s + \omega_0^2)$

$$G_D[s] = \frac{s}{s + \omega_D} \tag{3.4a}$$

$$= \frac{s}{\omega_D} + \mathcal{O}(s^2), \tag{3.4b}$$

we can approximate it for $\omega_D \gg |s|$ and obtain a D controller, where ω_D is some time constant. Indeed, as introduced in section 2.2.3, the high-pass filter is a D controller. In this case, the time constant is $\omega_D = 1/RC$. In the time domain, Eq. 3.4 is rewritten as

$$G_D(t) = \frac{d}{dt}(\Theta(t)\omega_D e^{-\omega_D t}). \tag{3.5}$$

The derivative control lets the output signal rapidly converge to the setpoint. However, we have to take this carefully because the noise increases with the frequency such that in the noisy environment the derivative control makes the noise contribution dominant.

The convergence performance of P, PI, and PID controller is demonstrated in Fig. 3.2.

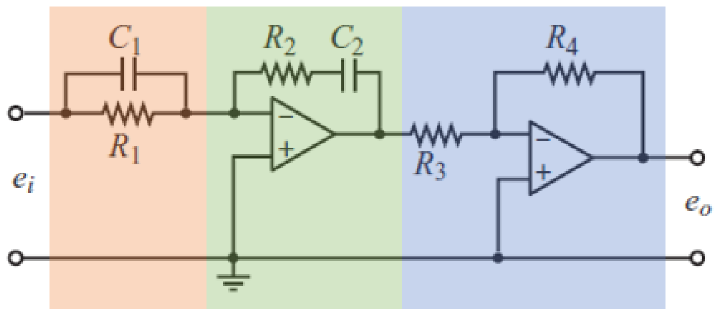

Figure 3.3: Realization of series PID controller using feedback amplifiers. Blue shaded controller is a P controller, green an I controller, and red a D controller. Figure adapted from [19].

3.2 Series PID Controller

As some readers have noticed, if we want to realize a PID controller with active filters in electronic circuits (see 2.2.3), there are no pure integral or derivative term, but its transfer function is added by ± 1. While current modern PID controllers are in parallel form, in analog circuits we have to use in series form [18, 19] (see Fig. 3.3). Since the coherent PID controller introduced in section 8 adopts the series form, we briefly explain the conversion between two types.

As depicted in Fig. 3.4, the PID control law is given in terms of a product of transfer functions

$$u[s] = K_P^{sr}(1 + \frac{K_I^{sr}}{s})(1 + K_D^{sr} s) \tag{3.6a}$$

$$= K_P^{sr}(1 + K_I^{sr} K_D^{sr}) + \frac{K_P^{sr} K_I^{sr}}{s} + K_P^{sr} K_D^{sr} s, \tag{3.6b}$$

where the first term is the effective P control with K_P, the second the effective I control with K_I, and the last the effective D control with K_D. The backtransformation is calculated as

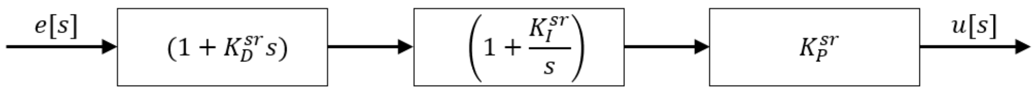

Figure 3.4: Series PID controller block diagram

$$K_P^{sr} = \frac{K_P}{2K_IK_D} \pm \sqrt{(\frac{K_P}{2K_IK_D})^2 - \frac{1}{K_IK_D}} \tag{3.7a}$$

$$K_I^{sr} = \frac{K_P}{2K_D} \pm \sqrt{(\frac{K_P}{2K_D})^2 - \frac{K_I}{K_D}} \tag{3.7b}$$

$$K_D^{sr} = \frac{K_P}{2K_I} \pm \sqrt{(\frac{K_P}{2K_I})^2 - \frac{1}{K_DK_I}} \tag{3.7c}$$

3.3 State Space Systems and PID Control

Here, we present the implementation of PID controller into the state space representation, which is very important for investigating and simulating the dynamical behaviour[18] and for calculating steady-state covariance matrix of state x e.g. due to the use of Lyapunov equation, which is needed in section 8. Further, we can discuss it generic and for multi-input-multi-output system. Thus, we exploit this opportunity to discuss it briefly.

The state space representation for a linear system is formulated as follows

$$\dot{x}(t) = Ax(t) + Bu(t) \tag{3.8}$$

$$y(t) = Cx(t) + Du(t), \tag{3.9}$$

where x is system state variable, u input, and y output. In the physical point of view, we can interpret the first equation as the Langevin equation and the second one the input-output relation. In this case, u is a control input. Since the discussion here is on classical level, we investigate the further analysis with the commonly used value $D = \mathbf{0}$ under P-I, P-D, and P-I-D control.

P-I Control

Given the state space representation for a linear system in Eq. (3.9), the control input u is represented in the time domain as the sum of Eqs. (3.1a) and (3.2a) according to Fig. 3.1, so

$$u(t) = K_Pe(t) + K_I \int_0^t d\tau e(\tau), \tag{3.10}$$

where the error signal is given by

$$e(t) = y(t) - r(t). \tag{3.11}$$

Combining both equations with the input-output equation (3.9), we obtain the control input as a function of the state space variable x, integrated error signal $e_I := \int d\tau e(\tau)$, and reference signal r

$$u(t) = K_P C x(t) - K_P r(t) + K_I e_I(t). \tag{3.12}$$

Henceforth, the Langevin equation is read as

$$\dot{x}(t) = (A + BK_P C)x(t) + BK_I e_I(t) - BK_P r(t). \tag{3.13}$$

In addition to that, we know $\dot{e}_I = e$, so the first order differential equation representing the whole PI feedback system is given by

$$\frac{d}{dt}\begin{bmatrix} x \\ e_I \end{bmatrix} = \begin{bmatrix} A + BK_P C & BK_I \\ C & 0 \end{bmatrix}\begin{bmatrix} x \\ e_I \end{bmatrix} + \begin{bmatrix} -K_P B \\ -1 \end{bmatrix} r, \tag{3.14}$$

where we have omitted the time dependence expression for clarity.

P-D Control

As usual, we start with the control input giving

$$u(t) = K_P e(t) + K_D \frac{d}{dt} e(t). \tag{3.15}$$

Evaluating now the error signal, we obtain

$$\begin{aligned} u(t) =& K_P(Cx(t) - r(t)) + K_D\left(C\frac{d}{dt}x(t) - \frac{d}{dt}r(t)\right) \\ =& K_P(Cx(t) - r(t)) + K_D(C(Ax(t) + Bu(t)), \end{aligned}$$

which results to

$$u(t) = (\mathbf{1} - K_D CB)^{-1}\left((K_P C + K_D CA)\, x(t) - K_P r(t)\right), \tag{3.16}$$

where we have exploited the fact r is time independent for $t > 0$ because of $r(t) = r\Theta(t)$.

Therefore, the closed-loop state space representation for PD feedback system is described by

$$\frac{d}{dt}x = \left(A + B\left(\mathbf{1} - K_D CB\right)^{-1}\left(K_P C + K_D CA\right)\right)x - B\left(\mathbf{1} - K_D CB\right)^{-1} K_P r. \tag{3.17}$$

P-I-D Control

We start again with finding an expression of additional states for the augmented state space model by exploiting the fact that the control input $u(t)$ is following the dynamics

$$u(t) = K_P e(t) + K_I \int_{t_0}^{t} d\tau e(\tau) + K_D \frac{d}{dt} e(t) \tag{3.18}$$

and, we define $e_I(t) := \int_0^t d\tau e(\tau)$ and $e_D(t) := de(t)/dt$. Inserting Eq. (3.11) and the state space model into (3.18) to eliminate e_D, the control input changes to

$$u(t) = (\mathbf{1} - K_D CB)^{-1} \left((K_P C + K_D CA)\, x(t) + K_I e_I(t) - K_P r(t) \right). \tag{3.19}$$

As a result, we obtain a combination of Eqs. (3.14) and (3.17)

$$\begin{aligned} \begin{bmatrix} \dot{x} \\ \dot{e}_I \end{bmatrix} = & \begin{bmatrix} A + B\,(\mathbf{1} - K_D CB)^{-1} (K_P C + K_D CA) & B\,(\mathbf{1} - K_D CB)^{-1} K_I \\ C & 0 \end{bmatrix} \begin{bmatrix} x \\ e_I \end{bmatrix} \\ & - \begin{bmatrix} B\,(\mathbf{1} - K_D CB)^{-1} K_P \\ \mathbf{1} \end{bmatrix} r. \end{aligned} \tag{3.20}$$

Laplace s-domain

In case of Laplace s-domain, we can get the state space equation far more simply. First, the control input $u[s]$ is expressed as

$$\begin{aligned} u[s] &= G_{PID}[s] e[s] && (3.21a) \\ &= G_{PID}[s](r[s] - y[s]) && (3.21b) \\ &= (\mathbf{1} + G_{PID}[s])^{-1} G_{PID}[s](r[s] - Cx[s]) && (3.21c) \end{aligned}$$

where

$$G_{PID}[s] = K_P + \frac{K_I}{s} + K_D s. \tag{3.22}$$

We note that G_{PID} is a matrix form if the parameters are individually set for each input, otherwise it is a scalar. Now inserting Eq. (3.21) into Laplace-transformed Eq. (3.9), we obtain

$$x[s] = (s\mathbf{1} - A + \underbrace{B(\mathbf{1} + G_{PID}[s])^{-1}G_{PID}[s]C}_{fb\ term})^{-1}B(\mathbf{1} + G_{PID}[s])^{-1}G_{PID}[s]r[s]. \tag{3.23}$$

We can then prove the output y indeed converges to the reference r as follows

$$\begin{aligned}
y_\infty &= \lim_{t\to\infty} y(t) && (3.24a)\\
&= \lim_{s\to 0} sy[s] && (3.24b)\\
&= \lim_{s\to 0} s(Cx[s] + (\mathbf{1} + G_{PID}[s])^{-1}G_{PID}[s](r[s] - Cx[s]) && (3.24c)\\
&= \lim_{s\to 0} sr[s] && (3.24d)\\
&= r_\infty, && (3.24e)
\end{aligned}$$

where we have used the Finite Value Theorem in Eq. (3.24b) and in Eq. (3.24d) the fact

$$\begin{aligned}
(\mathbf{1} + G_{PID}[s])^{-1}G_{PID}[s] &= (s\mathbf{1} + K_P s + K_I + K_D s^2)^{-1}(K_P s + K_I + K_D s^2) && (3.25a)\\
&\to K_I^{-1}K_I && (3.25b)\\
&= \mathbf{1}. && (3.25c)
\end{aligned}$$

In this proof, no assumption has been made, thus for any linear system, PID controller is able to let the output signal tracks the reference signal, which is a strong statement. But we have to remind this perfect tracking is valid as long as the I controller is present.

3.4 PID Control Performance

So far we have discussed the ideal case, i.e., no noise in this feedback system has been considered. However in reality, this situation is nearly impossible, hence we want to know how well the output can converge to the reference under noisy environment.

There are four types of noise we want to consider: measurement noise N, bias rejection B, load disturbance D_L, and supply disturbance D_S. In this thesis, we do not consider bias rejection. The general system framework is depicted in Fig. 3.5.

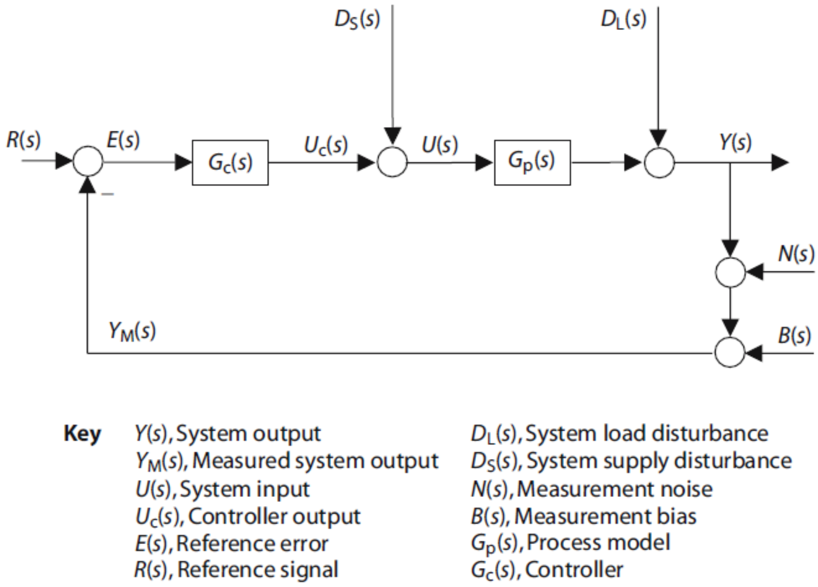

Figure 3.5: General PID system framework. Adapted from [18].

Before studying the PID control performance it is convenient to rewrite the transfer function of the plant system as

$$\begin{aligned} G_P[s] &= C(s\mathbf{1} - A)^{-1}B + \mathbf{1} && (3.26a) \\ &= \frac{1}{|s\mathbf{1} - A|}(C\mathrm{adj}(s\mathbf{1} - A)B + |s\mathbf{1} - A|\mathbf{1}) && (3.26b) \\ &=: \frac{g_P[s]}{d_P[s]}, && (3.26c) \end{aligned}$$

with $d_P[s] := |s\mathbf{1} - A|$. We note the degree of the characteristic polynomials in the numerator $g_P[s]$ and denominator $d_P[s]$ is both the same.

Closed-Loop Stability

In control engineering, it is critical to investigate the closed-loop stability as stated in section 2.2.1. The closed-loop transfer function is

$$\begin{aligned} G_{CL}[s] &= (\mathbf{1} + G_P[s]G_{PID}[s])^{-1}G_P[s]G_{PID}[s] && (3.27a) \\ &= (sd_P[s]\mathbf{1} + g_P[s](sK_P + K_I + s^2K_D))^{-1}g_P[s](sK_P + K_I + s^2K_D) && (3.27b) \\ &= \rho_{CL}[s]^{-1}g_P[s](sK_P + K_I + s^2K_D), && (3.27c) \end{aligned}$$

where the the roots of the closed-loop characteristic expression ρ_{CL} have to lie in the open left half of the complex plane for the closed-loop stability, i.e.,

$$\rho_{CL}[s] = sd_P[s]\mathbf{1} + g_P[s](sK_P + K_I + s^2K_D) = 0. \tag{3.28}$$

For example, for a standard second-order process with $G_P[s] = 1/(s^2 + \gamma s + \omega_0^2)$ we read

$$\rho_{CL}[s] = s^3 + (\gamma + K_D)s^2 + (1 + K_P)s + K_I,$$

hence we have a broader flexibility to assign closed-loop poles since we can regulate the PID parameters.

Measurement Noise Rejection

The transfer function of the measurement noise is the same as that of the reference signal, hence

$$y_N[s] = (\mathbf{1} + G_P[s]G_{PID}[s])^{-1}G_P[s]G_{PID}[s]N[s]. \tag{3.29}$$

For example in the case of a standard second-order process, we recognize

$$\begin{aligned} y_N[s] = & \quad \tfrac{sK_P+K_I+s^2K_D}{s^3+(\gamma+K_D)s^2+(1+K_P)s+K_I} \\ \xrightarrow{s\to\infty} & \quad \tfrac{K_D}{s}. \end{aligned} \tag{3.30}$$

So the noise rejection performance is of the order $1/s$.

Load Disturbance Rejection

System load disturbance let the controlled variables deviate from their respective set points. Physically, these load variables are white noises for instance due to thermal noises of electrons in transmission lines. Thus, those disturbances are low-frequency phenomena which can be modeled by a step-signal model $d_L[s] = d_L/s$. Applying this to calculate the steady state of the load disturbance rejection performance, we read

$$
\begin{aligned}
y_{d_L}(t \to \infty) =& \lim_{s \to 0} s\ y_{d_L}[s] \\
=& \lim_{s \to 0} s\ (\mathbf{1} + G_P[s]G_{PID}[s])^{-1} d_L[s] \\
=& \lim_{s \to 0} (s d_P[s]\mathbf{1} + g_P[s](sK_P + K_I + s^2 K_D))^{-1} s d_P[s]\ d_L \\
=& (g_P[0]K_I)^{-1} d_P[0] \lim_{s \to 0} s\ d_L \\
=& 0.
\end{aligned} \tag{3.31}
$$

As can be seen from this result, the integral term secures the load disturbance is rejected.

Supply Disturbance Rejection

As in the case of load disturbance, noises can affect the control input u, which is called supply disturbance phenomenon. In some case, this supply disturbance is a low-frequency noise, hence a white noise with $d_S[s] = d_S/s$. Since its transfer function is formulated as

$$
y_{d_S}[s] = (\mathbf{1} + G_P[s]G_{PID}[s])^{-1} G_P[s] d_S[s], \tag{3.32}
$$

the steady state of the supply disturbance leads to

$$
\begin{aligned}
y_{d_S}(t \to \infty) =& \lim_{s \to 0} s\ y_{d_S}[s] \\
=& \lim_{s \to 0} s\ (\mathbf{1} + G_P[s]G_{PID}[s])^{-1} G_P[s] d_S[s] \\
=& \lim_{s \to 0} (s d_P[s]\mathbf{1} + g_P[s](sK_P + K_I + s^2 K_D))^{-1} s g_P[s]\ d_S \\
=& (g_P[0]K_I)^{-1} g_P[0] \lim_{s \to 0} s\ d_S \\
=& 0.
\end{aligned} \tag{3.33}
$$

So as in the case of load disturbance rejection, the integral controller guarantees the perfect rejection.

4 Quantum Electromagnetic Circuit

Before we go into the detail of quantum electromagnetic circuit, we want to make some notes regarding it. Basically, the quantum electromagnetic circuit is a quantum mechanical version of microwave circuit (or also known as high-frequency technique). The reason why microwave circuit theory has branched off from the standard circuit theory is that its high frequency makes the behavior of an ordinary circuit element such as resistance deviate from its linear characteristic. For instance, the voltage applied to the resistance does not follow the Ohm's law anymore. That is because the device dimensions are now on the order of electric wavelength, which consideration has not been needed in the low-frequency regime due to the large wavelength and thus all the components of the electric circuit could be approximated linearly [3]. In addition to that, in case of superconducting circuits, interesting effects can be observed in all devices based on Josephson junctions by using the radio-frequency source [20, 21]. Especially since the quantum-limited amplifiers are mostly based on the three- or four-wave mixing, high-frequency operation is essential [11, 16]. Therefore, the quantum electromagnetic circuit is of significant importance in the analysis of superconducting circuits and devices.

4.1 Transmission Line Theory

The main physical variables used in circuit theory are obviously voltage and current, where lumped components such as a resistor, capacitor, inductor, and conductor make the explicit connection between them, while those used in field analysis are amplitude and phase, where the scattering matrix gives the relationship between input and output field. Hence to bridge this gap, transmission line theory, which connects the languages of the electronic circuit to that of (quantum) optics, is applied.

4.1.1 Classical Transmission Line Theory

In order to bridge its gap between two theories, we have to remind that the circuit theory basically uses four different lumped elements: the resistance, inductance, conductance, and capacitance. Additionally, if possible, we want to use those characteristic variables as linear elements, but we cannot neglect the fact that physical dimensions of the electrical wavelength are microscopic. Therefore, we take an infinitesimally small fraction of the transmission line as a lumped-element circuit and can approximate those four components linearly, where R is the series resistance per unit length, L the series inductance per unit length, G the shunt conductance per unit length, and C the

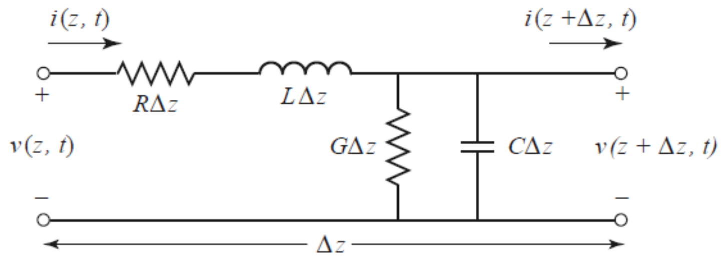

Figure 4.1: Transmission lines represented as a lumped-element circuit. Figure adapted from [3].

shunt capacitance per unit length (Fig. 4.1). Here, we note that two parallel transmission lines are always considered because of incoming and outgoing propagating waves through those lines. Thus, due to this parallel alignment not only series but also shunt elements have to be taken into account.

Solving the Kirchoff's voltage law

$$\frac{\partial V(z,t)}{\partial z} = -RI(z,t) - L\frac{\partial I(z,t)}{\partial t} \tag{4.1}$$

and current law

$$\frac{\partial I(z,t)}{\partial z} = -GV(z,t) - C\frac{\partial I(z,t)}{\partial t} \tag{4.2}$$

as depicted in Fig. 4.1, we obtain from those two wave Eqs. (4.1) and (4.2) as a traveling wave solutions by transforming into the frequency space

$$V(z) = V_{in}e^{-\gamma z} + V_{out}e^{\gamma z} \tag{4.3}$$

$$I(z) = I_{in}e^{-\gamma z} + I_{out}e^{\gamma z}, \tag{4.4}$$

where

$$\gamma = \sqrt{(R + i\omega L)(G + i\omega C)}. \tag{4.5}$$

The terms with $e^{-\gamma z}$ represents the incoming wave propagation in the +z direction and the term with $e^{\gamma z}$ the outgoing wave propagation in the -z direction with carrier frequency ω. Then, $V_{in,out}$ is the voltage amplitude of incoming and outgoing wave, respectively, and $I_{in,out}$ is the current amplitude. Furthermore, we obtain the so-called characteristic impedance Z_0 from the Eqs. (4.1), (4.2), (4.3) and (4.4)

$$Z_0 = \sqrt{\frac{R + i\omega L}{G + i\omega C}} \tag{4.6}$$

and therefore the Eq. (4.4) can be rewritten as

$$I(z) = \frac{1}{Z_0}(V_{in}e^{-\gamma z} - V_{out}e^{\gamma z}). \tag{4.7}$$

Hence, we can describe the whole dynamics by V_{in} and V_{out}[4]. In case of lossless line, $R = G = 0$ such that the characteristic impedance reduces to

$$Z_0 = \sqrt{\frac{L}{C}}. \tag{4.8}$$

Now, we want to connect this voltage and current representation with the field representation, which will be later related to the field creation and annihilation operator in quantum mechanics. The good starting point is to begin with the Lagrangian by first introducing the flux variable[5] [16, 22]

$$\varphi(z,t) \equiv \int_{-\infty}^{t} d\tau V(z,\tau)$$

[4]Strictly speaking, we have to distinguish between incoming wave and +z propagating wave, and outgoing wave and -z propagating wave, respectively, when dealing with equations (4.3) and (4.7). The reason lies that normally the relationships written in equations (4.3) and (4.7) hold only for ±z traveling waves and V_{in} and V_{out} are arbitrary independent functions. But when two transmission lines are somehow connected such as in case of semi-infinite lines, the incoming and outgoing waves are suddenly related due to the boundary conditions and thus the equality of both wave types holds [3, 16].

[5]Another approach is to start with the Maxwell equations, which would provide a clearer connection between the voltage and current representation and the field representation than the Lagragian approach, but then the analogy with the quantum optics would be difficult to see. For interested readers, the author refers to Ref. [3].

or

$$V(z,t) = \partial_t \varphi(z,t). \tag{4.9}$$

The local value of the current is then calculated as

$$I(z,t) = -\frac{1}{L}\partial_z \varphi(z,t). \tag{4.10}$$

Having obtained the flux representation, we can derive the Lagragian density

$$\mathcal{L}(z,t) \equiv \frac{C}{2}(\partial_t \varphi(z,t))^2 - \frac{1}{2L}(\partial_z \varphi(z,t))^2, \tag{4.11}$$

for which we obtain the momentum conjugate of $\varphi(z,t)$ as a charge density

$$q(z,t) \equiv \frac{\delta \mathcal{L}(z,t)}{\delta \partial_t \varphi(z,t)} = C\partial_t \varphi(z,t). \tag{4.12}$$

The Hamiltonian is then given by

$$H(t) \equiv \int dz \frac{1}{2C}(q(z,t))^2 + \frac{1}{2L}(\partial_z \varphi(z,t))^2. \tag{4.13}$$

Since we will see a wave equation described by the flux, if we calculate the Euler-Lagrange equation, the charge density and the flux are oscillating variables, i.e., the Hamiltonian given in Eq. (4.13) demonstrates a simple harmonic oscillator. Therefore, we want to rewrite this as a field variable to see the quantum analogy of the Hamiltonian written in creation and annihilation operators. This can be obtained by defining

$$A_k(t) \equiv \frac{1}{\sqrt{l}} \int dz e^{-ikz} \left(\frac{1}{\sqrt{2C}} q(z,t) - i\sqrt{\frac{k^2}{2L}} \varphi(z,t) \right), \tag{4.14}$$

where the fields as a function of wave vector k obey periodic boundary condition on a length l. Then we have

$$H(t) = \frac{1}{2}\sum_k (A_k^* A_k + A_k A_k^*). \tag{4.15}$$

From Eqs. (4.9) and (4.14), the input voltage V_{in} and output voltage V_{out} can be written as

$$V_{in}(z,t) = \sqrt{\frac{1}{2lC}}\sum_{k>0}[A_k(0)e^{+i(kz-\omega_k t)} + A_k^*(0)e^{-i(kz-\omega_k t)}] \tag{4.16a}$$

$$V_{out}(z,t) = \sqrt{\frac{1}{2lC}}\sum_{k<0}[A_k(0)e^{+i(kz-\omega_k t)} + A_k^*(0)e^{-i(kz-\omega_k t)}], \tag{4.16b}$$

where the frequency ω_k is dependent on k. By defining

$$A_{in}(z,t) \equiv \sqrt{\frac{1}{2lL}}\sum_{k>0}[A_k(0)e^{+i(kz-\omega_k t)} + A_k^*(0)e^{-i(kz-\omega_k t)}] \tag{4.17a}$$

$$A_{out}(z,t) \equiv \sqrt{\frac{1}{2lL}}\sum_{k<0}[A_k(0)e^{+i(kz-\omega_k t)} + A_k^*(0)e^{-i(kz-\omega_k t)}] \tag{4.17b}$$

we can describe the input voltage V_{in} and output voltage V_{out} as a function of input and output field, respectively,

$$A_{in}(z,t) = \frac{1}{\sqrt{Z_0}}V_{in}(z,t) \tag{4.18a}$$

$$A_{out}(z,t) = \frac{1}{\sqrt{Z_0}}V_{out}(z,t). \tag{4.18b}$$

4.1.2 Quantization of Transmission Line Theory

As we have obtained the relationship between voltage-current representation and field representation in classical transmission line theory, we begin with its quantization. When introducing Lagragian density, the momentum conjugate of $\varphi(z,t)$ has been derived, which was the charge density. Using the correspondence principle [16], we can just set those two physical variables as operators obeying the commutation relation

$$[\hat{q}(z), \hat{\varphi}(z')] = -i\hbar\delta(z - z'),$$

in which follows that the quantized field amplitude of Eq. (4.14) obeys

$$\left[\hat{A}_k, \hat{A}_{k'}\right] = \hbar\omega_k\delta_{k,k'}.$$

Therefore, we can write down the quantized field operator with creation $\hat{a}_k^\dagger$ and annihilation operators $\hat{a}_k$ by

$$\hat{A}_k = \sqrt{\hbar\omega_k}\hat{a}_k. \tag{4.19}$$

Thus, we see by expressing the quantized Hamiltonian with Eq. (4.19) it is consistent with the classical Hamiltonian form in Eq. (4.15)

$$\hat{\mathcal{H}} = \sum_k \hbar\omega_k \left[\hat{a}_k^\dagger\hat{a}_k + \frac{1}{2}\right]. \tag{4.20}$$

The quantization of input and output voltage (4.16) reads

$$\hat{V}_{in}(t) = \sqrt{\frac{1}{2lC}}\sum_{k>0}\sqrt{\hbar\omega_k}\left[\hat{a}_k e^{-i\omega_k t} + h.c.\right] \tag{4.21a}$$

$$= \int_0^\infty \frac{d\omega}{2\pi}\sqrt{\frac{\hbar\omega Z_0}{2}}\left[\hat{a}_{in}[\omega]e^{-i\omega t} + h.c.\right] \tag{4.21b}$$

$$\hat{V}_{out}(t) = \sqrt{\frac{1}{2lC}} \sum_{k<0} \sqrt{\hbar\omega_k} \left[\hat{a}_k e^{-i\omega_k t} + h.c.\right] \tag{4.22a}$$

$$= \int_0^\infty \frac{d\omega}{2\pi} \sqrt{\frac{\hbar\omega Z_0}{2}} \left[\hat{a}_{out}[\omega] e^{-i\omega t} + h.c.\right], \tag{4.22b}$$

where

$$\hat{a}_{in,out}[\omega] \equiv 2\pi \sqrt{\frac{1}{l}\frac{1}{LC}} \sum_{k \gtrless 0} \hat{a}_k \delta(\omega - \omega_k) \tag{4.23}$$

is the input/output field annihilation operator obeying the commutation relation

$$\left[\hat{a}_{in,out}[\omega], (\hat{a}_{in,out}[\omega'])^\dagger\right] = 2\pi\delta(\omega - \omega'). \tag{4.24}$$

Finally, we obtain for the quantized voltage and current in frequency domain as

$$\hat{V}[\omega] = \hat{V}_{in}[\omega] + \hat{V}_{out}[\omega] = \sqrt{\frac{\hbar\omega Z_0}{2}} (\hat{a}_{in}[\omega] + \hat{a}_{out}[\omega]) \tag{4.25a}$$

$$\hat{I}[\omega] = \frac{1}{Z_0}(\hat{V}_{in}[\omega] - \hat{V}_{out}[\omega]) = \sqrt{\frac{\hbar\omega}{2Z_0}} (\hat{a}_{in}[\omega] - \hat{a}_{out}[\omega]). \tag{4.25b}$$

Now, the next question may arise how to deal with the load impedance Z_L, if we want to express it only by incoming and outgoing wave amplitude $V_{in,out}$. This can be solved by using Ohm's law

$$V = Z_L I, \tag{4.26}$$

where the voltage reflection coefficient Γ is read as[6] $(z = 0)$

$$a_{out} = \Gamma a_{in} = \frac{Z_L - Z_0}{Z_L + Z_0} a_{in}. \tag{4.27}$$

[6]From now on, we will omit the hat for operators.

So if $Z_L \neq Z_0$, part of the incident wave is reflected. In other words, to achieve no reflection, we have to set $Z_L = Z_0$[7]. In this case, the impedances are *matched*, and this is of significant importance to deliver the power without loss or to obtain no reflection, which is favored, e.g. in environment-sensible qubit measurement[16, 13, 23, 15, 24, 25].

To summarize this subsection, we have the relationship between voltage-current representation and field representation classically and quantum mechanically.

4.2 Hybrid and Scattering Parameters

In this network analysis, which considers more than one input and one output, we restrict ourselves to study the behavior of two inputs and outputs through a scattering element. In microwave network analysis, if the component is connected only by two transmission lines - each for one input and one output -, it is called "one-port network", while it is called "two-port network", if the element is connected by four transmission lines - every two inputs and two outputs -.

If we study the outputs through a device for some inputs, we have to decide, what kind of input and output we want to consider, because this consideration determines the characterization of the electronic component. For example, if we apply a current as an input, we can measure the voltage as an output. Hence, the component can be characterized by an impedance, which can be also called as a transfer function in the language of control theory. In the two-port network case, if two different currents are flowing through the element as inputs from each port, obviously two different voltages can be measured at each side (Fig. 4.2). Then, the device is described as a 2×2 impedance matrix (also called as Z parameters)

$$\begin{bmatrix} V_1 \\ V_2 \end{bmatrix} = \underbrace{\begin{bmatrix} Z_{11} & Z_{12} \\ Z_{21} & Z_{22} \end{bmatrix}}_{Z} \begin{bmatrix} I_1 \\ I_2 \end{bmatrix}, \tag{4.28}$$

[7] At first glance, it may be confusing because two lines are connected and thus some would naively expect $a_{out} = a_{in}$. However, $Z_L = Z_0$ does not mean a simple line, but a disconnection, because Z_L consists of the same "medium" as Z_0 as it was for $z < 0$

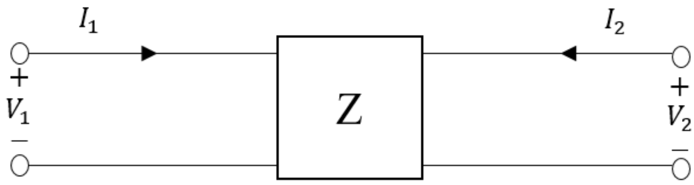

Figure 4.2: Schematic representation of impedance matrix Z. Two currents are flowing as an input and two voltages are measured at each port. In case of admittance matrix Y, the inputs and outputs are interchanged.

or, if the inputs and outputs are switched, a 2×2 admittance matrix (also called as Y parameters)

$$\begin{bmatrix} I_1 \\ I_2 \end{bmatrix} = \underbrace{\begin{bmatrix} Y_{11} & Y_{12} \\ Y_{21} & Y_{22} \end{bmatrix}}_{Y} \begin{bmatrix} V_1 \\ V_2 \end{bmatrix}. \tag{4.29}$$

Furthermore, such as in voltage feedback amplifier, voltage *and* current can be used as inputs, where we apply the voltage, e.g. at port 1 and want to have the current as an output at port 2 and vice versa. In this case, the so-called H or G parameters fulfill this requirement, namely,

$$\begin{bmatrix} V_1 \\ I_2 \end{bmatrix} = \underbrace{\begin{bmatrix} H_{11} & H_{12} \\ H_{21} & H_{22} \end{bmatrix}}_{H} \begin{bmatrix} V_2 \\ I_1 \end{bmatrix} \tag{4.30}$$

and

$$\begin{bmatrix} V_2 \\ I_1 \end{bmatrix} = \underbrace{\begin{bmatrix} G_{11} & G_{12} \\ G_{21} & G_{22} \end{bmatrix}}_{G} \begin{bmatrix} V_1 \\ I_2 \end{bmatrix}. \tag{4.31}$$

The abstract model of the network parameters Z, Y, G, and H is depicted in Fig. 4.3.
If we connect the components in cascade, it is convenient to use the so-called $ABCD$ matrix, which transmits the voltage and current at port 2 to

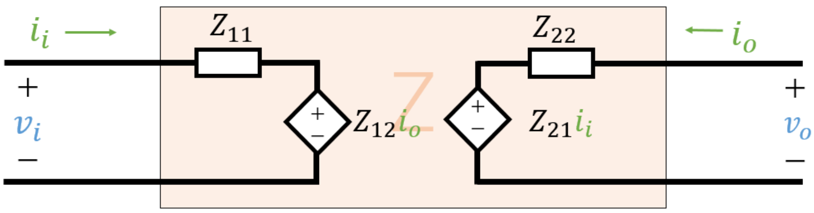

(a) Network parameter Z

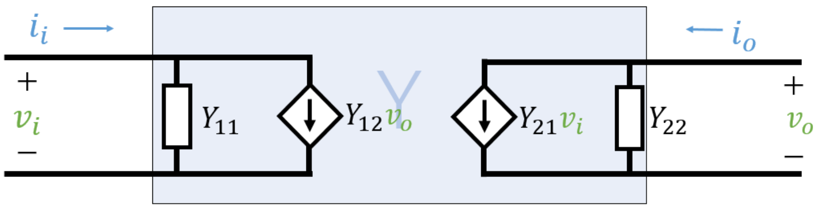

(b) Network parameter Y

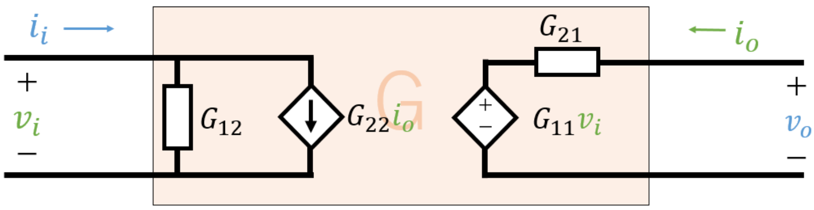

(c) Network parameter G

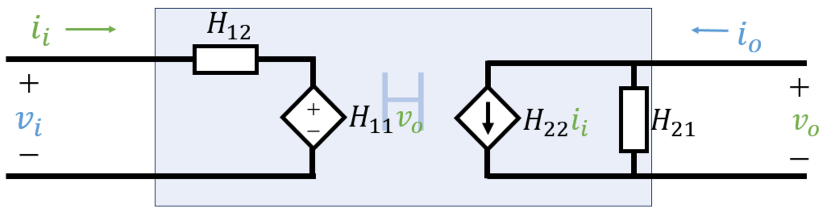

(d) Network parameter H

Figure 4.3: Network parameters Z, Y, G, H represented as an abstract circuit model. Green variables correspond to inputs, and blue ones to outputs. As described in general model of amplifier, (a) models the transresistance amplifier with gain Z_{21}, (b) the transconductance amplifier with gain Y_{21}, (c) the voltage amplifier with gain G_{11}, and (d) the current amplifier with gain H_{22}.

1 directly, in particular,

$$\begin{bmatrix} V_1 \\ I_1 \end{bmatrix} = \begin{bmatrix} A & B \\ C & D \end{bmatrix} \begin{bmatrix} V_2 \\ I_2 \end{bmatrix}. \tag{4.32}$$

As we can see from Eqs. (4.3) and (4.4), it is difficult to measure voltages and currents at high frequencies because the direct measurement of those quantities requires the magnitude and phase of a traveling or of a standing wave. Therefore, physical insights are somewhat lost. On the other hand, the so-called scattering matrix which relates the incident and reflected waves to each other can be directly obtained by a vector network analyzer. Once the scattering parameters of the device are known, the conversion to network parameters (Z, Y, H, G, and $ABCD$) (4.28) - (4.32) is possible. The scattering matrix S is defined as

$$\begin{bmatrix} a_{out} \\ b_{out} \end{bmatrix} = \begin{bmatrix} S_{11} & S_{12} \\ S_{21} & S_{22} \end{bmatrix} \begin{bmatrix} a_{in} \\ b_{in} \end{bmatrix}. \tag{4.33}$$

Each conversion to different parameters can be found in appendix A.

5 Directional Microwave SQUID Amplifier

Josephson effect is certainly one of the most important phenomena in the field of superconductivity due to its various applications in electronics, sensors, and high-frequency devices. A practical magnetic sensor is the Superconducting Quantum Interference Detector (SQUID), which consists of a superconducting loop interrupted by one or more Josephson junctions, devices with the Josephson effect. Another application is using them as directional microwave SQUID amplifier (MWSA), which is a quantum amplifier based on dc-SQUID. Its advantages over other amplifiers such as Josephson Parametric Amplifier are high gain, wide bandwidth, near-quantum-limited operation and physical separation of input-output signal (nonreciprocity) [15]. The essences of directional amplification of MWSA are nonreciprocity in spatial channels (such as circulator) and temporal channels (asymmetric frequency conversion).

But before going into the details, we review the basics of Josephson Junction and dc-SQUID.

5.1 Josephson Junction

Josephson junction (JJ) is a device forming a superconductor-insulator-superconductor layer[8]. This system makes use of the quantum phenomenon called tunnel effect, which allows two superconductors to interact such that an interesting effect arises - the celebrated Josephson effect. The fact that this effect has so many applications is owned by its high nonlinearity. Indeed, as in this MWSA the JJ is used for nonreciprocal frequency conversion[21], which will be discussed at the end of this subsection.

Josephson Equations

The supercurrent J_s is a direct consequence of the macroscopic quantum feature of superconductivity. That is, because we can describe the macroscopic coherent quantum wave function as $\Psi(\mathbf{r},t) = \Psi_0(\mathbf{r},t)e^{i\theta(\mathbf{r},t)}$, we can say $n_s^* = |\Psi_0|^2$ as a Cooper pair density and

$$J_s(\mathbf{r},t) = \frac{q^* n_s^* \hbar}{m^*}\left(\nabla\theta(\mathbf{r},t) - \frac{2\pi}{\Phi_0}\mathbf{A}(\mathbf{r},t)\right)$$

[8]The insulator part is not a must, it can be replaced, e.g. by semiconductor or metal, as well.

as a supercurrent density, where θ is the global phase of the wave function, q^* the charge and m^* the mass of the Cooper pair, $\Phi_0 = h/2e$ the quantum flux and $\mathbf{A}$ the vector potential. This result is analogous to the wave functions of quantum particles with $|\Psi_0|$ as a probability density and J_p as a probability current, which can be obtained from the continuity equation. We want to calculate the supercurrent density J_s flowing between two superconductors (thus in the insulator). In the microscopic derivation, we model the system (macroscopic wavefunction inside the insulator) as

$$\begin{aligned} i\hbar\frac{\partial}{\partial t}\Psi_L =& \mu_L\Psi_L + K\Psi_R \\ i\hbar\frac{\partial}{\partial t}\Psi_R =& \mu_R\Psi_R + K\Psi_L \end{aligned}$$

with $\Psi_k = \sqrt{n_k}e^{i\theta_k}, k = L, R$, where $\Psi_{L/R}$ denotes the wave function from the left and right side of the insulator, respectively, and $\mu_{L/R}$ its chemical potential. Then, we obtain the magnetic flux sensitive Josephson current

$$I_s(\phi) = I_0 \sin(\phi)$$

with $\phi(\mathbf{r}, t) = \theta_R(\mathbf{r}, t) - \theta_L(\mathbf{r}, t) - \frac{2\pi}{\Phi_0}\int_L^R d\mathbf{l}\cdot \mathbf{A}(\mathbf{r}, t)$ and the characteristic current I_0, and the voltage dependent time varying phase difference ϕ

$$\frac{\partial\phi}{\partial t} = \frac{2\pi}{\Phi_0}V$$

with $eV = \mu_R - \mu_L$.

Response to a dc Current Source

The first Josephson equation is a result for current smaller than the characteristic current I_0. However, if we apply a dc current greater than $I_0 < I_B$, part of the current changes to a normal current, since it exceeds the capable superconducting current flowing across the junction. So, we obtain

$$I_B = I_0 \sin(\phi(t)) + \frac{V(t)}{R}. \tag{5.1}$$

The reason for the time-dependency in the voltage $V(t)$ despite the fact that the constant bias current I_B is flowing across the resistance R lies on Eq. (5.1) itself. Since I_B is fixed and the superconducting current $I_0 \sin\phi(t)$ is alternating, the normal voltage is the only remaining part oscillating. This

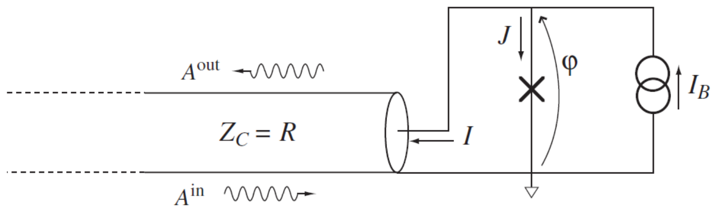

Figure 5.1: Model of Current-biased resistively shunted junction (RSJ). Adapted from [26].

plays an important role as a fluctuation term of the phase part $\Pi(t)$ in the harmonic balance treatment and contributes to generation of higher Josephson harmonics $n\omega_J,\ n \in \mathbb{Z}$ (see following subsections).

Nonreciprocity in Frequency Conversion

Kamal et al. has derived the nonreciprocity in frequency conversion of resistively-shunted JJ (RSJ) by using harmonic balance treatment[15, 21, 26](see Fig. 5.1). The harmonic balance analysis is a method to find the steady state of a nonlinear differential equation, which system has a single or multitone excitation. But strictly speaking, they have not used the harmonic balance analysis, but the related *small signal analysis*, where the nonlinear circuits are excited by two tones, one of which is very large (in this case JJ is excited by a "local oscillator" with the Josephson frequency $\omega_J = 2eV/\hbar$) and the other is vanishing small (signal frequency ω_m)[27]. The circuit is first analyzed via harmonic balance under local oscillation alone. After that, we examine the small-signal linear, time-varying circuit as a quasi-linear circuit under small-signal MW excitation.

What we need for the analysis are the two Josephson equations[9]

$$\hat{\omega} = \omega_0 \sin\phi \tag{5.2a}$$

$$\check{\omega} = \dot{\phi} \tag{5.2b}$$

with $\hat{\omega} := IR/\phi_0$, $\check{\omega} := V/\phi_0$, and $\omega_0 := I_0 R/\phi_0$. From this, we can obtain the boundary condition by making use of the result of the quantized transmission lines (see Eq. (4.25))

$$\check{\omega} + \hat{\omega} = \omega_B + 2\omega_{in} \tag{5.3}$$

[9] We adopt the notations of the original paper[15, 26].

with $\omega_B = I_B R/\phi_0$ the "bias current". We assume the phase consists of the running state term ($\omega_J t$) and fluctuation terms due to bias (Π)[10] and signal modulation (Σ), which are treated separately and thus gives

$$\phi(t) = \omega_J t + \delta\phi(t) = \omega_J t + \Pi(t) + \Sigma(t),$$

where

$$\begin{aligned}
\Pi(t) &:= \sum_{k=1}^{K} p_k^x \cos(k\omega_J t) + p_k^y \sin(k\omega_J t) \\
\Sigma(t) &:= \sum_{n=-N}^{N} s_n^x \cos(n\omega_J t + \omega_m t) + s_n^y \sin(n\omega_J t + \omega_m t).
\end{aligned}$$

K denotes the number of Josephson harmonics ($k\omega_J$) in steady state and N the number of Josephson harmonics ($n\omega_J + \omega_m$) in small signal modulation we want to consider.

As pointed out previously, we first attack this nonlinearity problem with the harmonic balance treatment with the large local oscillation ω_J. Since we have to analyze the steady-state response, we do not consider the signal contribution such as ω_{in} and Σ. Thus, by putting the Josephson equations (5.2) into (5.3)[11], collecting both quadratures (sin and cos) and comparing the pump coefficients $p_k^{x/y}$, we obtain for example for $K = 1$

$$\Pi(t) = \epsilon \cos(\omega_J t)$$

and for $K = 2$

$$\Pi(t) = \left(\epsilon + \frac{\epsilon^3}{4}\right) \cos(\omega_J t) - \frac{\epsilon^2}{4} \sin(2\omega_J t),$$

where $\epsilon = \omega_0/\omega_B$ can be interpreted as a measure of nonlinearity, since for $\epsilon \to 1$ the temporal behavior of the voltage $\breve{\omega}$ is highly nonlinear[26, 28]. The meaning of this result is the "colored" pump: As mentioned before, Π represents the pumping from the bias current ω_B and normally this pump should have a monochromatic contribution. Indeed, in the first harmonic treatment ($K = 1$) we see only frequency ω_J, but in the additional Josephson harmonic ($K = 2$) we further obtain $2\omega_J$, which breaks the symmetry between the up- and down-frequency conversion *amplitudes*.

[10] This treatment is justified by Eq. (5.1).

[11] Here, we expand the current-phase relation by Π, namely $\sin(\phi) = \sin(\omega_J t + \Pi) \approx \sin(\omega_J t) + \cos(\omega_J t)\Pi$

After the harmonic balance analysis, we are left with dealing the quasi-linear circuit under small MW excitation. The participation of the signal into the system leads to *spatial* asymmetry between the up- and down-frequency conversion amplitudes. This can be confirmed by studying the scattering matrix. For this purpose, we aim to get a relation

$$\begin{aligned}\vec{\omega} =& \hat{\mathbb{M}}\vec{\Sigma} \quad (current - phase\ relation)\\ \vec{\omega} =& \check{\mathbb{M}}\vec{\Sigma} \quad (voltage - phase\ relation)\end{aligned}$$

with the bases

$$\vec{X} = \begin{bmatrix} X[\omega_m] \\ X[\omega_J + \omega_m] \\ X[-\omega_J + \omega_m] \\ X[-\omega_m] \\ X[-\omega_J - \omega_m] \\ X[\omega_J - \omega_m] \end{bmatrix},$$

because we can transform the admittance matrix $\mathbb{Y}_J = \hat{\mathbb{M}}\check{\mathbb{M}}^{-1}$ to the scattering matrix $\mathbb{S} = \mathbb{W}^{-1}(1+\mathbb{Y}_J)^{-1}(1-\mathbb{Y}_J)\mathbb{W}$ with $\mathbb{W} = \mathrm{diag}(|\omega_J+\omega_m|, |\omega_m|, |\omega_J-\omega_m|)/\omega_B$ (see section 4.2). Henceforth, for this matrix representation above we use those Josephson equations (5.2), where for the current-phase relation we make the following approximation

$$\sin(\phi(t)) \approx \sin(\omega_J t) + \cos(\omega_J t)\Pi(t) - \sin(\omega_J t)\Pi(t)\Sigma(t).$$

Finally, the scattering matrix that gives the relationship between each incoming and outgoing mode of the system

$$\begin{bmatrix} a_{out}[\omega_m] \\ a_{out}[\omega_J + \omega_m] \\ a_{out}[-\omega_J + \omega_m] \end{bmatrix} = \begin{bmatrix} r_m & t_d & s_d \\ t_u & r_+ & v_{+-} \\ s_u & v_{-+} & r_- \end{bmatrix} \begin{bmatrix} a_{in}[\omega_m] \\ a_{in}[\omega_J + \omega_m] \\ a_{in}[-\omega_J + \omega_m] \end{bmatrix},$$

where

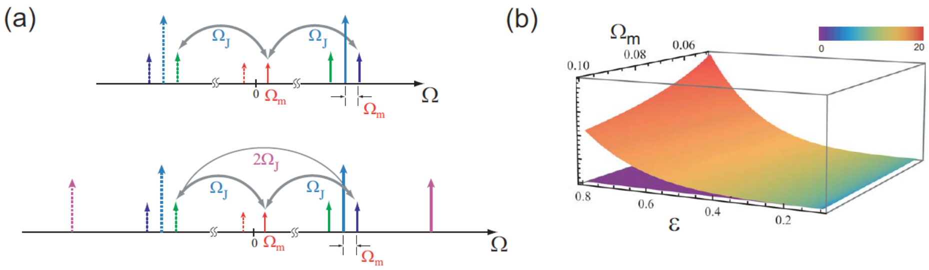

Figure 5.2: Asymmetry in frequency conversion in RSJ. (a) Frequency landscape for different expansions: three-wave mixing with $(K = 1, N = 1)$ (upper panel) and three- and four-wave mixing $(K = 2, N = 1)$. While the frequency conversion occurs symmetric in the first Josephson harmonic case (ω_J), due to the appearance of the second Josephson harmonics $(2\omega_J)$ the symmetric conversion is broken. (b) Asymmetry in frequency conversion for the two cases discussed above parametrized as $(|t_u|^2 + |s_u|^2) - (|t_d|^2 + |s_d|^2)$. The lower plot (purple) represents $(K = 1, N = 1)$ and shows no asymmetry, while in $(K = 2, N = 1)$ case the strong nonreciprocal frequency up-conversion can be recognized. Adapted from [26].

$$
\begin{aligned}
r_m =& 1 + \frac{\epsilon^2}{1 - (\omega_m/\omega_B)^2}, \\
r_\pm =& 1 \mp \frac{\epsilon^2}{2\omega_m/\omega_B(1 - \omega_m/\omega_B)}, \\
t_u =& \frac{-i\epsilon}{\sqrt{\omega_m/\omega_B(1 + \omega_m/\omega_B)}} \left(1 + \frac{\epsilon^2}{4} \frac{3 + (\omega_m/\omega_B)^2}{1 - (\omega_m/\omega_B)^2}\right), \\
t_d =& \frac{-i\epsilon}{\sqrt{\omega_m/\omega_B(1 + \omega_m/\omega_B)}} \left(1 + \frac{\epsilon^2}{4} \frac{1 - \omega_m/\omega_B}{1 + \omega_m/\omega_B}\right), \\
s_u =& \frac{i\epsilon}{\sqrt{\omega_m/\omega_B(1 + \omega_m/\omega_B)}} \left(1 + \frac{\epsilon^2}{4} \frac{3 + (\omega_m/\omega_B)^2}{1 - (\omega_m/\omega_B)^2}\right), \\
s_d =& \frac{i\epsilon}{\sqrt{\omega_m/\omega_B(1 + \omega_m/\omega_B)}} \left(1 + \frac{\epsilon^2}{4} \frac{1 - \omega_m/\omega_B}{1 + \omega_m/\omega_B}\right), \\
v_{\pm\mp} =& \pm \frac{\epsilon^2}{2\omega_m/\omega_B} \sqrt{\frac{1 \mp \omega_m/\omega_B}{1 \pm \omega_m/\omega_B}}.
\end{aligned}
$$

This result tells us two key points regarding to pumped JJ: Firstly, this device has a preferred frequency conversion due to the bias current. Secondly, the scattering matrix is not symmetric. That is, there is a favored direction for each input with different frequencies (see also Fig. 5.2). So, this pumped JJ already tells us the dc-SQUID possesses a very interesting effect. Indeed, this asymmetric up- and down-frequency conversion amplitudes of JJ plays an essential key in the directional MWSA.

5.2 dc-SQUID

A superconducting quantum interference device (SQUID) consists of two JJs connected parallel and joined by a superconducting loop. The device is called dc-SQUID if a dc-current flows through the SQUID. In MWSA, this dc-current works as a pump into the amplifier together with an external flux. Now, the dc-SQUID is responsible for the nonreciprocity in a temporal channel as in case of JJ, which yields to the "colored" pump and hence to nonequality in gain and reverse gain (cf. 2).

Superconducting current of a dc-SQUID

The key point of the high nonlinearity is the fluxoid quantization in the superconducting loop given by $\oint_c d\mathbf{l}\cdot \nabla\theta = \oint_c d\mathbf{l}\cdot 2\pi/\Phi_0(\Lambda \mathbf{J}_s + \mathbf{A}) = 2\pi n, n \in \mathbb{Z}$, because as a consequence the phase difference ϕ_L and ϕ_R are connected to each other with

$$\phi_R - \phi_L = \frac{2\pi\Phi}{\Phi_0} =: 2\phi_D,$$

where Φ is the total flux enclosed by the loop. As a result, by Kirchhoff's law, we obtain with a common phase $\phi_C := (\phi_R + \phi_L)/2$

$$\begin{aligned} I_B =& I_{s,L} + I_{s,R} = I_0(\sin\phi_L + \sin\phi_R) = 2I_0\cos(\frac{\phi_R - \phi_L}{2})\sin(\frac{\phi_R + \phi_L}{2}) \\ =& 2I_0\cos(\pi\frac{\Phi}{\Phi_0})\sin(\phi_C). \end{aligned} \tag{5.4}$$

Now, we have to consider the inductance effect of the superconducting loop, which follows

$$\Phi = \Phi_{ext} + \Phi_{loop}$$

and

$$
\begin{aligned}
I_{s,L} =& I_C + I_D \\
I_{s,R} =& I_C - I_D
\end{aligned}
$$

with

$$
\begin{aligned}
I_C =& I_0 \cos(\pi \frac{\Phi}{\Phi_0}) \sin(\phi_C) \\
I_D =& - I_0 \sin(\pi \frac{\Phi}{\Phi_0}) \cos(\phi_C),
\end{aligned}
$$

which leads to asymmetry in the current flow. So, the nonequality $\phi_L \neq \phi_R$ is the cause of this high nonlinearity. Hence,

$$
\Phi = \Phi_{ext} + LI_D = \Phi_{ext} - LI_0 \sin(\pi \frac{\Phi}{\Phi_0}) \cos(\phi_C). \tag{5.5}
$$

It is also important to note regarding the biases that the bias current I_B plays the role of common mode bias and the external flux Φ_{ext} the role of differential mode. Indeed, in MWSA analysis, I_B is responsible for energy supply and Φ_{ext} for transferability of the input signal (differential mode) into the output signal (common mode)[15, 20, 26].

Hamiltonian of dc-SQUID

Since in the next subsection we will discuss the current-phase relation and voltage-phase relation for the dc-SQUID, we shall write its Hamiltonian[20]

$$
\mathcal{H}_{SQUID} = \frac{Q_C^2}{2C} + \frac{Q_D^2}{2C} + \underbrace{2E_J \left(\frac{1}{\pi \beta_L} \left(\phi_D - \frac{\phi_{ext}}{2} \right)^2 - \cos(\phi_D)\cos(\phi_C) - \frac{I_B}{2I_0}\phi_C \right)}_{U_{SQUID}}
$$

with

$$
\begin{aligned}
\phi_D =& \frac{1}{2}\left(\phi_L - \phi_R\right), & \phi_C =& \frac{1}{2}\left(\phi_L + \phi_R\right), & & \\
I_D =& \frac{1}{2}\left(I_L - I_R\right), & I_C =& \frac{1}{2}\left(I_L + I_R\right), & & \\
\beta_L =& \frac{2LI_0}{\Phi_0}, & E_J =& \frac{I_0 \Phi_0}{2\pi}, & & \\
\Phi_0 =& \frac{h}{2e}, & \phi_0 =& \frac{\hbar}{2e}, & \phi_{ext} =& \frac{2\pi \Phi_{ext}}{\Phi_0},
\end{aligned}
$$

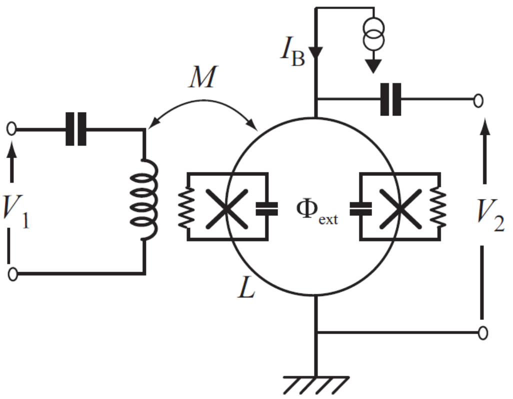

Figure 5.3: Circuit schematic of a conventional MWSA. The SQUID loop is biased by a direct current I_B and an external flux Φ_{ext}. An input voltage V_1 generates an oscillating current, which is transformed through an inductance as a small flux modulation $\delta\Phi$. This causes an output voltage $V_2 = V_{out} = V_\Phi \delta\Phi$. Adapted from [26].

where we have already transformed the operators into common and differential modes.

Voltage State and Amplification

Voltage state occurs, if the constant bias current goes above the maximal superconducting current I_0 at zero applied magnetic flux. We introduce this subsection because it is important to physically understand the directional MWSA, which cannot really be read out from the next section. Let us consider the case $\beta_L \ll 1$, which aim is to see, where the gain actually comes from. In this limit, Eq. (5.5) reduces to

$$\frac{\Phi}{\Phi_0} = \frac{\Phi_{ext}}{\Phi_0} - \frac{\beta_L}{2} \sin(\pi \frac{\Phi}{\Phi_0}) \cos(\phi_C) \approx \frac{\Phi_{ext}}{\Phi_0} = const.. \tag{5.6}$$

Since there is a normal current flowing across the junctions, we add in Eq. (5.4) the voltage term proportional to time derivative of the common phase ϕ_C

$$I_B = 2I_0 \cos(\pi \frac{\Phi}{\Phi_0}) \sin(\phi_C) + \frac{2}{R} \frac{\Phi_0}{2\pi} \frac{d}{dt} \phi_C.$$

We can then obtain the time-averaged voltage

$$\langle V(t) \rangle = I_0 R \sqrt{\left(\frac{I_B}{2I_0}\right)^2 - \cos^2\left(\pi \frac{\Phi_{ext}}{\Phi_0}\right)}, \tag{5.7}$$

which is relevant to define the "gain" of the amplifier $V_\Phi := \partial \langle V(t) \rangle / \partial \Phi_{ext}$. Usually, this sensitivity of the flux to voltage is called flux-to-voltage transfer coefficient. The highest sensitivity can be achieved for $\Phi_{ext} = \Phi_0/4$[20, 26, 28]. The reason for interpreting V_Φ as a gain can be found by investigating the time-averaged voltage $\langle V(t) \rangle$. If we expand it by the flux Φ_{ext} at $\Phi_0/4$, we have

$$\langle V(t) \rangle (\Phi_{ext}) = \underbrace{\langle V(t) \rangle (\Phi_0/4)}_{bias \quad term} + \underbrace{V_\Phi (\Phi_0/4)\, \delta\Phi}_{V_{out}} + ... \quad ,$$

henceforth sensitive to small flux variations(see Fig. 5.3). But the problem is the constant flux Φ due to $\beta_L \ll 1$ because this yields to no differential voltage, thus no input in the SQUID loop, which is in differential mode, can be amplified[12]. On top of that, it is better to take $\beta_L \sim 1$ to increase the sensitivity, but avoiding hysteresis curves. It turns out the differential current appears as an inductive current term I_{circ} circulating around the SQUID loop described by

$$I_{circ} = \frac{I_0}{\pi \beta_L} \left(-2\phi_D + \phi_{ext}\right).$$

The detailed current-phase relation of common and differential mode is held in the next section.

5.3 Directional Microwave SQUID Amplifier

The directional MWSA is a dc-SQUID connected with external circuits for incoming input signals and outgoing output signals (see Fig. 5.4). This signal input contributes to the second nonreciprocity, the physical separation of input-output signals.

In this thesis, we are working with the scattering matrix of MWSA. Thus we want to discuss its derivation briefly. The calculation flow is analogous to that of RSJ, but now with two different modes in this case.

[12]Nevertheless, the flux will fluctuate in time due to oscillating voltage contributing to steady-state response as $\Pi(t)$.

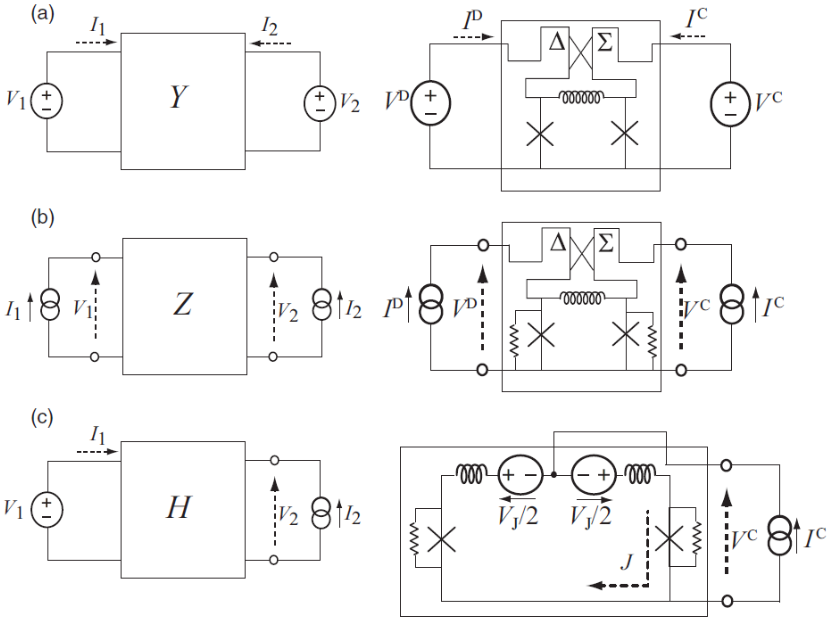

Figure 5.4: Representations of two-port amplifiers (a) in network parameters Y, (b) Z, and (c) H (see 2 for details). The left pictures are representing the corresponding network parameters, and the right ones the configurations for the dc-SQUID. As mentioned in the main text, the boxed device is the dc-SQUID connected by external circuits. Figure dapted from [15].

Small Signal Analysis

Inserting the result of the dc-SQUID Hamiltonian into the equation $I_{C,D}/I_0 = -\partial(U_{SQUID}/2E_J)/\partial\phi_{C,D}$, the current-phase and voltage-phase relation is given by

$$\begin{aligned} \hat{\omega}_C &= \frac{\omega_B}{2} - \omega_0 \sin\phi_C \cos\phi_D, & \check{\omega}_C &= \frac{\dot{\phi}_C}{\phi_0} \\ \hat{\omega}_D &= \frac{\omega_0}{\pi\beta_L}(-2\phi_D + \phi_{ext}) - \omega_0 \cos\phi_C \sin\phi_D, & \check{\omega}_D &= \frac{\dot{\phi}_D}{\phi_0}. \end{aligned}$$

Now, we want to use the boundary condition for common and differential modes with the input-output relation (see Eq. (4.25)). These common and differential inputs and outputs come from the same bias port as illustrated by Fig. 5.4 and are separated into left and right currents and voltages in the SQUID-loop. Since we want to utilize the wave amplitude representation, we model the resistance of JJ as a semi-infinite transmission line by making

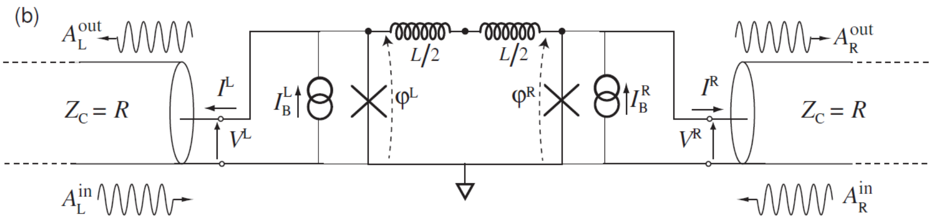

Figure 5.5: Model of the directional microwave SQUID amplifier. $I_B = I_B^L + I_B^R$ is the common mode bias current and $\phi_D = \phi_R - \phi_L$ is the differential mode bias flux. We stress the "real" input and output come from the bias port as depicted in Fig. 5.4 and are separated into "left" and "right" currents. Figure dapted from [26].

use of Caldeira-Leggett model [15, 22, 29, 26]. Henceforth, these lead to the appearance of two input and output signals representing the currents and voltages dropped across the left/right resistance(see Fig. 5.5). Since we obtain the common and differential modes by inserting into the left and right propagating waves, the left and right resistance of JJ has also the meaning of representing the common and differential modes. That is, we can neglect the external circuit.
Finally, we get using the above relations

$$\check{\omega}_{C,D}(t) = \hat{\omega}_{C,D}(t) + 2\omega_{in,(C,D)}(t).$$

Since we have everything to start with the harmonic balance analysis, we again distinguish between fluctuations due to the bias ($\Pi_{C,D}$) and due to the signal modulations ($\Sigma_{C,D}$)

$$\begin{aligned}\phi_C(t) =& \omega_J t + \delta\phi_C(t) = \omega_J t + \Pi_C(t) + \Sigma_C(t),\\ \phi_D(t) =& \varphi_0 + \delta\phi_D(t) = \varphi_0 + \Pi_D(t) + \Sigma_D(t),\end{aligned}$$

where $\omega_J = V_{dc}/\phi_0$ and φ_0 are the average static values of each phases. In dc-SQUID case, V_{dc} is the static voltage applied across the SQUID loop biased in the running state of the phase particle. As usual we expand $\Pi_{C,D}$ and $\Sigma_{C,D}$ as

$$\Pi_{C,D}(t) := \sum_{k=1}^{K} p^x_{k,(C,D)} \cos(k\omega_J t) + p^y_{k,(C,D)} \sin(k\omega_J t)$$

$$\Sigma_{C,D}(t) := \sum_{n=-N}^{N} s^x_{n,(C,D)} \cos(n\omega_J t + \omega_m t) + s^y_{n,(C,D)} \sin(n\omega_J t + \omega_m t)$$

such that we can evaluate the coefficients of $\Pi_{C,D}$ by putting into the steady-state boundary conditions

$$\check{\omega}_{C,D} - \hat{\omega}_{C,D} = 0.$$

One will then notice that the external flux ϕ_{ext} plays an important role regarding to asymmetry. The essence in this discussion is ϕ_{ext} can change the number of harmonics of the Josephson oscillation involved in Π. For example, $\Pi_D = 0$ for $\phi_{ext} = 0$, which means Π_D cannot contribute to the asymmetric frequency conversion. As pointed out in [20] and [15] the trajectory in the SQUID potential is maximized for $\phi_{ext} = \pi/2$ and will lead to directional gain in the MWSA.

As we get the steady-state response, we can move on to the small signal analysis. Hence, we include $\Sigma_{C,D}$ term in our calculation as the small signal perturbation. For this, as in RSJ case, we describe the current-phase and voltage-phase relationship in matrix form as

$$\begin{bmatrix} \vec{\hat{\omega}}_C \\ \vec{\hat{\omega}}_D \end{bmatrix} = \underbrace{\begin{bmatrix} \hat{\mathbb{M}}_{CC} & \hat{\mathbb{M}}_{CD} \\ \hat{\mathbb{M}}_{DC} & \hat{\mathbb{M}}_{DD} \end{bmatrix}}_{\hat{\mathbb{M}}} \begin{bmatrix} \vec{\Sigma}_C \\ \vec{\Sigma}_D \end{bmatrix}$$

$$\begin{bmatrix} \vec{\check{\omega}}_C \\ \vec{\check{\omega}}_D \end{bmatrix} = \underbrace{\begin{bmatrix} \check{\mathbb{M}}_{CC} & \check{\mathbb{M}}_{CD} \\ \check{\mathbb{M}}_{DC} & \check{\mathbb{M}}_{DD} \end{bmatrix}}_{\check{\mathbb{M}}} \begin{bmatrix} \vec{\Sigma}_C \\ \vec{\Sigma}_D \end{bmatrix}$$

giving

$$\mathbb{Y} = \hat{\mathbb{M}}\check{\mathbb{M}}^{-1}.$$

The basis of those vectors are defined in all signal and sideband frequencies of interest, namely $(\Sigma_C[n\omega_J + \omega_m], \Sigma_D[n\omega_J + \omega_m]), n \in [-N, +N]$ yielding to a $4(2N+1) \times 4(2N+1)$ admittance matrix.

Scattering Matrix of MWSA

Using the result of the admittance matrix, we use the identity to obtain the scattering representation of the quantum amplifier

$$\mathbb{S} = (\mathbf{1} + \mathbb{Y})^{-1} (\mathbf{1} - \mathbb{Y}).$$

Since we are only interested in signal frequencies ω_m and not their sideband frequencies $n\omega_J + \omega_m$, the 2-input-2-output relation is expressed as

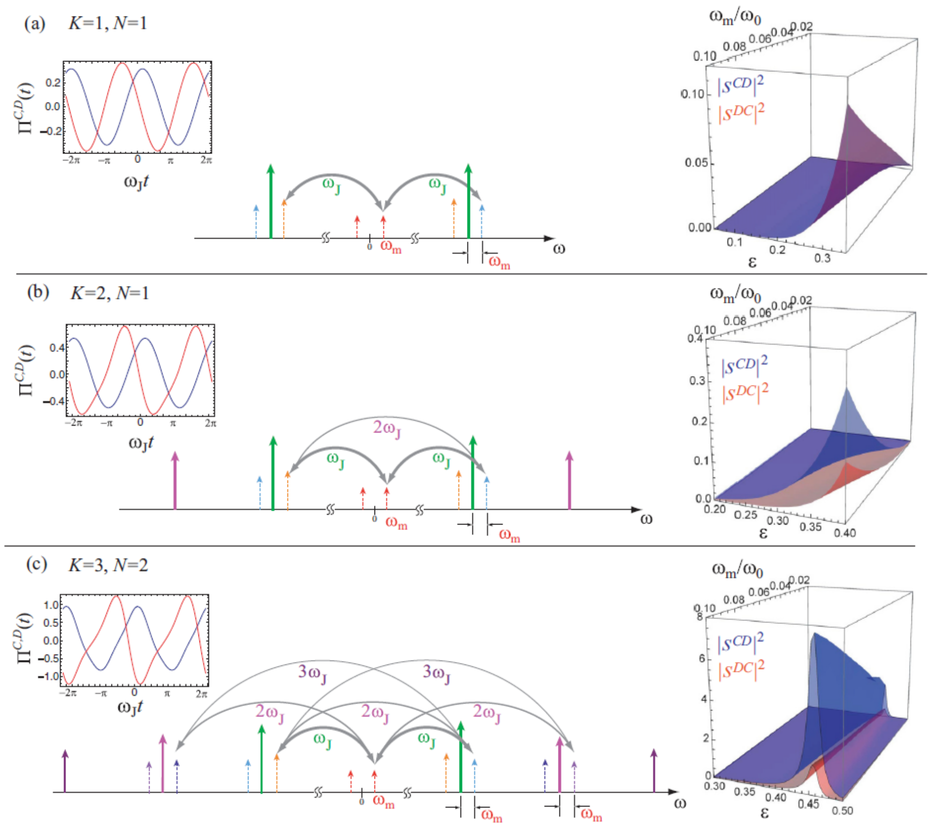

Figure 5.6: Frequency spectrum of Josephson harmonics, and small scattering gain and reverse gain of dc-SQUID with different expansions of nonlinearity: (a) to the first, (b) third, and (c) fifth order. Parameters used were $\Phi_{ext} = \Phi_0/4$, $\beta_L = 1$, and $\Omega_C = 1$. Figure dapted from [15].

$$\begin{bmatrix} A_{C,out}[\omega_m] \\ A_{D,out}[\omega_m] \end{bmatrix} = \begin{bmatrix} s_{CC}[\omega_m] & s_{CD}[\omega_m] \\ s_{DC}[\omega_m] & s_{DD}[\omega_m] \end{bmatrix} \begin{bmatrix} A_{C,in}[\omega_m] \\ A_{D,in}[\omega_m] \end{bmatrix}$$

The numerical result is shown in Fig. 5.6. But this is not a correct input-output relation, and henceforth we need to add idlers to be able to require $|s_{CD}[\omega_m]| > 1$, i.e.,

$$\begin{bmatrix} A_{C,out}[\omega_m] \\ A_{D,out}[\omega_m] \end{bmatrix} = \begin{bmatrix} s_{CC}[\omega_m] & s_{CD}[\omega_m] \\ s_{DC}[\omega_m] & s_{DD}[\omega_m] \end{bmatrix} \begin{bmatrix} A_{C,in}[\omega_m] \\ A_{D,in}[\omega_m] \end{bmatrix} + \begin{bmatrix} F_C[\omega_m] \\ F_D[\omega_m] \end{bmatrix}. \tag{5.8}$$

in order to fulfill the commutation relation

$$\left[A_{C,out}[\omega_m], A^{\dagger}_{C,out}[\omega_m]\right] = |s_{CC}[\omega_m]|^2 + |s_{CD}[\omega_m]|^2 + \left[F_C[\omega_m], F^{\dagger}_C[\omega_m]\right] = 1 \tag{5.9a}$$

$$\left[A_{D,out}[\omega_m], A^{\dagger}_{D,out}[\omega_m]\right] = |s_{DC}[\omega_m]|^2 + |s_{DD}[\omega_m]|^2 + \left[F_D[\omega_m], F^{\dagger}_D[\omega_m]\right] = 1. \tag{5.9b}$$

6 2-input-2-output Quantum Feedback Amplifier

In this section, we analyze properties of the 2-input-2-output QFA (2i2o QFA) in the feedback system because they have different features compared to the conventional quantum amplifiers (the phase-preserving amplifiers). Notably, while Yamamoto proved the feedback control of the signal is possible by using the idler in the phase-preserving amplifier case [30], it is not apparent the second signal coming into the 2i2o amplifier is able to feedback control the target signal. Here, we mean by feedback controllability, whether we get a similar result as in classical feedback amplifier case, namely, $G/(1 + GK)$. We also demonstrate the gain fluctuations of the MWSA can indeed be suppressed by the signal. In addition to that, we show the quantum-noise limit can be reached and how the added noise in the feedback system affects the total noise of the output.

6.1 Model

The model we study is shown in Fig. 6.1. At the moment, we do not consider added noises, that is, d_4, d_5, and F^K will be not investigated until subsection 6.3.

Obviously, the suggested model here is one of many possibilities to design, but the inputs and outputs of the MWSA G cannot be changed. I. e., a_3 and b_1 has to be the system output and input, respectively, and $\tilde{a}_2$ and b_2 is the input and output of the feedback loop. The reason is the scattering element s_{21}^G which is the only gain as mentioned in section 2. If we remember

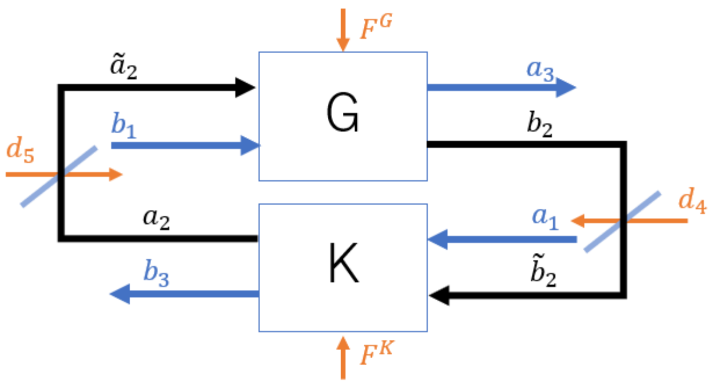

Figure 6.1: 2-input-2-output quantum feedback amplifier model.

the physical interpretation of the feedback amplifier mechanism in subsection 2.2.1, the key idea is that the multiplication of the controller and the gain is in the feedback loop circle. Therefore, the inputs and outputs of G cannot be replaced[13]. On the other hand, the inputs and outputs at the controller can be chosen arbitrarily. One can confirm that for each combination we will obtain different controller transfer function in the denominator, that is, $1 - s_{21}^{G} s_{ij}^{K}$.

The input-output relations of the amplifier and the controller is described as follows: Assume an arbitrary unitary coherent controller K (i.e. $s^{K,\dagger} s^{K} = s^{K} s^{K,\dagger} = \mathbf{1}$) with

$$\begin{bmatrix} a_2 \\ b_3 \end{bmatrix} = \begin{bmatrix} s_{11}^{K} & s_{12}^{K} \\ s_{21}^{K} & s_{22}^{K} \end{bmatrix} \begin{bmatrix} a_1 \\ b_2 \end{bmatrix}. \tag{6.1}$$

Now combining Eq. 6.1 with Eq. 5.8, where in this case $A_{D,in} = a_2$, $A_{C,in} = b_1$, $A_{D,out} = a_3$, and $A_{C,out} = b_2$, we obtain the feedback gain scattering matrix $s_{21}^{G,fb}$

$$\begin{aligned} \begin{bmatrix} a_3 \\ b_3 \end{bmatrix} =& \frac{1}{1 - s_{21}^{G} s_{12}^{K}} \begin{bmatrix} s_{11}^{G} s_{11}^{K} & s_{12}^{G} + s_{12}^{K} |s^{G}| \\ s_{21}^{K} + s_{21}^{G} |s^{K}| & s_{22}^{G} s_{22}^{K} \end{bmatrix} \begin{bmatrix} a_1 \\ b_1 \end{bmatrix} \\ &+ \frac{1}{1 - s_{21}^{G} s_{12}^{K}} \begin{bmatrix} 1 - s_{21}^{G} s_{12}^{K} & s_{12}^{G} s_{11}^{K} \\ 0 & s_{22}^{K} \end{bmatrix} \begin{bmatrix} F_1 \\ F_2 \end{bmatrix}. \end{aligned} \tag{6.2}$$

In the ideal quantum limit, we then have

$$\begin{bmatrix} a_3 \\ b_3 \end{bmatrix} = \begin{bmatrix} 0 & 0 \\ -\frac{|s^{K}|}{s_{12}^{K}} & 0 \end{bmatrix} \begin{bmatrix} a_1 \\ b_1 \end{bmatrix} + \begin{bmatrix} 1 & 0 \\ 0 & -\frac{s_{22}^{K}}{s_{12}^{K}} \frac{1}{s_{21}^{G}} \end{bmatrix} \begin{bmatrix} F_1 \\ F_2 \end{bmatrix}. \tag{6.3}$$

Hence, we obtain a similar structure as in classical case (Eq. (2.5)). We remind the readers that F_1^{G} scales with $\mathcal{O}(1)$, but F_2^{G} with $\mathcal{O}(s_{21}^{G})$. Thus, the order of the effective idler is accordingly reduced to $\mathcal{O}(1/s_{12}^{K})$.

How can we interpret this result physically? This feedback amplification physics is demonstrated in Fig. 6.2. For simplicity, we set a beam splitter (mirror) as a feedback controller, but as can be seen from the picture, this can be treated generically. We remind the readers the input signal a_1 does only have the option to be transmitted by s_{21}^{K} and reflected by s_{11}^{K}, and vice versa for b_2 in the feedback loop. If we now assume an ideal quantum amplifier with

[13] However, if the directionality is not present, and the device can amplify bidirectionally, the only restriction is the off-diagonal scattering element is in the feedback loop.

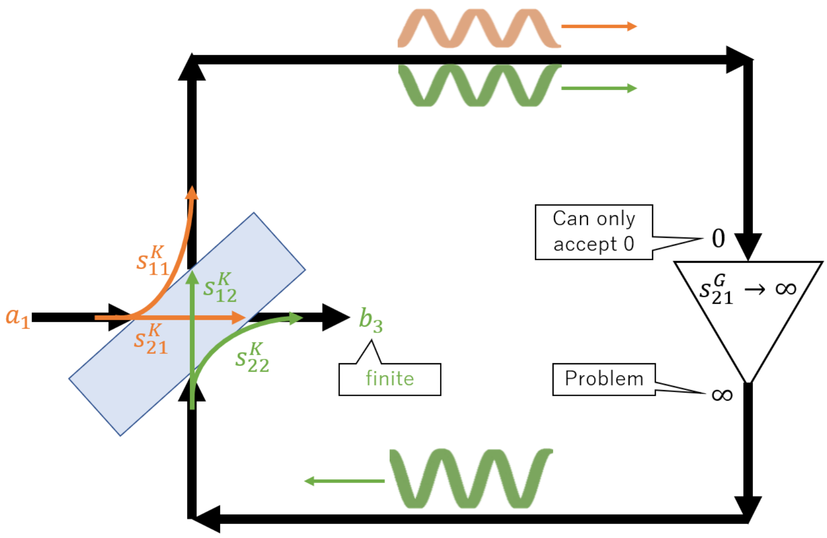

Figure 6.2: Physical interpretation of 2-input-2-output quantum feedback amplifier model. The ideal quantum amplifier is designated by a triangle, where the other port for b_1 and a_3 is not depicted for clarity, and the beam splitter (mirror) by a blue box. In the ideal amplifier limit, the gain is infinite.

infinite gain $s_{21}^G \to \infty$, then the output of a signal (b_2) would also be infinite. This is, however, a huge problem because the amplitude of b_3 is finite[14]. So, the only solution is to require the input of the amplifier a_2 is 0[15]. Then, let us begin with the incoming signal a_1, which will be partly transmitted to b_3 by s_{21}^K and partly reflected by s_{11}^K. The reflected signal $s_{11}^K a_1$ is traveling to the amplifier, but this device only accepts zero-amplitude. The only way to fulfill this requirement is to send another signal which is π-shifted in order to obtain destructive interference. But from where? This signal is provided by the quantum amplifier, which output gives $-s_{11}^K/s_{12}^K a_1$. So, this signal then transmits through the beam splitter to eliminate the wave from a_1, and the reflected one finally ends up with

$$b_3 = \left(s_{21}^K - \frac{s_{11}^K s_{22}^K}{s_{12}^K} \right) a_1 = -\frac{|s^K|}{s_{12}^K} a_1.$$

6.2 Feedback Gain Analysis

In this subsection, we want to analyze the relative sensitivity of each element as a function of the relative sensitivity of the original gain $\Delta s_{21}^G / s_{21}^G$. Using

[14]In the reality, this means the gain is much higher than the expected output.
[15]In the real consideration, this means small enough amplitude.

$|x+\epsilon| - |x| = \mathrm{Re}[x^\star \epsilon]/|x| + \mathcal{O}(\epsilon)$, we can prove the relative sensitivity looks similar to Eq. 2.12, namely,

$$\begin{aligned}
\frac{\Delta s_{11}^{G,fb}}{s_{11}^{G,fb}} &= \mathrm{Re}\left[\frac{\Delta s_{11}^G}{s_{11}^G} + \frac{s_{12}^K s_{21}^G}{1 - s_{21}^G s_{12}^K}\frac{\Delta s_{21}^G}{s_{21}^G}\right] \\
&= \mathrm{Re}\left[\frac{1}{1 - s_{21}^G s_{12}^K}\frac{\Delta s_{21}^G}{s_{21}^G}\right], \qquad \frac{\Delta s_{11}^G}{s_{11}^G} = \frac{\Delta s_{21}^G}{s_{21}^G} \qquad (6.4a) \\
\frac{\Delta s_{12}^{G,fb}}{s_{12}^{G,fb}} &= \mathrm{Re}\left[\frac{s_{12}^G}{s_{12}^G + s_{12}^K|s^G|}\frac{\Delta s_{12}^G}{s_{12}^G} + \frac{s_{12}^K s_{21}^G}{1 - s_{21}^G s_{12}^K}\frac{\Delta s_{21}^G}{s_{21}^G} + \frac{1}{1 + s_{12}^G/s_{12}^K|s^G|}\frac{\Delta|s^G|}{|s^G|}\right] \\
&= \mathrm{Re}\left[\frac{1}{1 - s_{21}^G s_{12}^K}\frac{\Delta s_{21}^G}{s_{21}^G} + \frac{1}{1 + s_{12}^G/s_{12}^K|s^G|}\frac{\Delta|s^G|}{|s^G|}\right], \qquad \frac{\Delta s_{12}^G}{s_{12}^G} = \frac{\Delta s_{21}^G}{s_{21}^G} \\
& \qquad (6.4b) \\
\frac{\Delta s_{21}^{G,fb}}{s_{21}^{G,fb}} &= \mathrm{Re}\left[\frac{1}{1 - s_{21}^G s_{12}^K}\frac{s_{11}^K s_{22}^K s_{21}^G}{s_{12}^K + s_{21}^G|s^K|}\frac{\Delta s_{21}^G}{s_{21}^G}\right] \qquad (6.4c)
\end{aligned}$$

$$\begin{aligned}
\frac{\Delta s_{22}^{G,fb}}{s_{22}^{G,fb}} &= \mathrm{Re}\left[\frac{\Delta s_{22}^G}{s_{22}^G} + \frac{s_{12}^K s_{21}^G}{1 - s_{21}^G s_{12}^K}\frac{\Delta s_{21}^G}{s_{21}^G}\right] \\
&= \mathrm{Re}\left[\frac{1}{1 - s_{21}^G s_{12}^K}\frac{\Delta s_{21}^G}{s_{21}^G}\right], \qquad \frac{\Delta s_{22}^G}{s_{22}^G} = \frac{\Delta s_{21}^G}{s_{21}^G}. \qquad (6.4d)
\end{aligned}$$

All relative sensitivities are suppressed by $\mathcal{O}(1/(1 - s_{21}^G s_{12}^K))$, thus robust against gain fluctuations. However, we see the relative sensitivity is dependent on $s_{21}^G s_{12}^K$, so thus increasing s_{21}^G is not enough, if s_{12}^K is taken very small. The result of gain without and with feedback is given in Fig. 6.3.

6.3 Quantum-Noise Limit and Added Noise

After we have evaluated the closed-loop feedback scattering matrix and the relative sensitivities of each scattering elements, questions may arise, how much the idler noise F^G or unwanted noises would contribute to the signal because these limit the detection performance of tiny signals. Therefore, we consider all noises as depicted in Fig. 6.1. To quantify the noise attributes, we make use of signal-to-noise ratio

$$(S/N) := \frac{|\langle x \rangle|^2}{\langle |\Delta x|^2 \rangle} \qquad (6.5)$$

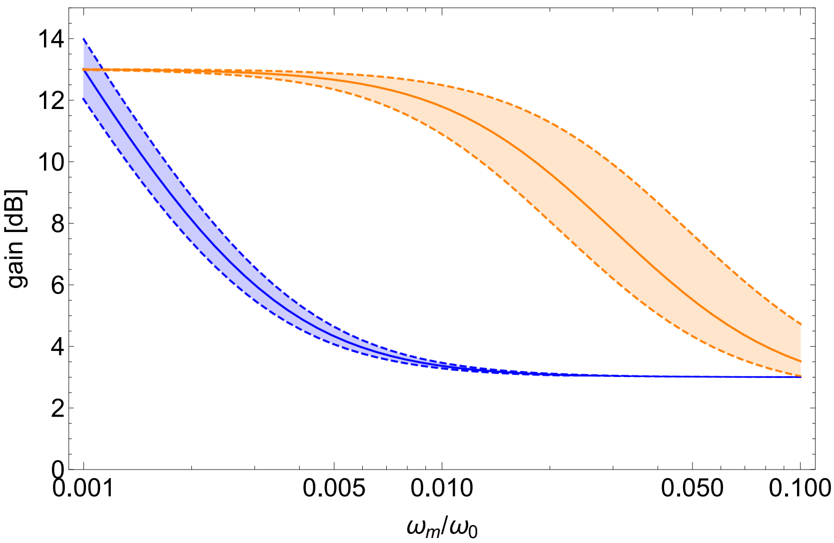

Figure 6.3: Power gain of the MWSA with no-feedback ($\epsilon = 0.16 \pm 0.016$) (blue) and with feedback with $\epsilon = 0.34 \pm 0.034$ and $s^K_{12} = -1/20$ (orange). The simulation is done with $K = 3$, $N = 2$. The parameters are chosen $\Phi_{ext} = \Phi_0/4$, $\beta_L = 1$, $\Omega_C = 1$.

where

$$\left\langle |\Delta x|^2 \right\rangle := \frac{1}{2} \left\langle \Delta x \Delta x^\dagger + \Delta x^\dagger \Delta x \right\rangle \tag{6.6}$$

with $\Delta x = x - \langle x \rangle$.

First, as an introduction, let us study only the output of a quantum amplifier G. We actually recognize the operational amplifier (op-amp) (and henceforth MWSA) is 2-signal-2-idler quantum amplifier [16], which can be described by

$$\begin{aligned} \begin{bmatrix} a_3 \\ b_2 \end{bmatrix} &= \begin{bmatrix} s^G_{11} & s^G_{12} \\ s^G_{21} & s^G_{22} \end{bmatrix} \begin{bmatrix} a_2 \\ b_1 \end{bmatrix} + \begin{bmatrix} F^G_1 \\ F^G_2 \end{bmatrix} \\ &= \begin{bmatrix} s^G_{11} & s^G_{12} \\ s^G_{21} & s^G_{22} \end{bmatrix} \begin{bmatrix} a_2 \\ b_1 \end{bmatrix} + \begin{bmatrix} s^G_{13} & s^G_{14} \\ s^G_{23} & s^G_{24} \end{bmatrix} \begin{bmatrix} d_1 \\ d^\dagger_2 \end{bmatrix}, \end{aligned} \tag{6.7}$$

with the vacuum noise d_i, so $\left\langle d^\dagger_i d_j \right\rangle = 0$ and $\left[d_i, d^\dagger_j \right] = \delta_{i,j}$. Applying Eqs. (6.5) and (6.6), the signal-to-noise ratio of b_2 is

$$
(\tilde{S/N})_2 = \frac{|\langle b_2\rangle|^2}{\langle|\Delta b_2|^2\rangle} = \frac{\left|\langle a_2\rangle + \frac{s_{22}^G}{s_{21}^G}\langle b_1\rangle\right|^2}{\langle|\Delta a_2|^2\rangle + \left|\frac{s_{22}^G}{s_{21}^G}\right|^2\langle|\Delta b_1|^2\rangle + \underbrace{\frac{1}{2}\left|\frac{s_{23}^G}{s_{21}^G}\right|^2 + \frac{1}{2}\left|\frac{s_{24}^G}{s_{21}^G}\right|^2}_{=\mathcal{A}}}, \tag{6.8}
$$

where $\mathcal{A}_2^{(0)}$ is called added noise. In this case, the added noise is just the idler of the quantum amplifier. This added noise can be generalized for $N-2$ noise sources as

$$
\mathcal{A}_2^{(0)} = \frac{1}{2|s_{21}^G|^2}\sum_{k=3}^{N}|s_{2k}^G|^2 = \frac{1}{2} - \frac{1-\left|s_{22}^G\right|^2}{2\left|s_{21}^G\right|^2} + \sum_{k\neq 4}^{N}|s_{2k}^G|^2 \tag{6.9}
$$

$$
= \left|\frac{s_{24}^G}{s_{21}^G}\right|^2 - \frac{1}{2} + \frac{1-\left|s_{22}^G\right|^2}{2\left|s_{21}^G\right|^2} \tag{6.10}
$$

$$
\geq \frac{1}{2} - \frac{1-\left|s_{22}^G\right|^2}{2\left|s_{21}^G\right|^2}, \tag{6.11}
$$

where the last two equality and inequality can be shown by using the canonical commutation relation (CCR) (see Appendix B for the proof). Because of the restriction to the degree of freedom in the added noises, we can actually express $\mathcal{A}_2^{(0)}$ only with three matrix elements. Furthermore, we notice the added noise can indeed reach the quantum noise limit $\mathcal{A}_2^{(0)} \geq 1/2$ for $|s_{21}^G| \to \infty$ since $|s_{22}| \leq 1$. We note we have not made any assumptions here except for being s_{21}^G the gain. That is, the added noise of any transfer functions, including closed-loop transfer functions, written by Eq. (6.7) with 21 matrix element as the gain can be expressed as the equation above. So, Eq. (6.11) is quite fundamental.

Now let us assume there are additional noise contributions in the following way: The quantum amplifier and the controller experience another noise source such that

$$
\begin{bmatrix} F_1^G \\ F_2^G \end{bmatrix} \to \begin{bmatrix} s_{13}^G & s_{14}^G & s_{15}^G \\ s_{23}^G & s_{24}^G & s_{25}^G \end{bmatrix} \begin{bmatrix} d_1 \\ d_2^\dagger \\ d_3 \end{bmatrix} \tag{6.12}
$$

and

$$
\begin{bmatrix} F_1^K \\ F_2^K \end{bmatrix} = \begin{bmatrix} s_{13}^K \\ s_{23}^K \end{bmatrix} d_4. \tag{6.13}
$$

In addition to that, we model the loss of transmission lines as a beam splitter such that the inputs a_2 at G and b_2 at K change to

$$
\begin{aligned}
b_2 \rightarrow \tilde{b}_2 &= \alpha_1 b_2 + \delta_1 d_5 && (6.14)\\
a_2 \rightarrow \tilde{a}_2 &= \alpha_2 a_2 + \delta_2 d_6. && (6.15)
\end{aligned}
$$

Finally, we reach to the following closed-loop input-output relation

$$
\begin{bmatrix} a_3 \\ b_3 \end{bmatrix} = \frac{1}{1-\alpha_1\alpha_2 s_{21}^G s_{12}^K} \begin{bmatrix} \alpha_2 s_{11}^G s_{11}^K & s_{12}^G + \alpha_1\alpha_2 s_{12}^K |s^G| \\ s_{21}^K + \alpha_1\alpha_2 s_{21}^G |s^K| & \alpha_1 s_{22}^G s_{22}^K \end{bmatrix} \begin{bmatrix} a_1 \\ b_1 \end{bmatrix} + \begin{bmatrix} \tilde{F}_1^G \\ \tilde{F}_2^G \end{bmatrix} + \begin{bmatrix} \tilde{F}_1^K \\ \tilde{F}_2^K \end{bmatrix}, \tag{6.16}
$$

with[16]

$$
\begin{bmatrix} \tilde{F}_1^G \\ \tilde{F}_2^G \end{bmatrix} = \begin{bmatrix} s_{13}^{G,fb} & s_{14}^{G,fb} & s_{15}^{G,fb} & s_{16}^{G,fb} \\ s_{23}^{G,fb} & s_{24}^{G,fb} & s_{25}^{G,fb} & s_{26}^{G,fb} \end{bmatrix} \begin{bmatrix} d_1 \\ d_2^\dagger \\ d_3 \\ d_6 \end{bmatrix} \tag{6.17}
$$

and

$$
\begin{bmatrix} \tilde{F}_1^K \\ \tilde{F}_2^K \end{bmatrix} = \begin{bmatrix} s_{13}^{K,fb} & s_{14}^{K,fb} \\ s_{23}^{K,fb} & s_{24}^{K,fb} \end{bmatrix} \begin{bmatrix} d_4 \\ d_5 \end{bmatrix}. \tag{6.18}
$$

So the matrix elements $s_{ij}^G (i,j=1,2)$ in Eq. (6.11) changes to

$$
\begin{aligned}
s_{11}^G \rightarrow s_{11}^{G,fb} &= \frac{\alpha_2 s_{11}^G s_{11}^K}{1-\alpha_1\alpha_2 s_{21}^G s_{12}^K}, \quad s_{12}^G \rightarrow s_{12}^{G,fb} = \frac{s_{12}^G + \alpha_1\alpha_2 s_{12}^K |s^G|}{1-\alpha_1\alpha_2 s_{21}^G s_{12}^K}, \\
s_{21}^G \rightarrow s_{21}^{G,fb} &= \frac{s_{21}^K + \alpha_1\alpha_2 s_{21}^G |s^K|}{1-\alpha_1\alpha_2 s_{21}^G s_{12}^K}, \quad s_{22}^G \rightarrow s_{22}^{G,fb} = \frac{\alpha_1 s_{22}^G s_{22}^K}{1-\alpha_1\alpha_2 s_{21}^G s_{12}^K}.
\end{aligned} \tag{6.19}
$$

[16] For the detailed description of those elements, see Appendix B.

Analogous to the proof in Appendix B, we then obtain

$$\begin{aligned}
\mathcal{A}_2^{(fb)} =& \frac{1}{2|s_{21}^{G,fb}|^2} \sum_{k=3}^{N=8} |s_{2k}^{G,fb}|^2 \\
=& \frac{1}{2} - \frac{1-\left|s_{22}^{G,fb}\right|^2}{2\left|s_{21}^{G,fb}\right|^2} + \sum_{k\neq 4}^{N} |s_{2k}^{G,fb}|^2 && (6.20a) \\
=& \left|\frac{s_{24}^{G,fb}}{s_{21}^{G,fb}}\right|^2 - \frac{1}{2} + \frac{1-\left|s_{22}^{G,fb}\right|^2}{2\left|s_{21}^{G,fb}\right|^2} && (6.20b) \\
\geq& \frac{1}{2} - \frac{1-\left|s_{22}^{G,fb}\right|^2}{2\left|s_{21}^{G,fb}\right|^2}. && (6.20c)
\end{aligned}$$

In the quantum amplifier limit, we have the following relations

$$\left|\frac{s_{24}^{G,fb}}{s_{21}^{G,fb}}\right| = \left|\frac{\alpha_1 s_{22}^K s_{24}^G}{s_{21}^K + \alpha_1\alpha_2 s_{21}^G\,|s^K|}\right| \to \left|\frac{s_{22}^K}{\alpha_2}\right|\left|\frac{s_{24}^G}{s_{21}^G}\right| \approx \left|\frac{s_{24}^G}{s_{21}^G}\right| \qquad (6.21a)$$

$$\left|\frac{s_{22}^{G,fb}}{s_{21}^{G,fb}}\right| = \left|\frac{\alpha_1 s_{22}^K s_{22}^G}{s_{21}^K + \alpha_1\alpha_2 s_{21}^G\,|s^K|}\right| \to \left|\frac{s_{22}^K}{\alpha_2}\right|\left|\frac{s_{22}^G}{s_{21}^G}\right| \approx \left|\frac{s_{22}^G}{s_{21}^G}\right|, \qquad (6.21b)$$

where we have assumed in the last approximation $\left|s_{22}^K\right| \approx |\alpha_2|$. If $\left|s_{22}^K\right| \approx |\alpha_2| \lesssim 1$, which indirectly requires high feedback gain limit $\left|s_{21}^{G,fb}\right| \approx 1/\left|s_{12}^K\right| \to \infty$ because of the unitary requirement of s^K, we obtain

$$\lim_{\left|s_{21}^{G,fb}\right|\to\infty} \mathcal{A}_2^{(fb)} \approx \lim_{\left|s_{21}^{G}\right|\to\infty} \mathcal{A}_2^{(0)} = \left|\frac{s_{24}^G}{s_{21}^G}\right|^2 - \frac{1}{2}, \qquad (6.22)$$

thus the added noise is only limited by the idler noise s_{24}^G and is independent of other noise sources. So to reach the quantum noise limit, the feedback system can be designed more or less roughly, but the quantum amplifier itself has to be noiseless as possible.

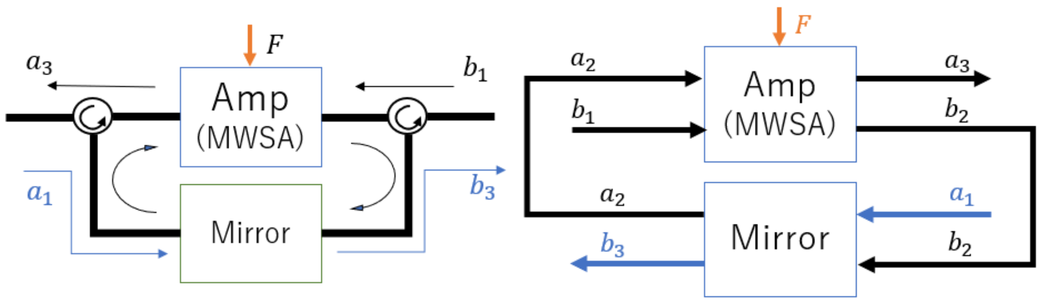

Figure 7.1: Coherent P controller in physical model (left) and in block diagram (right).

7 Directional Coherent Active P, I, and D Controller

Now, since we know the second signal can indeed feedback control the other signal, we go to the next stage, namely, giving the quantum feedback amplifier a certain functionality. For the realization of a CPID controller, we obviously need coherent P, I, and D controller. In this subsection, those three controllers are presented.
In contrast to NDPA, thanks to its directionality we only need two circulators for realizing a coherent P and D controller instead of three. On top of that, if we use the NDPA, constructing the coherent I controller would be difficult: For designing this with a cavity as a feedback controller we need a feedback loop involving only reflected waves. However, this kind of feedback loop violates the Ito rule, which is not the case for MWSA due to its nonreciprocity.
The focus mainly lies on the added noises in the whole feedback system by applying the result obtained in section 6. From here on, we assume a perfect directional quantum amplifier, that is, $s^G_{11} = s^G_{22} = 0$, and $|s^G| = 1$[17].

7.1 Coherent P Controller

The P control scheme uses a beam splitter or mirror as a controller as depicted in Fig. 7.1. The feedback controller is just

$$\begin{bmatrix} \alpha & -\beta \\ \beta & \alpha \end{bmatrix}.$$

[17]For non-ideal case, the result is given in Appendix B

Since it has the same structure as that introduced in section 6 and the control parameters are frequency-independent, further discussions are omitted.

7.2 Coherent D Controller

In case of D controller, the feedback structure is the same, but we replace the beam splitter with the cavity, where its transfer function s^K is written as

$$\begin{bmatrix} a_2 \\ b_3 \end{bmatrix} = \frac{1}{s - i\Delta + \gamma/2} \begin{bmatrix} s - i\Delta & -\gamma/2 \\ -\gamma/2 & s - i\Delta \end{bmatrix} \begin{bmatrix} a_1 \\ b_2 \end{bmatrix} \tag{7.1}$$

with the detuning from the carrier frequency $\Delta = \omega_P - \omega_{cav}$ and the decay rate γ. Applying this Eq. 7.1 to Eq. 6.2, we obtain

$$\begin{aligned}
\begin{bmatrix} a_3 \\ b_3 \end{bmatrix} =& s^D \begin{bmatrix} a_1 \\ b_1 \end{bmatrix} + \begin{bmatrix} F_1^D \\ F_2^D \end{bmatrix} \\
=& \frac{1}{1 - s_{21}^{G,D} s_{12}^{K,D}} \begin{bmatrix} 0 & s_{12}^{G,D} + s_{12}^{K,D} |s^{G,D}| \\ s_{21}^{K,D} + s_{21}^{G,D} |s^{K,D}| & 0 \end{bmatrix} \begin{bmatrix} a_1 \\ b_1 \end{bmatrix} \\
&+ \frac{1}{1 - s_{21}^{G,D} s_{12}^{K,D}} \begin{bmatrix} 1 - s_{21}^{G,D} s_{12}^{K,D} & 0 \\ 0 & s_{22}^{K,D} \end{bmatrix} \begin{bmatrix} F_1^{G,D} \\ F_2^{G,D} \end{bmatrix} \\
=& \frac{1}{s + (s_{21}^{G,D} + 1)\frac{\gamma_D}{2}} \begin{bmatrix} 0 & s_{12}^{G,D}(s + \frac{\gamma_D}{2}) - \frac{\gamma_D}{2} \\ s_{21}^{G,D}(s + \frac{\gamma_D}{2}) - \frac{\gamma_D}{2} & 0 \end{bmatrix} \begin{bmatrix} a_1 \\ b_1 \end{bmatrix} \\
&+ \begin{bmatrix} 1 & 0 \\ 0 & \frac{s}{s + (s_{21}^{G,D} + 1)\gamma_D/2} \end{bmatrix} \begin{bmatrix} F_1^{G,D} \\ F_2^{G,D} \end{bmatrix}
\end{aligned} \tag{7.2}$$

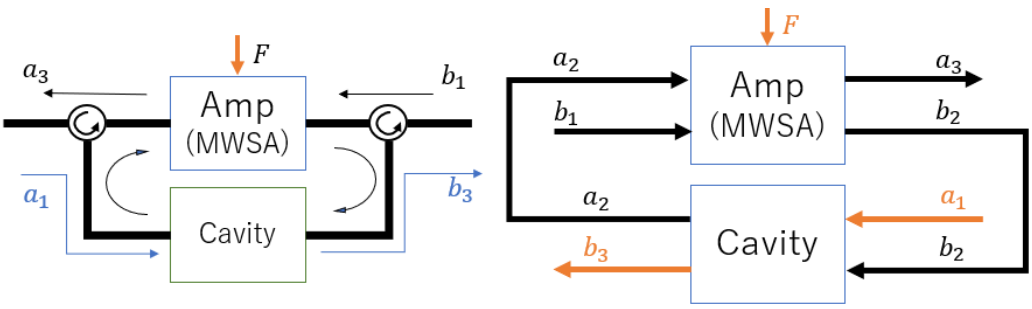

Figure 7.2: Coherent D controller in physical model (left) and in block diagram (right).

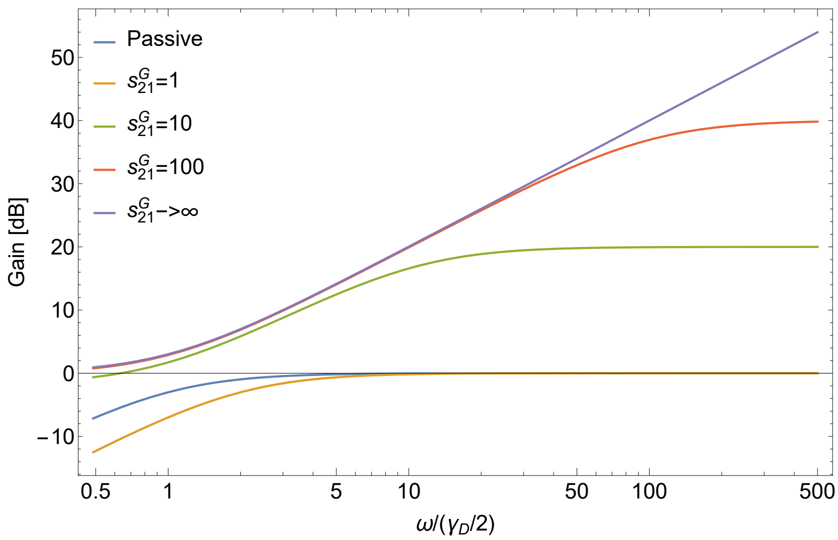

Figure 7.3: Gain plot of coherent passive and active D controller with different amplifier gains $s_{21}^{G} = 1,\ 10,\ 100,$ and ∞.

and in the ideal limit $s_{12}^{G,D} \to 0$ and $s_{21}^{G,D} \to \infty$

$$\begin{bmatrix} a_3 \\ b_3 \end{bmatrix} = \begin{bmatrix} 0 & 0 \\ \frac{s}{\gamma_D/2} + 1 & 0 \end{bmatrix} \begin{bmatrix} a_1 \\ b_1 \end{bmatrix} + \begin{bmatrix} 1 & 0 \\ 0 & -\frac{s}{s_{21}^{G}\gamma_D/2} \end{bmatrix} \begin{bmatrix} F_1^{G,D} \\ F_2^{G,D} \end{bmatrix}. \tag{7.3}$$

The superscript and subscript D stresses the elements are referring to the D controller. Thus we have a derivative control with an offset +1. The gain plot for different gains compared with a passive D controller is demonstrated in Fig. 7.3.

Some readers might be curious about its time domain representation. In the time domain, the transfer function for the input signal transforms to

$$\mathcal{L}^{-1}\left[\frac{s_{21}^{G,D}(s+\frac{\gamma_D}{2})-\frac{\gamma_D}{2}}{s+(s_{21}^{G,D}+1)\frac{\gamma_D}{2}}\right] = -\left({s_{21}^{G,D}}^2+1\right)\frac{\gamma_D}{2}e^{-\frac{\gamma_D}{2}(s_{21}^{G,D}+1)t} + s_{21}^{G,D}\delta(t), \tag{7.4}$$

which results in the high gain limit to

$$\mathcal{L}^{-1}\left[\frac{s_{21}^{G,D}(s+\frac{\gamma_D}{2})-\frac{\gamma_D}{2}}{s+(s_{21}^{G,D}+1)\frac{\gamma_D}{2}}\right] \to \frac{1}{\gamma_D/2}\frac{d}{dt}\delta(t)+\delta(t). \tag{7.5}$$

Let us consider the same transfer function with the signal, as well. In the rotating frame, the signal a_1 is just an operator $a_1(t) = \Theta(t)a_1$, which yields to $a_1[s] = a_1/s$ in s-domain. The inverse Laplace transformation of the 21 element of its transfer function multiplied with the signal is calculated as

$$\mathcal{L}^{-1}\left[\frac{s_{21}^{G,D}(s+\frac{\gamma_D}{2})-\frac{\gamma_D}{2}}{s+(s_{21}^{G,D}+1)\frac{\gamma_D}{2}}\frac{1}{s}\right] = \frac{s_{21}^{G,D^2}+1}{s_{21}^{G,D}+1}e^{-\frac{\gamma_D}{2}(s_{21}^{G,D}+1)t} + \frac{s_{21}^{G,D}-1}{s_{21}^{G,D}+1}, \qquad (7.6)$$

hence in the gain limit, we have

$$\begin{aligned}
&\frac{s_{21}^{G,D^2}+1}{s_{21}^{G,D}+1}e^{-\frac{\gamma_D}{2}(s_{21}^{G,D}+1)t} + \frac{s_{21}^{G,D}-1}{s_{21}^{G,D}+1} \\
&\to \frac{1}{\gamma_D/2}\delta(t) + 1 \\
&= \frac{1}{\gamma_D/2}\frac{d}{dt}\Theta(t) + 1 \\
&= \mathcal{L}^{-1}\left[\left(\frac{s}{\gamma_D/2}+1\right)\frac{1}{s}\right],
\end{aligned}$$

where we have used the fact $\delta(t) = \lim s_{21}\exp(-s_{21}t)$.
Analogously, the transfer function of idler in the time domain is described by

$$\mathcal{L}^{-1}\left[\frac{s}{s+(s_{21}^{G,D}+1)\frac{\gamma_D}{2}}\right] = -\frac{\gamma_D}{2}\left(s_{21}^{G,D}+1\right)e^{-\frac{\gamma_D}{2}(s_{21}^{G,D}+1)t} + \delta(t) \qquad (7.7)$$

$$\to \frac{1}{s_{21}^{G,D}\gamma_D/2}\dot{\delta}(t) + \delta(t), \qquad (7.8)$$

where we remind the readers that the idler $F_2^{G,D}$ is of $\mathcal{O}(s_{21}^{G,D})$ in the limit such that the coefficient $1/s_{21}^{G,D}$ in the first term is compensated.

Now, we have seen in the previous section 6 that the added noise effect can be hugely reduced to the sum of the added noise of the quantum amplifier and vacuum noise, if the feedback amplifier gain is high enough and the transmission lines are not that lossy. For example, for P controller small transmittance β of the beam splitter should be chosen, because its inverse gets very large. The question arises how we can obtain such huge gain in D controller or how can we reduce the added noise as much as possible. As in the case of the beam splitter, we now deal with the internal loss of the cavity

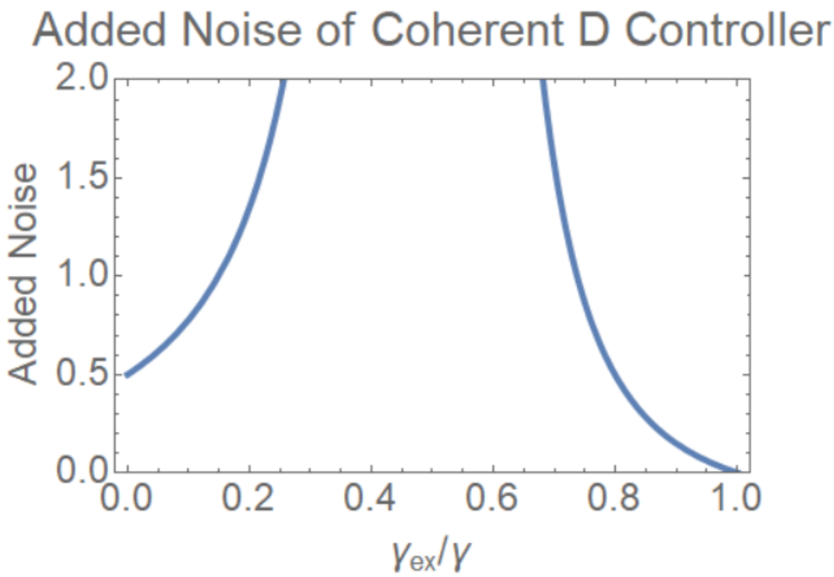

Figure 7.4: The added noise of coherent D controller as a function of external loss $\gamma_{D,ex}$.

and the transmission lines. The input-output relation of the cavity is then corrected

$$\begin{bmatrix} a_2 \\ b_3 \end{bmatrix} = \frac{1}{s - i\Delta + \gamma_D/2} \begin{bmatrix} s - i\Delta + \gamma_{D,0}/2 & -\gamma_{D,ex}/2 \\ -\gamma_{D,ex}/2 & s - i\Delta + \gamma_{D,0}/2 \end{bmatrix} \begin{bmatrix} a_1 \\ b_2 \end{bmatrix} + \frac{1}{s - i\Delta + \gamma_D/2} \begin{bmatrix} -\sqrt{\gamma_{D,0}\gamma_{D,ex}/2} \\ -\sqrt{\gamma_{D,0}\gamma_{D,ex}/2} \end{bmatrix} \xi_i, \tag{7.9}$$

where ξ_i represents the internal loss mode with $\left[\xi_i, \xi_i^\dagger\right] = 1$ and with internal decay rate $\gamma_{D,0}$. The total decay rate is the sum of internal and external decay rate, namely, $\gamma_D = \gamma_{D,0} + \gamma_{D,ex}$.

For the coherent D controller, we insert the Eq. (7.3) into Eq. (6.20a) and the added noise of the controller is then calculated as

$$
\begin{aligned}
\mathcal{A}_{2,D}^{(fb)} =& \frac{1}{2} - \frac{1}{2\left|s_{21}^{G,fb}\right|^2} + \left|\frac{s_{23}^{K,fb}}{s_{21}^{G,fb}}\right|^2 \\
=& \frac{1}{2} - \frac{1}{2}\left|\frac{-i\omega - i\Delta + \gamma_D/2 + s_{21}^{G}\gamma_{D,ex}/2}{-\gamma_{D,ex}/2 + s_{21}^{G}\left(-i\omega - i\Delta + (\gamma_{D,0} - \gamma_{D,ex})/2\right)}\right|^2 \\
&+ \left|\frac{s_{21}^{G}(-i\omega - i\Delta + \gamma_D/2) + (-i\omega - i\Delta + \gamma_D/2)}{-\gamma_{D,ex}/2 + s_{21}^{G}(-i\omega - i\Delta + (\gamma_{D,0} - \gamma_{D,ex})/2)}\right|^2 \frac{\gamma_{D,0}\gamma_{D,ex}/2}{|-i\omega - i\Delta + \gamma_D/2|^2}
\end{aligned} \tag{7.10a}
$$

$$
\to \frac{1}{2} - \frac{1}{2}\left|\frac{\gamma_{D,ex}/2}{-i\omega - i\Delta + \gamma_D/2}\right|^2 + \frac{\gamma_{D,0}\gamma_{D,ex}/2}{|-i\omega - i\Delta + \gamma_D/2|^2}, \tag{7.10b}
$$

or just insert into Eq. (6.20b) as a lower bound

$$
\begin{aligned}
\mathcal{A}_{2,D}^{(fb)} &= \frac{1}{2}\left|\frac{\gamma_{D,ex}/2}{-i\omega - i\Delta + \gamma_D/2}\right|^2 + \left|\frac{1}{\alpha_{D,2}}\frac{-i\omega - i\Delta + \gamma_{D,0}/2}{-i\omega - i\Delta + \gamma_D/2}\right|^2 \left|\frac{s_{24}^{G}}{s_{21}^{G}}\right|^2 - \frac{1}{2} \\
&\to \frac{1}{2}\left|\frac{\gamma_{D,ex}/2}{-i\omega - i\Delta + \gamma_D/2}\right|^2 + \frac{1}{2},
\end{aligned} \tag{7.11a}
$$

where $\alpha_{D,2}$ is the transmittance of the beam splitter modeled for its loss in the feedback path (a_2-$\tilde{a}_2$-path in Fig. 6.1), $\gamma_D = \gamma_{D,0} + \gamma_{D,ex}$ the total decay rate of the cavity composed of the internal loss decay rate $\gamma_{D,0}$ and external loss $\gamma_{D,ex}$. We have used the fact $\left|s_{24}^{G}\right| \to \left|s_{21}^{G}\right|$ in Eq. (7.11a). Additionally, the limit $\gamma_{D,ex} \ll \gamma_{D,0}$ has been taken, and thus $|\alpha_{D,2}| \approx |(-i\omega - i\Delta + \gamma_{D,0}/2)/(-i\omega - i\Delta + \gamma_D/2)|$ in Eq. (7.11a). That is, if the external loss is negligibly small such that it is even much smaller than the internal loss, the added noise effect can be reduced up to the vacuum noise in the ideal quantum amplifier limit. But this noise spectrum exactly has the form of a low pass filter (or band-pass filter). I.e., in order to suppress the noise contribution (that is low gain limit), we also have to design this filter as a good cavity $\gamma_D \ll \omega_{cav}$, since this limit makes the Lorentzian distribution sharp, and hence the bandwidth of the noise small. But this is simultaneously the demanded condition for a high gain D controller.
The reason why we have a high added noise in the center as shown in Fig. 7.4 can be explained by the last term of Eq. (7.9). The added noise has a peak at $\gamma_{D,0} = \gamma_{D,ex}$ and hence around the center.

7.3 Coherent I Controller

For the coherent I controller, we need to design a feedback structure as shown in Fig. 7.6. After a simple algebra calculation, we read for a general expression

$$\begin{aligned}\begin{bmatrix} a_3 \\ b_3 \end{bmatrix} =& \frac{1}{1+s_{21}^G s_{11}^K}\begin{bmatrix} -s_{11}^G s_{12}^K & -s_{12}^G + s_{11}^K|s^G| \\ s_{22}^K + s_{21}^G|s^K| & s_{22}^G s_{21}^K \end{bmatrix}\begin{bmatrix} a_1 \\ b_1 \end{bmatrix} \\ &+ \frac{1}{1+s_{21}^G s_{11}^K}\begin{bmatrix} -(1+s_{21}^G s_{11}^K) & s_{11}^G s_{11}^K \\ 0 & s_{21}^K \end{bmatrix}\begin{bmatrix} F_1^{G,I} \\ F_2^{G,I} \end{bmatrix}\end{aligned} \tag{7.12}$$

Therefore, we obtain in the perfect directionality limit

$$\begin{aligned}\begin{bmatrix} a_3 \\ b_3 \end{bmatrix} =& \frac{1}{s(s_{21}^{G,I}+1)+\frac{\gamma_I}{2}}\begin{bmatrix} 0 & s - s_{12}^{G,I}(s+\frac{\gamma_I}{2}) \\ s + s_{21}^{G,I}(s+\frac{\gamma_I}{2}) & 0 \end{bmatrix}\begin{bmatrix} a_1 \\ b_1 \end{bmatrix} \\ &+ \begin{bmatrix} -1 & 0 \\ 0 & \frac{-\gamma_I/2}{s(s_{21}^{G,I}+1)+\frac{\gamma_I}{2}} \end{bmatrix}\begin{bmatrix} F_1^{G,I} \\ F_2^{G,I} \end{bmatrix}\end{aligned} \tag{7.13}$$

and in the ideal case

$$\begin{bmatrix} a_3 \\ b_3 \end{bmatrix} = \begin{bmatrix} 0 & 0 \\ \frac{\gamma_I/2}{s}+1 & 0 \end{bmatrix}\begin{bmatrix} a_1 \\ b_1 \end{bmatrix} + \begin{bmatrix} 1 & 0 \\ 0 & -\frac{\gamma_I/2}{s s_{21}^G} \end{bmatrix}\begin{bmatrix} F_1^{G,I} \\ F_2^{G,I} \end{bmatrix}. \tag{7.14}$$

Hence, we obtain an integral term with the offset +1. The gain plot for different gains compared with a passive D controller is demonstrated in Fig. 7.5.

Using the inverse Laplace transform, the time domain description of the I controller is given by

$$\mathcal{L}^{-1}\left[\frac{s+s_{21}^{G,I}(s+\frac{\gamma_I}{2})}{s(s_{21}^{G,I}+1)+\frac{\gamma_I}{2}}\right] = \frac{\gamma_I}{2}\frac{s_{21}^{G,I}-1}{s_{21}^{G,I}+1}e^{-\frac{\gamma_I}{2}\frac{t}{s_{21}^{G,I}+1}} + \delta(t) \tag{7.15a}$$

$$\rightarrow \frac{\gamma_I}{2} + \delta(t), \tag{7.15b}$$

where the last limit gives the result in the high gain limit. Hence, we see the first term works as an integrator due to

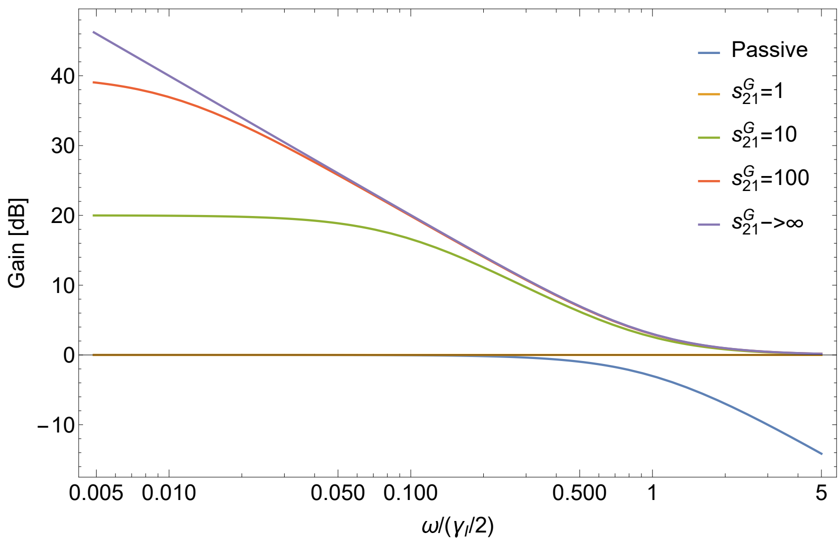

Figure 7.5: Gain plot of coherent passive and active I controller with different amplifier gains $s_{21}^G = 1,\ 10,\ 100,$ and ∞.

$$\mathcal{L}^{-1}\left[\frac{s + s_{21}^{G,I}(s + \frac{\gamma_I}{2})}{s(s_{21}^{G,I} + 1) + \frac{\gamma_I}{2}} a_1[s]\right] \to \int_0^t dt' \left(\frac{\gamma_I}{2} + \delta(t - t')\right) a_1(t')$$
$$= \int_0^t dt' \frac{\gamma_I}{2} a_1(t') + a_1(t).$$

For example, in the rotating frame, we have a time-independent signal a_1 yielding to

$$\mathcal{L}^{-1}\left[\frac{s + s_{21}^{G,I}(s + \frac{\gamma_I}{2})}{s(s_{21}^{G,I} + 1) + \frac{\gamma_I}{2}} \frac{1}{s}\right] = s_{21}^{G,I}\left(1 - e^{-\frac{\gamma_I}{2}\frac{t}{s_{21}^{G,I}+1}}\right) + e^{-\frac{\gamma_I}{2}\frac{t}{s_{21}^{G,I}+1}} \tag{7.16}$$

thus in the gain limit, we have

$$\begin{aligned}
& s_{21}^{G,I}\left(1 - e^{-\frac{\gamma_I}{2}\frac{t}{s_{21}^{G,I}+1}}\right) + e^{-\frac{\gamma_I}{2}\frac{t}{s_{21}^{G,I}+1}} \\
& \to \frac{\gamma_I}{2} t + 1 \\
& = \frac{\gamma_I}{2}\int d\tau \Theta(t - \tau) + 1 \\
& = \mathcal{L}^{-1}\left[\left(\frac{\gamma_I}{2}\frac{1}{s} + 1\right)\frac{1}{s}\right],
\end{aligned} \tag{7.17}$$

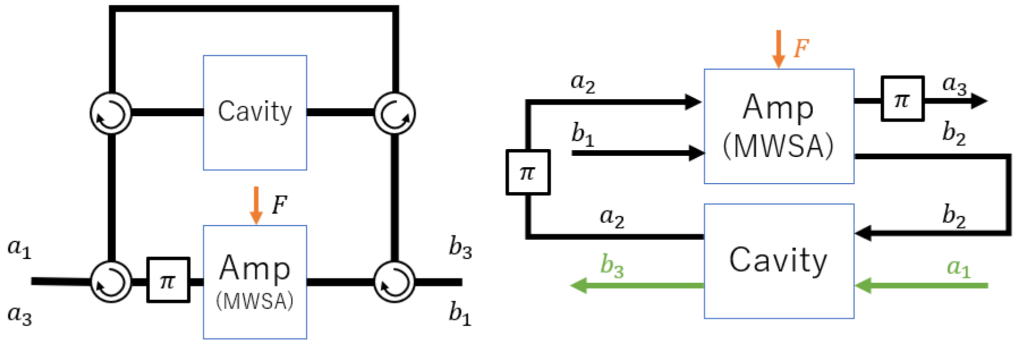

Figure 7.6: Coherent I controller in physical model (left) and in block diagram (right). The π shift is needed for the stability.

as expected.
In the idler case, its time domain is represented by

$$\mathcal{L}^{-1}\left[\frac{-\gamma_I/2}{s(s_{21}^{G,I}+1)+\frac{\gamma_I}{2}}\right] = -\frac{\gamma_I}{2}\frac{1}{s_{21}^{G,I}+1}e^{-\frac{\gamma_I}{2}\frac{t}{s_{21}^{G,I}+1}} \tag{7.18}$$

$$\rightarrow -\frac{\gamma_I}{2}\frac{1}{s_{21}^{G,I}}. \tag{7.19}$$

Analogously to the D controller, we can calculate the added noise of the coherent integral controller with Eq. (6.11), but with the following matrix elements $s_{ij}^{G}(i,j=1,2)$

$$s_{11}^{G} \rightarrow s_{11}^{G,fb} = \frac{\alpha_2 s_{11}^{G} s_{12}^{K}}{1+\alpha_1\alpha_2 s_{21}^{G} s_{11}^{K}}, \quad s_{12}^{G} \rightarrow s_{12}^{G,fb} = \frac{-s_{12}^{G}+\alpha_1\alpha_2 s_{11}^{K}|s^{G}|}{1+\alpha_1\alpha_2 s_{21}^{G} s_{11}^{K}},$$
$$s_{21}^{G} \rightarrow s_{21}^{G,fb} = \frac{s_{22}^{K}+\alpha_1\alpha_2 s_{21}^{G}|s^{K}|}{1+\alpha_1\alpha_2 s_{21}^{G} s_{11}^{K}}, \quad s_{22}^{G} \rightarrow s_{22}^{G,fb} = \frac{\alpha_1 s_{22}^{G} s_{21}^{K}}{1+\alpha_1\alpha_2 s_{21}^{G} s_{11}^{K}}. \tag{7.20}$$

Hence, the added noise in the ideal limit is given by

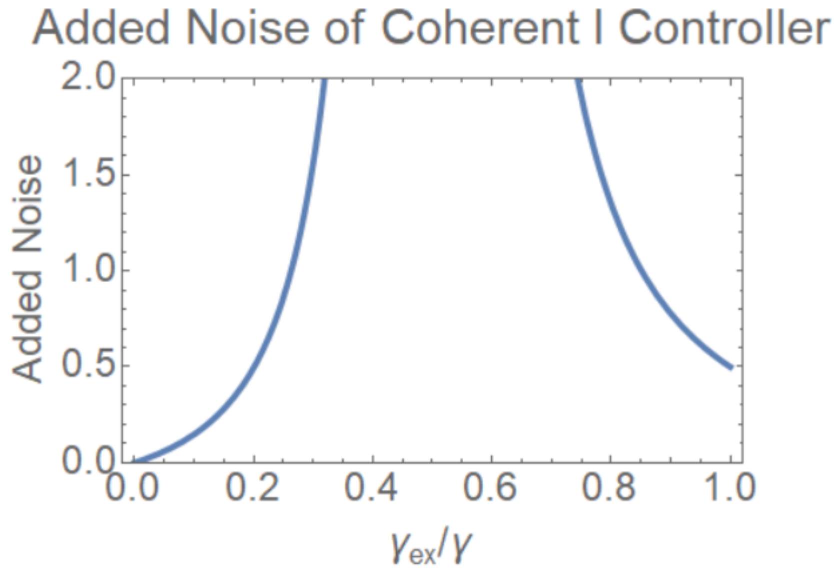

Figure 7.7: The added noise of coherent I controller as a function of external loss $\gamma_{I,ex}$.

$$\mathcal{A}_{2,I}^{(fb)} = \frac{1}{2} - \frac{1}{2\left|s_{21}^{G,fb}\right|^2} + \left|\frac{-s_{21}^K s_{13}^K s_{21}^G/(1+s_{11}^K s_{21}^G) + s_{23}^K}{s_{21}^{G,fb}}\right|^2 \tag{7.21a}$$

$$= \frac{1}{2} - \frac{1}{2}\left|\frac{-i\omega - i\Delta + \gamma_I + s_{21}^G(-i\omega - i\Delta + \gamma_{I,0}/2)}{-i\omega - i\Delta + \gamma_{I,0}/2 + s_{21}^G(-i\omega - i\Delta + (\gamma_{I,0} - \gamma_{I,ex})/2)}\right|^2 + \left|\frac{(s_{21}^G + 1)(-i\omega - i\Delta + \gamma_I/2)}{-i\omega - i\Delta + \gamma_{I,0}/2 + s_{21}^G(-i\omega - i\Delta + (\gamma_{I,0} - \gamma_{I,ex})/2)}\right|^2 \frac{\gamma_{I,0}\gamma_{I,ex}/2}{|-i\omega - i\Delta + \gamma_I/2|^2} \tag{7.21b}$$

$$\to \frac{1}{2} - \frac{1}{2}\left|\frac{-i\omega - i\Delta + \gamma_{I,0}/2}{-i\omega - i\Delta - \gamma_I}\right|^2 + \frac{\gamma_{I,0}\gamma_{I,ex}/2}{|-i\omega - i\Delta - \gamma_I/2|^2}, \tag{7.21c}$$

where the limit is the other way round of the derivative controller, namely, $\gamma_{I,0} \ll \gamma_{I,ex}$. In the low frequency limit $|\omega + \Delta| \ll \gamma_{I,0}$, even vacuum noise can be achieved. Thus, the noise spectrum of the I controller is, in this case, a high-pass filter (or a band rejection). I.e., we have to aim for a bad cavity limit, to reject the noise through a broad region, which is again a high gain I controller condition.
The reason for a high added noise in the center as demonstrated in Fig. 7.7 is the same as in the coherent D controller case.

8 Coherent PID Feedback Control

In experiments preparing a stable steady-state is one of difficult practical tasks. Indeed, experimentalists and theorists suggest a measurement-based feedback using system-based quantum filtering theory[11, 31, 32, 33, 34] and a classical PID control[35, 36, 37, 38, 39]. But its critical drawbacks are the significant signal loss and time delays due to the use of classical components such as detectors, signal processors, and actuators. In the coherent case, there is a systematic coherent feedback control strategy for achieving steady-state, but this requires engineering a certain Hamiltonian and perfect knowledge about the system itself which cannot be always fulfilled[40, 41, 42]. In contrast to these feedback strategies, a coherent PID (CPID) feedback control system uses only three controllers, namely P, I, and D controller, let the state automatically converge to the reference signal *without any need of detailed information about the system* and works on a coherent level.

In this thesis, we suggest the CPID feedback control system method with some concrete examples and primarily focus on the covariance (matrix) of system variable x, because in contrast to the classical PID controller the output of CPID controller contains idlers/added noises due to CCR restrictions, which have to be considered. In this thesis, the state variables are either annihilation/creation operators or its quadrature variables. Hence its covariance matrix is naturally related to particle numbers or just system energy.
We start this section with the basic idea of constructing the CPID feedback control system by combining the essential elements of classical PID feedback control system with the quantum elements, namely, the quantum detectors and converters.
In order to get familiar with this new feedback system, it is instructive, to begin with a coherent P (CP) feedback control, so just with a P controller. In the next subsection, the coherent PI (CPI) feedback control is introduced, and its associated problem. Furthermore, we study the coherent PD (CPD) feedback control with an application to cooling an optomechanical system with the so-called cold-damping method. Finally, the CPID feedback control will be shortly studied.

8.1 Basic Coherent PID Feedback Control System

As mentioned previously, for the construction of the coherent feedback system we look at the key elements of its quantum counterpart. With this observation, we then replace all classical parts with quantum ones.
As shown in Fig. 3.1, the fundamental points we have to implement are: error signal, PID controller, plant (system), and the feedback of system output.

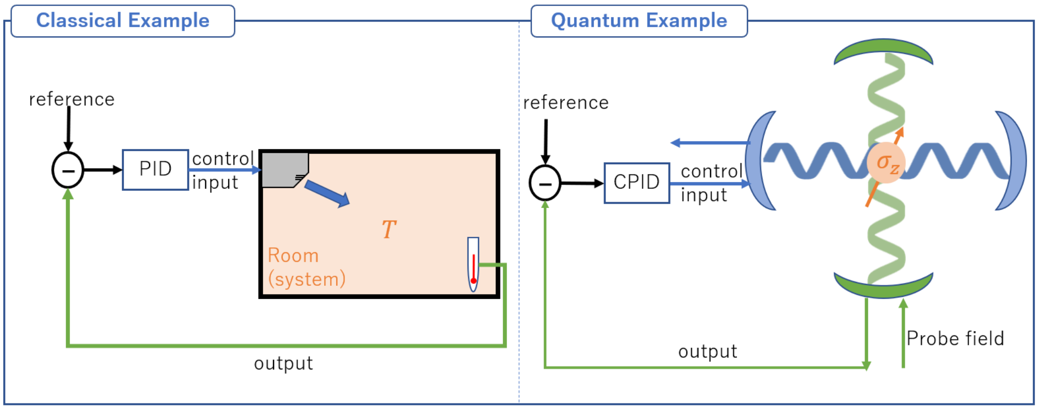

Figure 8.1: Image and example of conversion-system-detection concept in classical and quantum (coherent) PID feedback control system. (Classical) The temperature T (system state/variable) is electronically measured (detection) and modified via PID controller. This electronic control input is then converted to corresponding temperature control input (conversion). (Quantum) The spin state σ_z is transformed from a standing wave into a traveling wave and is "detected" (but no measurement). This traveling output is modified by a coherent PID controller to a traveling control input and converted again into a corresponding standing wave to regulate the spin state.

But if we think of a temperature regulator for example, where the system variable is temperature, but the output or the control is done electrically, there has to be also a measurement device and a converter (see Fig. 8.1).

Since we have recognized the key elements, we change our focus to the quantum world. The error signal is realized by a half mirror, which let the reference signal and output destructively interfere. As we have already CPID controller and a quantum system, we need to figure out the classical counterpart of a measurement device and a converter. Here, we make use of the idea written in the paper[16]. For example, the system-coupled cavity with the Hamiltonian $\mathcal{H}_{plant} = \mathcal{H}_{sys} + \hbar\omega_{cav} a^\dagger a(1 + Az)$ is a quantum detector and a quantum transducer simultaneously, where a is the annihilation operator in cavity mode and z is some system operator, because for weak coupling $A \ll 1$ the reflection phase shift can be approximated by $\theta \approx 4\omega_{cav} Az/\kappa$. Henceforth, we can gain information about z from the phase shift θ. The whole procedure is thus the cavity transforms laser input into a cavity photon, which couples to the system, and transforms back to laser output working as a quantum detector. We exploit this basic idea, where the system output y is going out from the quantum detector and the control input u is converted

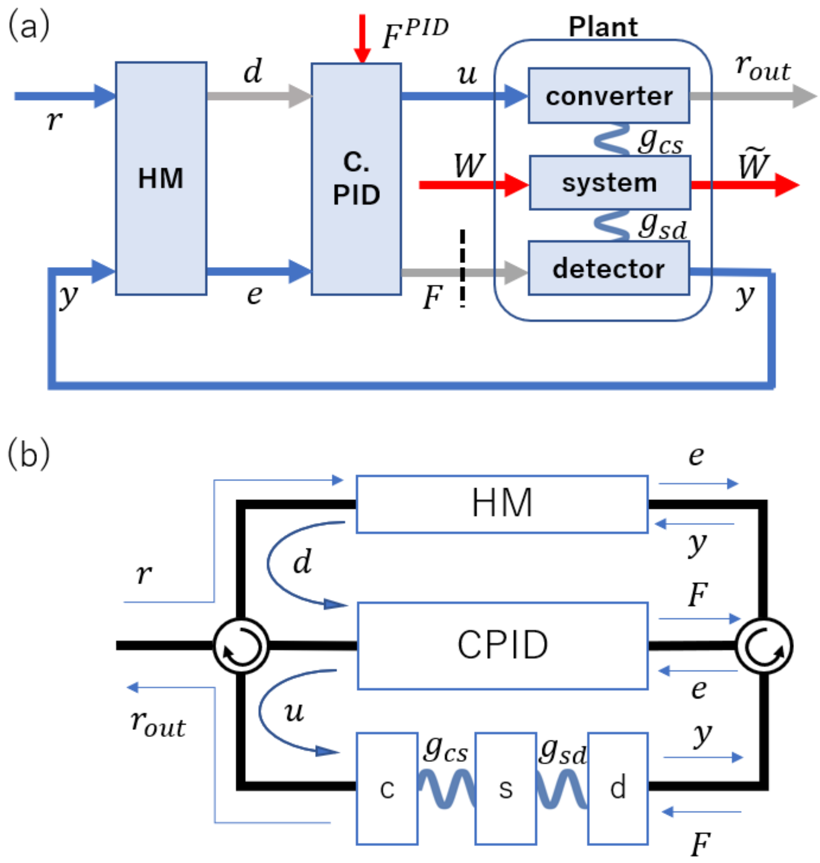

Figure 8.2: Basic coherent PID feedback control system (a) in a block diagram and (b) as a physical realization. The dashed line indicates this line can be cut if necessary.

to a system variable x in an appropriate Hilbert space. Finally, we end up with the following basic CPID feedback control system depicted in Fig. 8.2. Indeed, these concepts also appear in the measurement-based feedback control such as [38, 37, 35, 31].
The Hamiltonian of the plant is thus generally expressed by

$$\mathcal{H}_{plant} = \mathcal{H}_{conv} + \mathcal{H}_{c-s} + \mathcal{H}_{sys} + \mathcal{H}_{s-d} + \mathcal{H}_{det} \tag{8.1}$$

$$= \mathcal{H}_{conv} + \hbar g_{cs}(c^\dagger s + cs^\dagger) + \mathcal{H}_{sys} + \hbar g_{sd}(d^\dagger s + ds^\dagger) + \mathcal{H}_{det}, \tag{8.2}$$

where $\mathcal{H}_{conv,sys,det}$ are bare Hamiltonians of the converter, system, and detector, respectively. The interaction Hamiltonian $\mathcal{H}_{c-s}$ describes the interaction between the converters and system and $\mathcal{H}_{s-d}$ that between the system and detector. If these interactions can be modeled as a beam-splitter like Hamiltonian, then they are coupled with strength g_{cs} between the converter and system and with g_{sd} between the system and detector, respectively, where c, s, and d are annihilation operators involved in these interactions. If we can write the Hamiltonians as

$$\mathcal{H}_{conv} = \hbar\omega_c c^\dagger c \tag{8.3}$$

$$\mathcal{H}_{sys} = \hbar\omega_s s^\dagger s \tag{8.4}$$

$$\mathcal{H}_{det} = \hbar\omega_d d^\dagger d, \tag{8.5}$$

then the quantum Langevin equation is given by

$$\frac{d}{dt}\begin{bmatrix} c \\ s \\ d \end{bmatrix} = \begin{bmatrix} -i\omega_c - \frac{\kappa_c}{2} & -ig_{cs} & 0 \\ -ig_{cs} & -i\omega_s - \frac{\kappa_s}{2} & -ig_{sd} \\ 0 & -ig_{sd} & -i\omega_d - \frac{\kappa_d}{2} \end{bmatrix} \begin{bmatrix} c \\ s \\ d \end{bmatrix} - \begin{bmatrix} \sqrt{\kappa_c} & 0 & 0 \\ 0 & \sqrt{\kappa_s} & 0 \\ 0 & 0 & \sqrt{\kappa_d} \end{bmatrix} \begin{bmatrix} u \\ W \\ F \end{bmatrix} \tag{8.6}$$

and its input-output relation

$$\begin{bmatrix} r_{out} \\ \tilde{W} \\ y \end{bmatrix} = \begin{bmatrix} \sqrt{\kappa_c} & 0 & 0 \\ 0 & \sqrt{\kappa_s} & 0 \\ 0 & 0 & \sqrt{\kappa_d} \end{bmatrix} \begin{bmatrix} c \\ s \\ d \end{bmatrix} + \begin{bmatrix} u \\ W \\ F \end{bmatrix}. \tag{8.7}$$

with

$$u(t) = K_P e(t) + K_I \int_0^t e(t) + K_D \frac{d}{dt} e(t) + F^{PID}. \tag{8.8}$$

Details about the control input u will be discussed in each following sections. Thus, we have the same structure as the classical state space representation with some additional "noises", namely,

$$\frac{d}{dt} x = Ax + Bu + B_{add}\xi \tag{8.9a}$$

$$y = Cx + D\xi, \tag{8.9b}$$

where

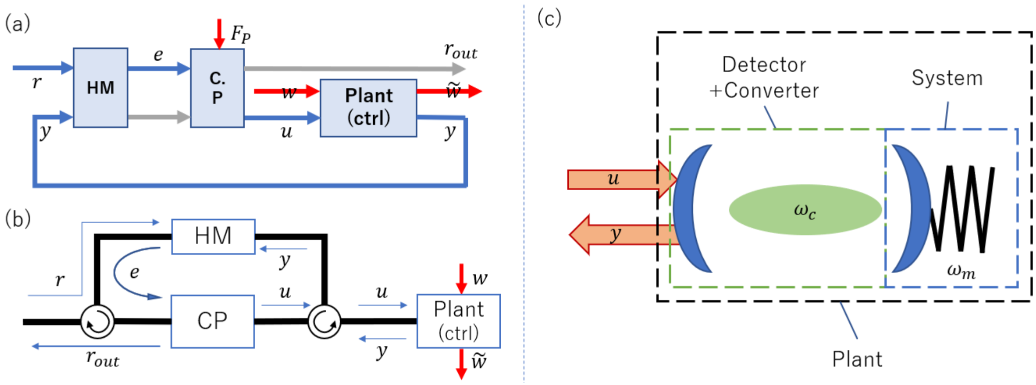

Figure 8.3: Coherent P feedback control system (a) in block diagram and (b) as a physical model. The coherent P controller is denoted by "C.P". For $|K_P| > 1$, we use the model depicted in Fig. 8.4 and the idler is added, while for $|K_P| < 1$ we just set a mirror. (c) The sideband-cooled optomechanical system as a concrete example for the special case, where the cavity acts as a detector and converter simultaneously.

$$B = \begin{bmatrix} -\sqrt{\kappa_c} \\ 0 \\ 0 \end{bmatrix}, \qquad B_{add} = \begin{bmatrix} 0 & 0 \\ -\sqrt{\kappa_s} & 0 \\ 0 & -\sqrt{\kappa_d} \end{bmatrix},$$

$$C = \begin{bmatrix} 0 & 0 & 1 \end{bmatrix}, \qquad D = \begin{bmatrix} 0 & 1 \end{bmatrix}, \qquad \xi = \begin{bmatrix} w \\ F \end{bmatrix}.$$

If we interpret the noises F^{PID} and $B_{add}\xi$ as the system supply disturbance and $D\xi$ as the system load disturbance in the language of PID control theory, we have shown in section 3 the output y indeed converges to the reference signal r.

8.2 Coherent P Feedback Control

In this subsection, we present the coherent P feedback control with a focus on the steady-state covariance matrix of system operator x. As a concrete example, we will prove the cooling performance is better than the no-feedback sideband-cooling method for optomechanical system.

8.2.1 State Space Representation

The state-space representation of the P controlled feedback system (see Fig. 8.3) is presented. This model is a *special case* of the feedback system suggested in Fig. 8.2, where the converter, system and the quantum detector are all in one. Since the input-output relation of the controller is different for the P parameter $|K_P| > 1$ and $|K_P| < 1$, we have to consider both cases: In $|K_P| > 1$ case, we are using the feedback amplified P controller introduced in section 6, while in $|K_P| < 1$ case we choose a mirror/beam-splitter as a P controller.

$|K_P| > 1$ case

The input-output relation of the coherent P controller for $|K_P| > 1$ is read (cf. Eq. (6.3))

$$\begin{bmatrix} r_{out} \\ u \end{bmatrix} = \begin{bmatrix} 0 & 0 \\ K_P & 0 \end{bmatrix} \begin{bmatrix} e \\ d \end{bmatrix} + \begin{bmatrix} 1 & 0 \\ 0 & \sqrt{K_P^2 - 1} \end{bmatrix} \begin{bmatrix} F_1^{G,P} \\ d^{P\dagger} \end{bmatrix}$$

with $K_P = 1/\beta$ in the ideal limit, if the scattering matrix of the feedback controller is

$$\begin{bmatrix} \alpha & -\beta \\ \beta & \alpha \end{bmatrix}.$$

The state-space representation for $|K_P| > 1$ is then

$$\dot{x} = \left(A - \frac{K_P}{\sqrt{2} - K_P} BB^T \right) x - \frac{K_P}{\sqrt{2} - K_P} Br + \frac{\sqrt{2}}{\sqrt{2} - K_P} BF_P + B_w w \tag{8.10}$$

$$y = - \frac{\sqrt{2}}{\sqrt{2} - K_P} B^T x - \frac{K_P}{\sqrt{2} - K_P} r + \frac{\sqrt{2}}{\sqrt{2} - K_P} F_P, \tag{8.11}$$

where $F_P = \sqrt{K_P^2 - 1} d^{P\dagger}$ is the idler of *P controller.*

$|K_P| < 1$ case

In $|K_P| < 1$ case, we have

$$\begin{bmatrix} r_{out} \\ u \end{bmatrix} = \begin{bmatrix} \alpha & -\beta \\ \beta & \alpha \end{bmatrix} \begin{bmatrix} e \\ d \end{bmatrix}$$

The state-space representation for $|K_P| < 1$ is

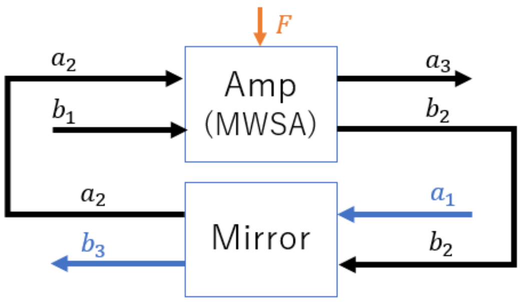

Figure 8.4: Coherent P controller for $|K_P| > 1$.

$$\dot{x} = \left(A - \frac{K_P}{\sqrt{2} - K_P} BB^T \right) x - \frac{\sqrt{2 - K_P^2}}{\sqrt{2} - K_P} Br + \frac{\sqrt{2}}{\sqrt{2} - K_P} BF_P + B_w w \tag{8.12}$$

$$y = - \frac{\sqrt{2}}{\sqrt{2} - K_P} B^T x - \frac{\sqrt{2 - K_P^2}}{\sqrt{2} - K_P} r + \frac{\sqrt{2}}{\sqrt{2} - K_P} F_P \tag{8.13}$$

with $K_P = \beta - \alpha$ and $F_P = \sqrt{1 - K_P^2} d^P$. It should be noted that for $K_P = 0$ we recover the original system with input $-r$.

As we can see, the only differences between them are the coefficient of the reference signal r is different and the operation of Hermitean conjugation in the idler. Thus, the system matrix A_P of the state space representation remains the same.
Now, we see we have a K_P dependent coefficient before every "input" matrix B. This seemingly by K_P modified input/decay rate is quite an interesting phenomenon since this coupling rate itself is just a naturally given value and therefore cannot be changed. The physical interpretation of this weird result is the following: The essence is the modification of the signal amplitude resulting in an effective modified decay rate. We start with the output of the plant $y = -B^T x + u$. After going through the half-mirror, the error signal e is changed by the coherent P controller, which gives

$$u = -B^T \frac{K_P}{\sqrt{2} - K_P} x - \frac{K_P}{\sqrt{2} - K_P} r + noise.$$

Here, the important point is the controller let the *signal*, x, interfere, but has not changed $-B^T$. This control input then goes into the plant, which results to add the x term in the Langevin Eq.. As it will be shown in Eq. (8.17) as an example, the decay term in the system matrix A_P can give

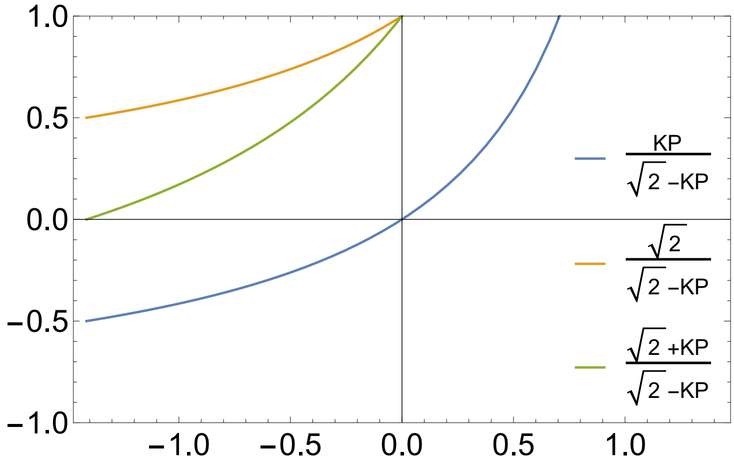

Figure 8.5: All coefficients depending on K_P.

$$\frac{1}{2}\kappa\left(\frac{\sqrt{2}+K_P}{\sqrt{2}-K_P}a\right)=\frac{1}{2}\left(\kappa\frac{\sqrt{2}+K_P}{\sqrt{2}-K_P}\right)a.$$

The above equation shows two ways of interpretation. First of all, in the SLH description the decay operator is written $\sqrt{\kappa}a$ and hence $-\kappa a/2$ in the system matrix A, which can be interpreted as *this decay rate is reserved for* ***one*** *amplitude quantum*. Now, the left-hand side expresses the modified photon amplitude. For example, in the stable case explained later, where the coefficient is below 1, the amplitude is reduced. That is, it takes more time to let an amplitude quantum decay. The right-hand side, on the other hand, says this delay can be modeled by the reduced decay rate for ***one*** *quantum*. We can easily prove the stability region ranges $K_P \in \left(-\sqrt{2}\,,0\right]$. This can be physically explained by input and decay rate. We observe the coefficient of input rate of r in the Langevin equation is $\sqrt{2}/(\sqrt{2}-K_P)$ for $|K_P|>1$ and $\sqrt{2-K_P^2}/(\sqrt{2}-K_P)$ for $|K_P|<1$, while the decay rate in the input-output relation is $\sqrt{2}/(\sqrt{2}-K_P)$. As plotted in Fig. 8.5, the effective decay rate is equal or larger than the effective input rate for $K_P \in \left(-\sqrt{2}\,,0\right]$. So it does not produce more internal state than it decays, which means stability. For $K_P>0$ this relation changes and causes instability.

8.2.2 Steady-State Covariance Matrix of state x

For the calculation of the steady-state covariance matrix $P_x := \left\langle xx^\dagger\right\rangle_{ss}$, we use the Lyapunov equation

$$AP_x + P_xA^\dagger + Q = 0, \tag{8.14}$$

where A is the system matrix and Q is the dissipation matrix with

$$Q = BR_w B^T. \tag{8.15}$$

Here, $R_w = \left\langle \mathrm{diag}(uu^\dagger, \xi\xi^\dagger) \right\rangle_{ss}$ is the covariance matrix of signal inputs u and noise inputs ξ. Generally speaking, the physical meaning of P_x and Q are the generalized total energy and the generalized dissipation, respectively. In the linear quantum system case, P_x contains information about the number of (quasi-)particles and correlations between them and Q about its dissipation energy. The steady-state covariance matrix can be directly calculated by

$$P_x = \int_0^\infty dt e^{A^\dagger t} Q e^{At}. \tag{8.16}$$

Now let us start with the study of steady-state covariance matrix through a concrete example: the optomechanical system. The idea behind this choice is the following: It is known in (no-feedback) sideband-cooling method there exists an optimal optical decay rate κ as a function of mechanical frequency ω_m ($\kappa/\omega_m = 1/\sqrt{32}$ in [43] and $\kappa/\omega_m \approx 0.2$ in [39]). Now, looking at the quantum Langevin equations (8.10) and (8.12) we notice the "decay matrix" B is associated with the parameter K_P. That is, we can freely choose and control the value of the decay rate. Therefore, thanks to this feedback we can have an optimal effective decay rate. But because its dependence on parameter K_P is everywhere not the same, a careful analytical calculation will be performed in the following.

We deal this problem within the rotating-wave approximation, i.e., as a beam-splitter-like Hamiltonian or as a passive system, to be able to calculate analytically, which system matrix gives

$$A_P = \begin{bmatrix} -i\omega_m - \frac{\gamma_m}{2} & ig^* \\ ig & i\Delta - \frac{1}{2}\frac{\sqrt{2}+K_P}{\sqrt{2}-K_P}\kappa \end{bmatrix}, \tag{8.17}$$

where ω_m is the mechanical eigenfrequency, γ_m its coupling strength with the heat bath, $\Delta = -\omega_m$ the detuning of the cavity, g the coupling strength between them, and κ is the external coupling of the cavity. The modified dissipation matrix Q_P is expressed as

$$
\begin{aligned}
Q_P =& B_P R_w B_P^T \\
=& \left(\frac{K_P^2}{(\sqrt{2}-K_P)^2} \Theta(|K_P|-1) + \frac{2-K_P^2}{(\sqrt{2}-K_P)^2} \Theta(1-|K_P|) \right) BB^T + B_w \left\langle ww^\dagger \right\rangle B_w^T \\
=& \begin{bmatrix} \gamma_m \coth\left(\frac{\hbar\omega_m}{2k_BT}\right) & 0 \\ 0 & \frac{K_P^2}{(\sqrt{2}-K_P)^2}\kappa\Theta(|K_P|-1) + \frac{4-3K_P^2}{(\sqrt{2}-K_P)^2}\kappa\Theta(1-|K_P|) \end{bmatrix}, \qquad (8.18) \\
=:& \mathrm{diag}\left(q_1, q_{21}\right) \qquad (8.19)
\end{aligned}
$$

where due to $\left\langle F_P F_P^\dagger \right\rangle = (K_P^2 - 1)\left\langle d^{P\dagger} d^P \right\rangle = 0$ and

$$
R_w = \begin{cases} \left\langle \mathrm{diag}\left(rr^\dagger, F_P F_P^\dagger, ww^\dagger\right) \right\rangle_{ss} = \mathrm{diag}\left(1, 0, \coth\left(\frac{\hbar\omega_m}{2k_BT}\right)\right), & |K_P| > 1 \\ \left\langle \mathrm{diag}\left(rr^\dagger, ww^\dagger\right) \right\rangle_{ss} = \mathrm{diag}\left(1, \coth\left(\frac{\hbar\omega_m}{2k_BT}\right)\right), & |K_P| < 1. \end{cases}
$$

To be able to consider the idler effect, we have to take attention into the Hermitean conjugate of the system, as well, namely, $A_P^\dagger$ and $Q_P^\dagger$ yielding to

$$
\begin{aligned}
Q_P^\dagger =& B_P R_w^\dagger B_P^T \\
=& \left(\frac{2K_P^2 - 2}{(\sqrt{2}-K_P)^2} \Theta(|K_P|-1) \right) BB^T \\
=& \begin{bmatrix} 0 & 0 \\ 0 & \frac{2K_P^2-2}{(\sqrt{2}-K_P)^2}\Theta(|K_P|-1)\kappa \end{bmatrix}, \qquad (8.20) \\
=:& \mathrm{diag}\left(0, q_{22}\right) \qquad (8.21)
\end{aligned}
$$

where

$$
R_w^\dagger = \begin{cases} \left\langle \mathrm{diag}\left(r^\dagger r, F_P^\dagger F_P, w^\dagger w\right) \right\rangle_{ss} = \mathrm{diag}\left(0, K_P^2 - 1, 0\right), & |K_P| > 1 \\ \left\langle \mathrm{diag}\left(r^\dagger r, w^\dagger w\right) \right\rangle_{ss} = \mathrm{diag}\left(0, 0\right), & |K_P| < 1. \end{cases}
$$

Since

$$
P_x = \begin{bmatrix} n_{Phonon,ss}+1 & \left\langle ba^\dagger \right\rangle_{ss} & 0 & 0 \\ \left\langle ab^\dagger \right\rangle_{ss} & n_{Photon,ss}+1 & 0 & 0 \\ 0 & 0 & n_{Phonon,ss} & \left\langle b^\dagger a \right\rangle_{ss} \\ 0 & 0 & \left\langle a^\dagger b \right\rangle_{ss} & n_{Photon,ss} \end{bmatrix}, \qquad (8.22)
$$

where $n_{Phonon,ss}$ and $n_{Photon,ss}$ are steady-state number, and a and b annihilation operator of phonons and photons, respectively, we obtain

$$\begin{aligned}
2n_{Phonon,ss}+1 =& \frac{q_1}{||V||^2}\left(\frac{-|v_-|^2}{\lambda_+ + \lambda_+^*} + \mathrm{Re}\left[\frac{2}{\lambda_+ + \lambda_-^*}\right] + \frac{-|v_+|^2}{\lambda_- + \lambda_-^*}\right)\\
&+ \frac{q_2}{||V||^2}\left(\frac{-1}{\lambda_+ + \lambda_+^*} + \mathrm{Re}\left[\frac{2}{\lambda_+ + \lambda_-^*}\right] + \frac{-1}{\lambda_- + \lambda_-^*}\right) \quad (8.23)\\
2n_{Photon,ss}+1 =& \frac{q_2}{||V||^2}\left(\frac{-|v_-|^2}{\lambda_+ + \lambda_+^*} + \mathrm{Re}\left[\frac{2}{\lambda_+ + \lambda_-^*}\right] + \frac{-|v_+|^2}{\lambda_- + \lambda_-^*}\right)\\
&+ \frac{q_1}{||V||^2}\left(\frac{-1}{\lambda_+ + \lambda_+^*} + \mathrm{Re}\left[\frac{2}{\lambda_+ + \lambda_-^*}\right] + \frac{-1}{\lambda_- + \lambda_-^*}\right), \quad (8.24)
\end{aligned}$$

where

$$\begin{aligned}
\lambda_\pm =& -\frac{1}{2}\left(2i\omega_m + \frac{\gamma_m}{2} + \frac{1}{2}\frac{\sqrt{2}+K_P}{\sqrt{2}-K_P}\kappa\right) \pm \sqrt{\left(\frac{\gamma_m}{4} - \frac{1}{4}\frac{\sqrt{2}+K_P}{\sqrt{2}-K_P}\kappa\right)^2 - |g|^2}\\
v_\pm =& \frac{1}{ig^*}\left(\frac{\gamma_m}{4} - \frac{1}{4}\frac{\sqrt{2}+K_P}{\sqrt{2}-K_P}\kappa \pm \sqrt{\left(\frac{\gamma_m}{4} - \frac{1}{4}\frac{\sqrt{2}+K_P}{\sqrt{2}-K_P}\kappa\right)^2 - |g|^2}\right)\\
|V| =& v_- - v_+, \qquad q_2 = q_{21} + q_{22}.
\end{aligned}$$

8.2.3 Quantum Limit of Steady State Covariance Matrix

It is interesting to consider the lower bound of $\mathrm{tr}(P_x)$, since this corresponds to the lower bound of the total number of (quasi-)particles because any physical observables can be expressed by annihilation and creation operators. If we have the Lyapunov equation (8.14), then the trace bound can be calculated by[45, 46]

$$\mathrm{tr}(P_x) \geq -\frac{\mathrm{tr}(Q)}{\mathrm{tr}(A+A^\dagger)} = \frac{\mathrm{tr}(BR_wB^T)}{\mathrm{tr}(B^TB)}. \quad (8.25)$$

We can physically interpret this inequality that the total number of particles is lower bounded by the *averaged dissipated particle number*, because the numerator gives the total dissipation energy and the denominator the total dissipation energy in the ground state (zero-point fluctuation included). However, we have to be careful that this result is the average per particle (mode). Hence, for $T \to 0$ this lower bound does not show the real lower

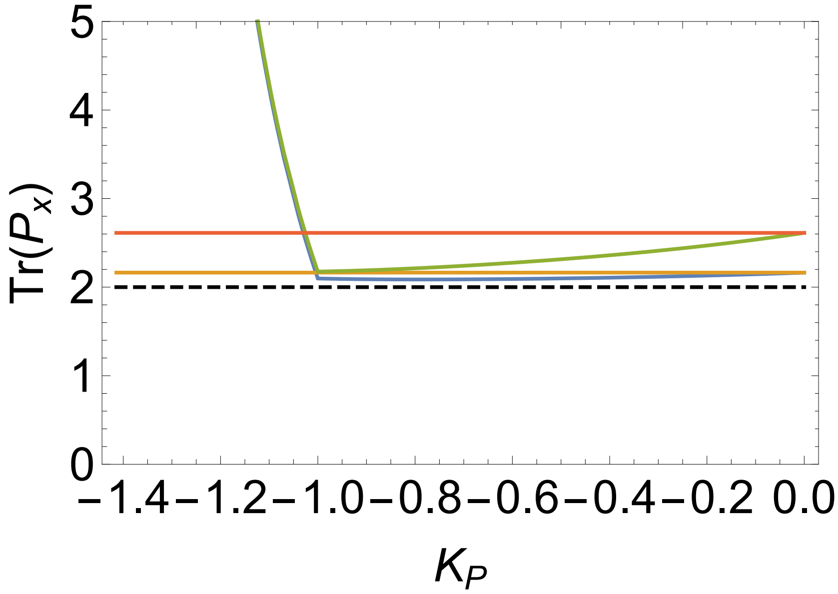

Figure 8.6: Trace of Steady State Covariance Matrix as a function of K_P at $T = 0.01$K. Total particle number with P-controlled system in rotating-wave approximation(blue) and without control (orange). Total particle number with P-controlled system without rotating-wave approximation (green) and without control (red). As expected, they are lower bounded by $\mathrm{tr}(P_x) \geq 2$ due to two particle modes: phonon and cavity photon. We have used for the simulation: $\omega_m = 2\pi \times 10.56$ MHz, $g_m = 2\pi \times 32$ Hz, $g = 2\pi \times 20$ kHz, and $\kappa = 2\pi \times 200$ kHz. Values adapted from [44].

bound. In the linear quantum system, the quantum limit is directly obtained from P_x itself by

$$\mathrm{tr}(P_x) = \sum_{k=1}^{m} \coth\left(\frac{\hbar\omega_k}{2k_B T_{eff,k}}\right) \geq m, \tag{8.26}$$

where m is the number of particle modes in the system, ω_k the eigenfrequency and $T_{eff,k}$ the effective temperature of k-th particle mode.

8.2.4 Which System is the Best?

Now, we want to study, which system can cool the phonon better: sideband-cooled, coherent P controlled system with $|K_P| > 1$ or with $|K_P| < 1$. It turns out the coherent P controller feedback system with $|K_P| < 1$ can perform the best cooling.

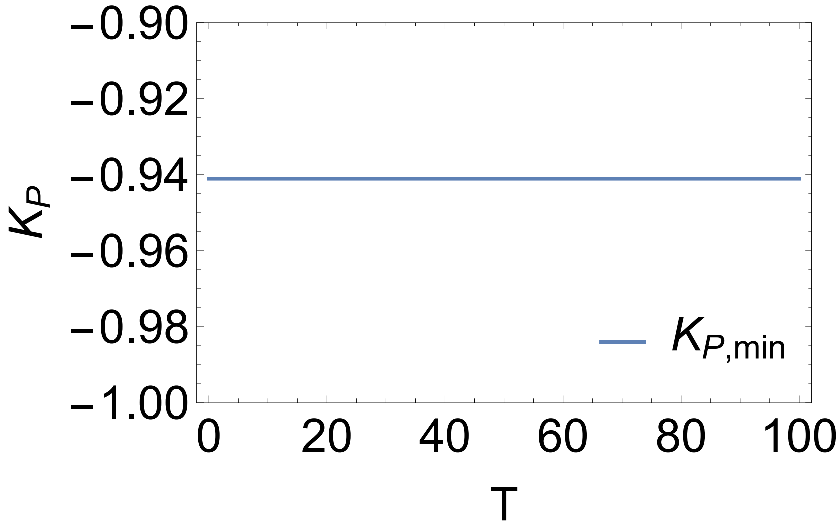

Figure 8.7: The best parameter $K_{P,<1}^{min}$ as a function of T. One can recognize the position of the minimum does not change. We have used for the simulation: $\omega_m = 2\pi \times 10.56$ MHz, $g_m = 2\pi \times 32$ Hz, $g = 2\pi \times 20$ kHz, $\kappa = 2\pi \times 200$ kHz, and $T = 4.4$ K. Values adapted from [44].

no P controlled vs. P controlled system

One can get the sideband-cooled steady state phonon number from Eq. (8.23) by putting $K_P = 0$

$$n_{Phonon,ss}(K_P=0) = \frac{\kappa}{\gamma_m+\kappa}\frac{4g^2}{4|g|^2+\gamma_m\kappa} + \frac{\gamma_m}{\gamma_m+\kappa}\frac{4|g|^2+\kappa(\gamma_m+\kappa)}{4|g|^2+\gamma_m\kappa}\coth\left(\frac{\hbar\omega_m}{2k_BT}\right). \tag{8.27}$$

In order to know, which is the best, the simple approach to take is: Is there a parameter $K_P \neq 0$, which decreases the steady state phonon number more than for $K_P = 0$? So let us expand $n_{Phonon,ss}$ to the first order, which results to

$$\begin{aligned} n_{Phonon,ss}(K_P) =& n_{Phonon,ss}(0) \\ &+ \frac{\gamma_m\kappa}{(\gamma_m+\kappa)^2}\frac{\sqrt{2}4|g|^2\left(\kappa^2-4|g|^2\right)}{\left(4|g|^2+\gamma_m\kappa\right)^2}\left(\coth\left(\frac{\hbar\omega_m}{2k_BT}\right)-1\right)K_P \\ &+ \mathcal{O}\left(K_P^2\right). \end{aligned} \tag{8.28}$$

Thus, indeed, there exists a $K_P \neq 0$ which perform better cooling than for $K_P = 0$, namely,

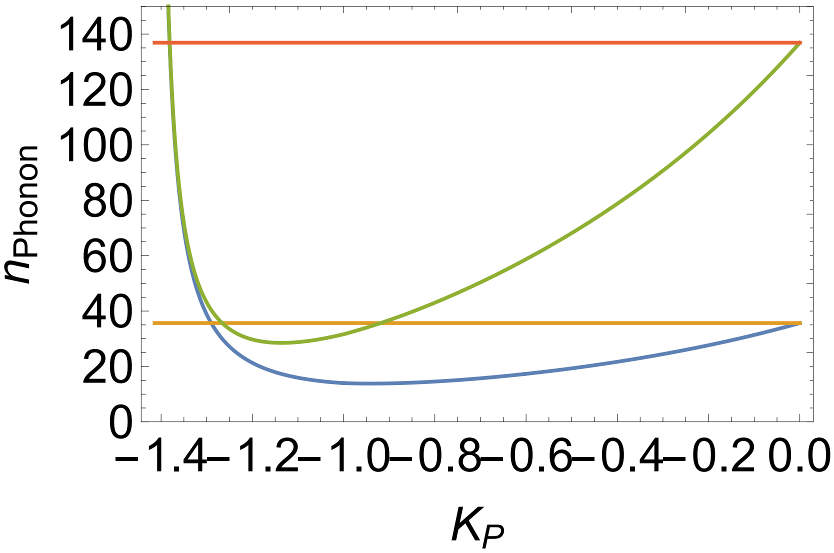

Figure 8.8: Steady State Phonon Number as a function of K_P. Phonon number with P-controlled system in rotating-wave approximation(blue) and without control (orange). Phonon number with P-controlled system without rotating-wave approximation (green) and without control (red). We have used for the simulation: $\omega_m = 2\pi \times 10.56$ MHz, $g_m = 2\pi \times 32$ Hz, $g = 2\pi \times 20$ kHz, $\kappa = 2\pi \times 200$ kHz, and $T = 4.4$ K. Values adapted from [44].

$$
\begin{aligned}
K_P &< 0 \quad for\ \kappa^2 - 4|g|^2 > 0 \\
K_P &> 0 \quad for\ \kappa^2 - 4|g|^2 < 0.
\end{aligned}
$$

$|K_P| > 1$ **vs.** $|K_P| < 1$

We are now left with $|K_P| > 1$ and $|K_P| < 1$ system. In this steady state problem, the only difference is q_2 in Eq. (8.18). If we introduce

$$K^{min}_{P,\gtrless 1} := \min_{|K_P| \gtrless 1} n_{Phonon,ss}(K_P), \tag{8.29}$$

we have just to check, which $K^{min}_{P,\gtrless 1}$ decreases q_2 even more. One can prove for the feedback system with $|K_P| > 1$ the phonon number is monotonically decreasing for $\kappa^2 - 4|g|^2 > 0$ and $K_P < -1$, so the best parameter one can choose is $K^{min}_{P,>1} = -1$. Since it is an large intense equation, we do not write it down, but we can show

$$n_{Phonon,ss}(K_P = -1) > n_{Phonon,ss}(K_P = -1 + 0^+) \geq n_{Phonon,ss}(K^{min}_{P,<1}) \quad \forall T > 0.$$

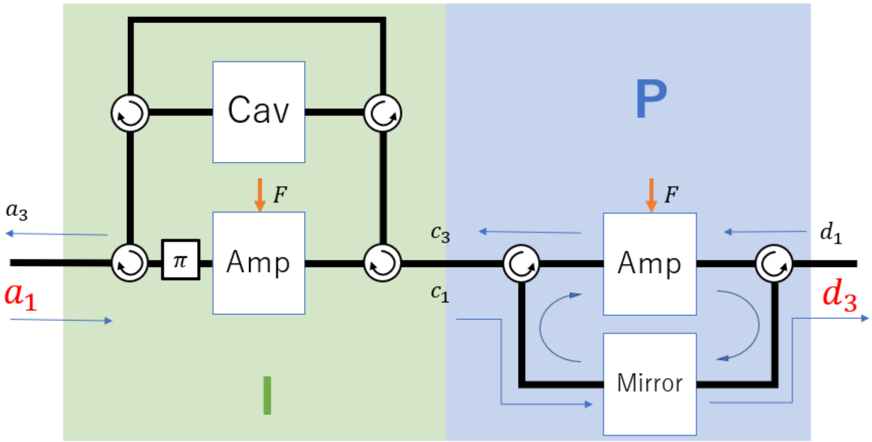

Figure 8.9: Coherent PI controller scheme. a_1 is the input signal and d_3 is the output signal. When implemented in the feedback scheme, the input is an error signal and the output a control input of the plant.

One can find that $K_{P,>1}^{min}$ is temperature independent (see Fig. 8.7).
Fig. 8.8 shows the steady state phonon number as a function of P parameter, where the exact calculation (active system) case is also plotted. In an active system case, there is a temperature T, which best parameter K_P lies in $K_P < -1$.

So, the essence of this enhanced cooling compared to the no-feedback scheme is the controllable effective decay rate $\kappa_{eff}(K_P)$.

8.3 Coherent PI Feedback Control

In this subsection, we show the idler from the coherent I controller largely contributes to the added noise such that the steady-state variance of the system operator x spreads dramatically for huge amplifier gain in I controller. This effect will be demonstrated with a simple toy model and with an optomechanical system.

8.3.1 Coherent PI Controller

From now on, we see the advantage of directional I controller. Thanks to this nonreciprocity, we can align the coherent P and I controller in series without having the input d_1 in Fig. 8.9 in output $d_3 = u$ in the ideal quantum amplifier limit, namely,

$$\begin{bmatrix} r_{out} \\ u \end{bmatrix} = \begin{bmatrix} 0 & 0 \\ s_{21}^I s_{21}^P & 0 \end{bmatrix} \begin{bmatrix} e \\ d_1 \end{bmatrix} + \begin{bmatrix} s_{12}^P & 0 \\ 0 & 1 \end{bmatrix} \begin{bmatrix} F_1^P \\ F_2^P \end{bmatrix} + \begin{bmatrix} 1 & 0 \\ 0 & s_{21}^P \end{bmatrix} \begin{bmatrix} F_1^I \\ F_2^I \end{bmatrix}, \tag{8.30}$$

where the matrix $s^{P,I}$ is the scattering matrix of the signal in coherent P and I controller, respectively (see Eqs. (6.3) and (7.14))[18]. The added noise of the coherent P controller is described $F_2^P = \sqrt{|K_P^2 - 1|} d^{P(\dagger)}$ for $|K_P| < 1$ and $|K_P| > 1$, respectively. Then, the control input u can be written as

$$\begin{aligned} u[s] =& s_{21}^I[s] s_{21}^P[s] e[s] + F_2^P[s] + s_{21}^P F_2^I[s] \qquad (8.31) \\ =& \left(1 + \frac{\gamma_I/2}{s}\right) s_{21}^P e[s] + F_2^P[s] + s_{21}^P F_2^I[s] \\ =:& K_P e[s] + K_I \frac{e[s]}{s} + F_2^P[s] + K_P F_2^I[s]. \qquad (8.32) \end{aligned}$$

Thus,

$$K_P := s_{21}^P, \qquad K_I := s_{21}^P \gamma_I/2.$$

8.3.2 $\left\langle F_{PI}^\dagger(t) F_{PI}(t') \right\rangle$ Divergence Problem

Here, we want to study the behavior of $\left\langle F_{PI}^\dagger(t) F_{PI}(t') \right\rangle$. To evaluate it, we switch to the QSDE (quantum stochastic differential equation) form and define

$$d\tilde{F}_{PI}(t) := \int_t^{t+dt} d\tau F_{PI}(\tau) \tag{8.33}$$

$$dD_{P,I}(t) := \int_t^{t+dt} d\tau d^{P,I}(\tau). \tag{8.34}$$

Then, the calculation steps are as follows:

[18]For non-ideal case, see Appendix B.

$$
\begin{aligned}
&\left\langle d\tilde{F}^{\dagger}_{PI}(t)\ d\tilde{F}_{PI}(t')\right\rangle \\
&\overset{(7.18)}{=} \left(K_P^2-1\right)\Theta\left(|K_P|-1\right)\left\langle dD_P(t)dD_P^{\dagger}(t')\right\rangle \\
&\quad + K_I^2\frac{s_{21}^{G,I\,2}-1}{(s_{21}^{G,I}+1)^2}\int_0^t d\tau_1\int_0^{t'} d\tau_2 \\
&\quad \exp\left(-\frac{\gamma_I}{2}\frac{t+t'-(\tau_1+\tau_2)}{s_{21}^{G,I}+1}\right)\left\langle dD_I(\tau_1)dD_I^{\dagger}(\tau_2)\right\rangle
\end{aligned}
\tag{8.35}
$$

$$
\begin{aligned}
&= \left(K_P^2-1\right)\Theta\left(|K_P|-1\right)\left\langle dD_P(t)dD_P^{\dagger}(t')\right\rangle \\
&\quad + K_I^2\frac{s_{21}^{G,I\,2}-1}{(s_{21}^{G,I}+1)^2}\exp\left(-\frac{\gamma_I}{2}\frac{t+t'}{s_{21}^{G,I}+1}\right) \\
&\quad \times\int_0^t d\tau_1\int_0^{t'} d\tau_2 \exp\left(\frac{\gamma_I}{2}\frac{(\tau_1+\tau_2)}{s_{21}^{G,I}+1}\right)\left\langle dD_I(\tau_1)dD_I^{\dagger}(\tau_2)\right\rangle
\end{aligned}
\tag{8.36}
$$

$$
\begin{aligned}
&\overset{(8.34)}{=} \left(K_P^2-1\right)\Theta\left(|K_P|-1\right)\left\langle dD_P(t)dD_P^{\dagger}(t')\right\rangle \\
&\quad + K_I^2\frac{s_{21}^{G,I\,2}-1}{(s_{21}^{G,I}+1)^2}\exp\left(-\frac{\gamma_I}{2}\frac{t+t'}{s_{21}^{G,I}+1}\right) \\
&\quad \times\int_0^t d\tau_1\int_0^{t'} d\tau_2 \exp\left(\frac{\gamma_I}{2}\frac{(\tau_1+\tau_2)}{s_{21}^{G,I}+1}\right)\underbrace{\int_{\tau_1}^{\tau_1+d\tau_1} dT_1\int_{\tau_2}^{\tau_2+d\tau_2} dT_2\delta(T_1-T_2)}_{=d\tau_1}
\end{aligned}
\tag{8.37}
$$

$$
\begin{aligned}
&= \left(K_P^2-1\right)\Theta\left(|K_P|-1\right)\left\langle dD_P(t)dD_P^{\dagger}(t')\right\rangle \\
&\quad + K_I^2\frac{s_{21}^{G,I\,2}-1}{(\gamma_I/2)^2} \\
&\quad \times\left(d\tau_1(t)-\exp\left(-\frac{\gamma_I}{2}\frac{t}{s_{21}^{G,I}+1}\right)d\tau_1(0)\right)\left(1-\exp\left(-\frac{\gamma_I}{2}\frac{t'}{s_{21}^{G,I}+1}\right)\right)
\end{aligned}
\tag{8.38}
$$

$$
\xrightarrow{t=t'\to\infty} \left(K_P^2-1\right)\Theta\left(|K_P|-1\right)dt + K_P^2\left(s_{21}^{G,I\,2}-1\right)dt, \tag{8.39}
$$

where we have used $K_I = K_P\gamma_I/2$ and $d\tau_1(t) = dt$ in the last equation. The equality $d\tau_1(t) = dt$ holds because of the definition in Eq. (8.34)

$$
dD_I(\tau_1 = t) = \int_{\tau_1=t}^{(\tau_1=t)+d(\tau_1=t)} d\tau d^I(\tau).
$$

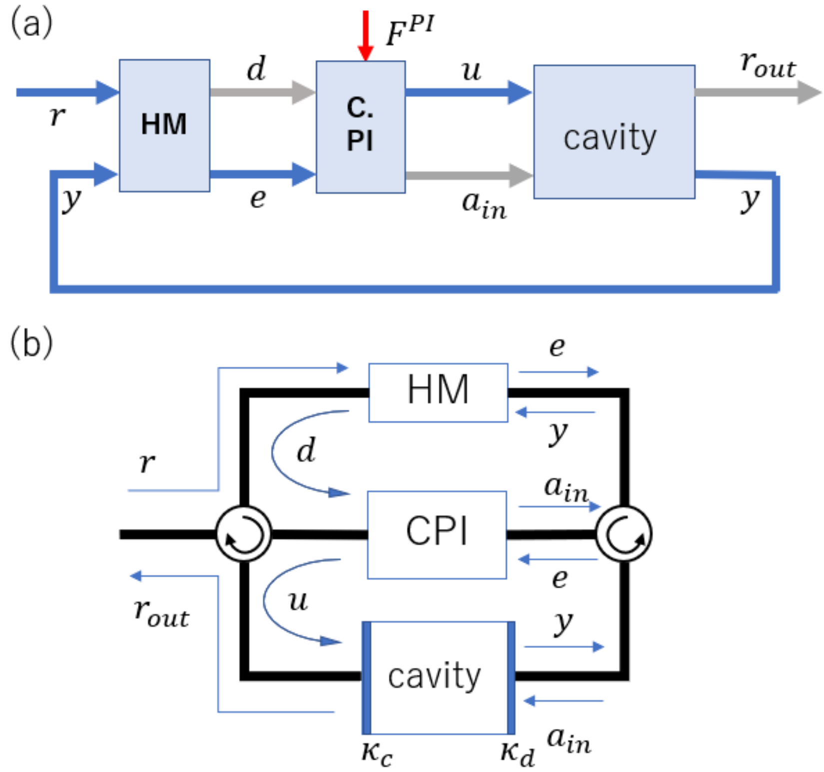

Figure 8.10: Coherent PI Feedback Control System depicted as (a) block diagram and (b) physical realization.

The reason lies merely on the fact that the integration effect occurs on the idler, as well, to satisfy the CCR. Henceforth, increasing the amplifier gain means extending the integration time (see Eq. (7.15)), and thus its amplitude, which is needed because the purpose of the coherent I controller is to eliminate the steady-state error by increasing (integrating) the signal.

Toy model: Cavity Photon

To see how this will affect to the system variable, we use a simple cavity system as a toy model. The whole state space representation is given by

$$\frac{d}{dt}\begin{bmatrix} a \\ e_I \end{bmatrix} = \begin{bmatrix} -i\Delta - \frac{1}{2}\left(\kappa_c + \kappa_d + K_P\sqrt{2\kappa_c\kappa_d}\right) & -K_I\sqrt{\kappa_c} \\ \sqrt{\frac{\kappa_d}{2}} & 0 \end{bmatrix}\begin{bmatrix} a \\ e_I \end{bmatrix}$$
$$+ \begin{bmatrix} -\left(\sqrt{\kappa_d} + K_P\sqrt{\frac{\kappa_c}{2}}\right) & K_P\sqrt{\frac{\kappa_c}{2}} & -\sqrt{\kappa_c} \\ \frac{1}{\sqrt{2}} & -\frac{1}{\sqrt{2}} & 0 \end{bmatrix}\begin{bmatrix} a_{in} \\ r \\ F_{PI} \end{bmatrix}, \quad (8.40)$$

where the detuning of the cavity is represented by $\Delta = \omega_c - \omega_L$ with the cavity frequency ω_c and laser frequency ω_L, the decay rate at converter side by κ_c, and the decay rate at quantum detector side by κ_d.
To obtain the steady state cavity photon number, we solve the Lyapunov equations

$$
\begin{aligned}
A_{PI}P + PA_{PI}^{\dagger} + Q =&0 && (8.41)\\
P^{\dagger}A_{PI}^{\dagger} + A_{PI}P^{\dagger} + Q^{\dagger} =&0, && (8.42)
\end{aligned}
$$

where we note $P \neq P^{\dagger}$ and $Q \neq Q^{\dagger}$, because the operators are non-commutative, i.e.,

$$
\begin{aligned}
P =& \left\langle \begin{bmatrix} a \\ e_I \end{bmatrix} \begin{bmatrix} a^{\dagger} & e_I^{\dagger} \end{bmatrix} \right\rangle = \begin{bmatrix} \langle aa^{\dagger}\rangle & \left\langle ae_I^{\dagger}\right\rangle \\ \langle e_I a^{\dagger}\rangle & \left\langle e_I e_I^{\dagger}\right\rangle \end{bmatrix}\\
P^{\dagger} =& \left\langle \begin{bmatrix} a^{\dagger} \\ e_I^{\dagger} \end{bmatrix} \begin{bmatrix} a & e_I \end{bmatrix} \right\rangle = \begin{bmatrix} \langle a^{\dagger}a\rangle & \langle a^{\dagger}e_I\rangle \\ \left\langle e_I^{\dagger}a\right\rangle & \left\langle e_I^{\dagger}e_I\right\rangle \end{bmatrix}
\end{aligned}
$$

and

$$
\begin{aligned}
Q =& B_{PI} \begin{bmatrix} \left\langle a_{in}a_{in}^{\dagger}\right\rangle & 0 & 0 \\ 0 & \langle rr^{\dagger}\rangle & 0 \\ 0 & 0 & \left\langle F_{PI}F_{PI}^{\dagger}\right\rangle \end{bmatrix} B_{PI}^{T}\\
=& \begin{bmatrix} \left(\sqrt{\kappa_d + K_P\sqrt{\frac{\kappa_c}{2}}}\right)^2 + K_P^2\frac{\kappa_c}{2} & -\sqrt{\frac{\kappa_d}{2}} - K_P\sqrt{\kappa_c} \\ -\sqrt{\frac{\kappa_d}{2}} - K_P\sqrt{\kappa_c} & 1 \end{bmatrix}\\
=:& \begin{bmatrix} q_{11} & q_{12} \\ q_{12} & q_{22} \end{bmatrix}\\
Q^{\dagger} =& B_{PI} \begin{bmatrix} \left\langle a_{in}^{\dagger}a_{in}\right\rangle & 0 & 0 \\ 0 & \langle r^{\dagger}r\rangle & 0 \\ 0 & 0 & \left\langle F_{PI}^{\dagger}F_{PI}\right\rangle \end{bmatrix} B_{PI}^{T}\\
=& \begin{bmatrix} \left(\left(K_P^2 - 1\right)\left(\Theta\left(|K_P| - 1\right) - \Theta\left(1 - |K_P|\right)\right) + K_P^2\left({s_{21}^{G,I}}^2 - 1\right)\right)\kappa_c & 0 \\ 0 & 0 \end{bmatrix}\\
=:& \begin{bmatrix} q_{11}^{(\dagger)} & 0 \\ 0 & 0 \end{bmatrix}.
\end{aligned}
$$

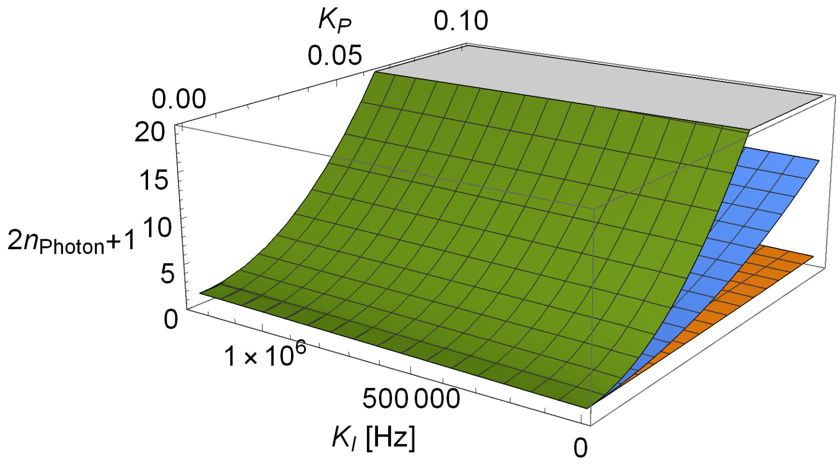

Figure 8.11: Steady state cavity photon number for (orange) $s_{21}^{G,I} = 10$, (blue) $s_{21}^{G,I} = 50$, and (green) $s_{21}^{G,I} = 100$. Parameters are chosen as $\Delta = 0$, $\kappa_c = \kappa_d = 2\pi \times 200$ kHz. For a high gain, the photon number n_{photon} is very sensitive to the parameter change K_P.

That is, $q_{11}^{(\dagger)}$ is proportional to the gain squared.
Finally, we obtain for the steady state photon number as

$$\begin{aligned} 2n_{Photon,ss} + 1 =& \frac{q_1}{||V||^2}\left(\frac{-|v_-|^2}{\lambda_+ + \lambda_+^*} + \mathrm{Re}\left[\frac{\sqrt{2\kappa_d/\kappa_c}}{\lambda_+ + \lambda_-^*}\right] + \frac{-|v_+|^2}{\lambda_- + \lambda_-^*}\right) \\ &+ \frac{q_{22}}{||V||^2}\frac{\kappa_d}{2\kappa_c K_I}\left(\frac{-1}{\lambda_+ + \lambda_+^*} + \mathrm{Re}\left[\frac{2}{\lambda_+ + \lambda_-^*}\right] + \frac{-1}{\lambda_- + \lambda_-^*}\right) \\ &+ 2\frac{q_{12}}{||V||^2}\frac{1}{\sqrt{K_I}}\mathrm{Re}\left[\frac{-v_-}{2\mathrm{Re}[\lambda_+]}\frac{v_+}{\lambda_- + \lambda_+^*} + \frac{-v_+}{2\mathrm{Re}[\lambda_-]}\right] \end{aligned} \tag{8.43}$$

where

$$\begin{aligned}
\lambda_\pm =& -\frac{1}{2}\left(i\Delta + \frac{\kappa_c + \kappa_d + K_P\sqrt{2\kappa_c\kappa_d}}{2}\right) \\
&\pm \sqrt{\frac{1}{4}\left(i\Delta + \frac{\kappa_c + \kappa_d + K_P\sqrt{2\kappa_c\kappa_d}}{2}\right)^2 - K_I\sqrt{\kappa_c\kappa_d/2}} \\
v_\pm =& \frac{1}{\sqrt{K_I\kappa_c}}\left(\frac{1}{2}\left(i\Delta + \frac{\kappa_c + \kappa_d + K_P\sqrt{2\kappa_c\kappa_d}}{2}\right)\right. \\
&\left.\pm\sqrt{\frac{1}{4}\left(i\Delta + \frac{\kappa_c + \kappa_d + K_P\sqrt{2\kappa_c\kappa_d}}{2}\right)^2 - K_I\sqrt{\kappa_c\kappa_d/2}}\right) \\
|V| =& v_- - v_+, \qquad q_1 = q_{11} + q_{11}^{(\dagger)}.
\end{aligned}$$

The result for various gains is shown in Fig. 8.11.
If we only focus on F_{PI} contribution to the cavity photon, we have

$$\begin{aligned}
2n_{Photon,ss} + 1 =& \frac{q_1^{(\dagger)}}{||V||^2}\left(\frac{-|v_-|^2}{\lambda_+ + \lambda_+^*} + \mathrm{Re}\left[\frac{\sqrt{2\kappa_d/\kappa_c}}{\lambda_+ + \lambda_-^*}\right] + \frac{-|v_+|^2}{\lambda_- + \lambda_-^*}\right) \\
& \propto {s_{21}^{G,I}}^2 .
\end{aligned} \tag{8.44}$$

This means the photon cavity number increases by the gain squared. For example, let us choose the reference power such that $\langle r \rangle_{ss} = \sqrt{\kappa_d}$ and let $\langle a_{in} \rangle_{ss} = 0$ be a vacuum state. In this case the mean cavity photon amplitude results to

$$\langle a \rangle_{ss} = 1,$$

then the amplitude of cavity photon number gives $a = 1 \pm \mathcal{O}(10)$, even if we choose $s_{21}^{G,I} = 10$. Of course, we can regulate this variance by K_P, however, this must be chosen much smaller than the inverse of the gain, such that we can achieve a stable mean number.

8.3.3 State Space Representation of the Special Case

Analogous to the classical P-I control case, we can derive the augmented state space representation, but with the differences $C = -B^T$ and the existence of idlers and noises in the system.

The control input u changes to

$$u(t) = K_P e(t) + K_I \int_0^t d\tau e(\tau) + F_{PI}(t), \tag{8.45}$$

with

$$\begin{aligned} F_{PI}(t) &= F_2^P + K_P F_2^I(t) \\ &\to \mp\sqrt{|K_P^2 - 1|} d_2^P(t)^{(\dagger)} - K_I \int_0^t dt' d_2^I(t')^\dagger. \end{aligned} \tag{8.46}$$

Henceforth, the augmented coherent equation of motion is changed to

$$\begin{aligned} \frac{d}{dt}\begin{bmatrix} x \\ e_I \end{bmatrix} &= \begin{bmatrix} A - \frac{K_P}{\sqrt{2}-K_P}BB^T & \frac{K_I}{1-K_P/\sqrt{2}}B \\ -\frac{1}{\sqrt{2}-K_P}B^T & \frac{K_I}{\sqrt{2}-K_P} \end{bmatrix}\begin{bmatrix} x \\ e_I \end{bmatrix} + \frac{-1}{\sqrt{2}-K_P}\begin{bmatrix} K_P B \\ 1 \end{bmatrix} r \\ &+ \begin{bmatrix} B_w \\ 0 \end{bmatrix} w + \frac{1}{\sqrt{2}-K_P}\begin{bmatrix} \sqrt{2}B \\ \mathbf{1} \end{bmatrix} F_{PI}, \end{aligned} \tag{8.47}$$

where we have omitted the time dependence for clarity, as usual.

8.3.4 Stability Analysis

The closed-loop stability for the coherent PI feedback system with no internal loss is provided.

But before going into the analysis, we first want to prove a lemma: In the linear quantum system, we can express the state space representation, i.e., the quantum Langevin equations and the input-output relation, in terms of $ABCD$ model (see Eq. (3.9)), which is a function of the bare system Hamiltonian and the interaction Hamiltonian with the environment or just the decay rate. Now, the bare passive system Hamiltonian is described as $\mathcal{H}_{sys} = \mathbf{a}^\dagger \Omega \mathbf{a}$ with the annihilation operators in vector form $\mathbf{a} = [a_1\ a_2\ ...\ a_n]^T$, while B is representing the decay rate. Keeping these in mind, we want to state the following lemma:

Lemma 8.1 *If a square matrix $A = -i\Omega - \frac{1}{2}BB^T \in \mathbb{C}^{n\times n}$ with $\Omega = \Omega^\dagger$ has its complex eigenvalues $\{\lambda_k\}_{k=1,\dots,n}$, then we can express its eigenvalues as $\lambda_k = -i\omega_k - \gamma_k/2$ with $\Omega = U^\dagger \mathrm{diag}_k(\omega_k)U$ and $BB^T = U^\dagger \mathrm{diag}_k(\gamma_k)U$, where U is the change of basis matrix with $UU^\dagger = U^\dagger U = \mathbf{1}$. Moreover, $\gamma_k \geq 0\ \forall k$.*

Proof. Since $\lambda_k \in \mathbb{C}$, we can write $\lambda_k = -i\lambda_{i,k} - \lambda_{r,k}$ with $\lambda_{i,k}, \lambda_{r,k} \in \mathbb{R}\ \ \forall k$. Since A is diagonalizable, we can decompose it as

$$
\begin{aligned}
A =& U^\dagger \mathrm{diag}_k(\lambda_k)U \\
=& U^\dagger \mathrm{diag}_k(-i\lambda_{i,k} - \lambda_{r,k})U \\
=& U^\dagger \mathrm{diag}_k(-i\lambda_{i,k})U + U^\dagger \mathrm{diag}_k(-\lambda_{r,k})U \\
=& - i\Omega - \frac{1}{2}BB^T.
\end{aligned}
$$

We also consider its Hermitean conjugate

$$
\begin{aligned}
A^\dagger =& U^\dagger \mathrm{diag}_k(i\lambda_{i,k})U + U^\dagger \mathrm{diag}_k(-\lambda_{r,k})U \\
=& i\Omega - \frac{1}{2}BB^T.
\end{aligned}
$$

Summing and subtracting both equations we obtain

$$
\Omega = U^\dagger \mathrm{diag}_k(\lambda_{i,k})U, \qquad \frac{1}{2}BB^T = U^\dagger \mathrm{diag}_k(\lambda_{r,k})U.
$$

Hence, $\lambda_{i,k} = \omega_k$ and $\lambda_{r,k} = \gamma_k/2$ for all $k = 1, ..., n$. Since $1/2BB^T$ is a semi-positive definite matrix, we naturally obtain $\gamma_k \geq 0$. Therefore,

$$
\lambda_k = -i\omega_k - \gamma_k/2, \qquad \forall k = 1, ..., n. \ \square
$$

This means we can treat the "imaginary" Hermitean matrix and the "real" Hermitean matrix independently in terms of diagonalization.

For the stability analysis, we have to find the conditions where the solutions of a characteristic polynomial are all lying in the left side of the complex plane. If we consider the augmented differential equation as in Eq. (3.14) with $A = -i\Omega - 1/2BB^T$ and $C = -B^T$, we have to calculate

$$
\begin{aligned}
&\left| \begin{bmatrix} s\mathbf{1} - A + \frac{K_P}{\sqrt{2}-K_P}BB^T & -\frac{K_I}{1-K_P/\sqrt{2}}B \\ \frac{1}{\sqrt{2}-K_P}B^T & s\mathbf{1} - \frac{K_I}{\sqrt{2}-K_P}\mathbf{1} \end{bmatrix} \right| \\
&= \left| s - \frac{K_I}{\sqrt{2}-K_P} \right|^2 \left| s\mathbf{1} - A + \frac{K_P}{\sqrt{2}-K_P}BB^T + \frac{1}{s - \frac{K_I}{\sqrt{2}-K_P}} \frac{\sqrt{2}K_I}{(\sqrt{2}-K_P)^2}BB^T \right|.
\end{aligned}
\tag{8.48}
$$

Now let us assume the plant is composed of the quantum detector and system such that only the detector feels the signal input into the plant. Other noise inputs are not considered because those are providing further decays and widen the stability region. Hence, the quantum Langevin equation of the plant is

$$\frac{d}{dt}\begin{bmatrix} x_{sys} \\ x_{det} \end{bmatrix} = \begin{bmatrix} -i\Omega_{sys} & -iG_{sys-det} \\ -iG^{\dagger}_{sys-det} & -i\Omega_{det} - 1/2B_{det}B^{T}_{det} \end{bmatrix} \begin{bmatrix} x_{sys} \\ x_{det} \end{bmatrix} + \begin{bmatrix} 0 \\ B_{det} \end{bmatrix} u, \tag{8.49}$$

where $\Omega_{sys/det}$ is the system/detector Hamiltonian matrix, $G_{sys-det}$ the coupling matrix between them, and B_{det} the "input matrix" to the detector. Using the lemma above we can diagonalize A for SISO configuration as

$$A = U^{\dagger}\mathrm{diag}(-i\omega_1, i\omega_1, ..., -i\omega_n, i\omega_n, -i\omega_{det} - \frac{\gamma}{2}, i\omega_{det} - \frac{\gamma}{2})U, \tag{8.50}$$

where ω_k is the k-th eigenfrequency, which is equivalent to the eigenvalue of system matrix A, and ω_{det} is the eigenfrequency affected by the coupling strength γ with

$$BB^T = \begin{bmatrix} 0 & 0 \\ 0 & B_{det}B^{T}_{det} \end{bmatrix} = U^{\dagger}\mathrm{diag}(0, ..., 0, \gamma, \gamma)U. \tag{8.51}$$

Since the second factor of Eq. (8.48) is only composed of the matrices Ω and BB^T, we can rewrite (8.48) thanks to the lemma above stating that the imaginary and real part can be treated independently when diagonalizing as

$$\begin{aligned}
&\left| s - \frac{K_I}{\sqrt{2} - K_P} \right|^2 \left| s\mathbf{1} - A + \frac{K_P}{\sqrt{2} - K_P} BB^T + \frac{1}{s - \frac{K_I}{\sqrt{2} - K_P}} \frac{\sqrt{2}K_I}{(\sqrt{2} - K_P)^2} BB^T \right| \\
&= \left| s^2 + (i\omega_{det} + \frac{1}{2}\frac{\sqrt{2} + K_P}{\sqrt{2} - K_P}\gamma - \frac{K_I}{\sqrt{2} - K_P})s \right. \\
&\qquad \left. + \left(-i\omega_{det} - \frac{1}{2}\frac{\sqrt{2} + K_P}{\sqrt{2} - K_P}\gamma \right) \frac{K_I}{\sqrt{2} - K_P} + \frac{\sqrt{2}K_I}{(\sqrt{2} - K_P)^2}\gamma \right| \\
&\quad \times \prod_{k=1}^{n} |s - i\omega_k| \, |s + i\omega_k| \\
&= 0.
\end{aligned} \tag{8.52}$$

So, we have changed the complex characteristic polynomial of an augmented state space representation into a simple quadratic problem. For convenience, we define

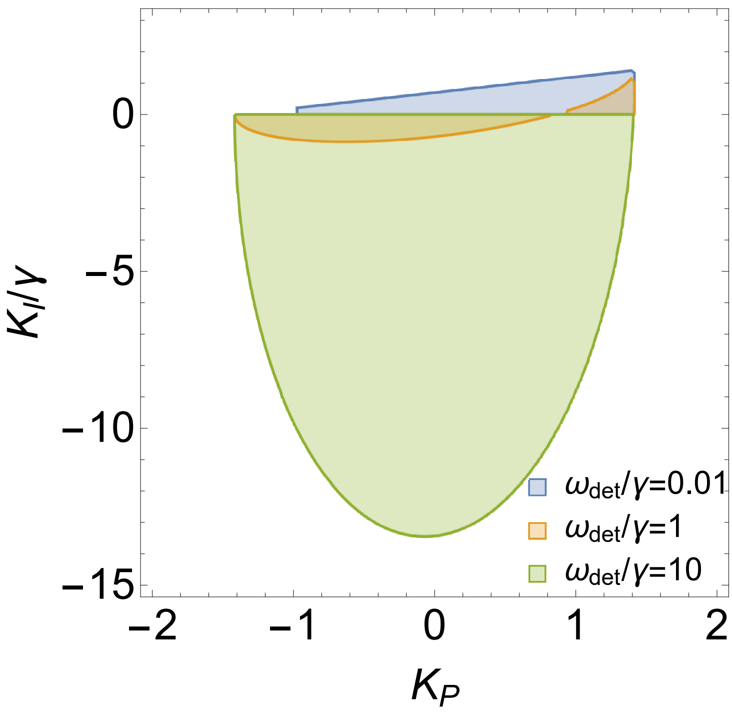

Figure 8.12: Stability region as a function of K_P and K_I with different eigenfrequency-decay ratio: $\omega_{det}/\gamma = 0.01, 1, 10$.

$$\begin{aligned} a_1 :=& i\omega_{det} + \frac{1}{2}\frac{\sqrt{2}+K_P}{\sqrt{2}-K_P}\gamma \\ a_2 :=& \frac{K_I}{\sqrt{2}-K_P} \\ b :=& \frac{\sqrt{2}K_I}{(\sqrt{2}-K_P)^2}\gamma. \end{aligned}$$

Thus, the eigenvalues are solved as

$$s = -\frac{1}{2}\left(a_1 - a_2\right) \pm \sqrt{\frac{1}{4}\left(a_1 + a_2\right)^2 - b}. \tag{8.53}$$

Finally, for stability we have to require $\mathrm{Re}[s] < 0$. The result of stable regions for different ratios ω_{det}/γ is plotted in Fig. 8.12.

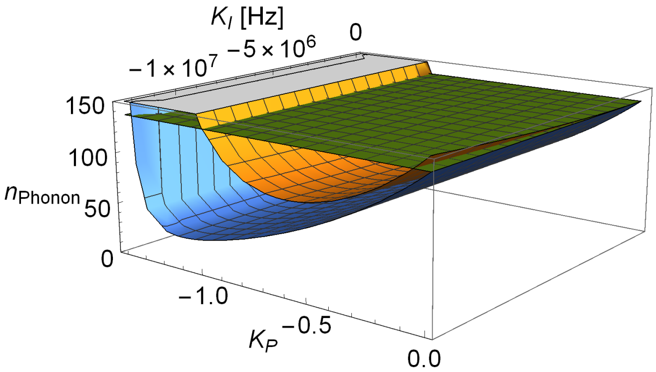

Figure 8.13: Steady State Phonon Number as a function of K_P and K_I. Phonon number without feedback control (green), with CP-controlled system (blue), and with CPI-controlled system ($s_{21}^{G,I} = 10$) (orange). We have used for the simulation: $\omega_m = 2\pi \times 10.56$ MHz, $g_m = 2\pi \times 32$ Hz, $g = 2\pi \times 20$ kHz, $\kappa = 2\pi \times 200$ kHz, and $T = 4.4$ K. Values adapted from [44].

8.3.5 Comparison with Coherent P Controller

While we have demonstrated the effectiveness of the added noise F_{PI} in the previous subsection via a simple toy model, we go to more practical level. We have seen in section 8.2 the coherent P control is proven to be very useful to cool the optomechanical system. Hence, the comparison between the CP feedback controlled and CPI feedback controlled optomechanical cooling system gives us a clearer picture with respect to the effect of idlers.

Since the calculation procedure is the same as in previous ones, we just write down the dissipation matrix Q_{PI}. If the system variables are in quadrature forms, we obtain

$$Q_{PI} = \begin{bmatrix} Q_w & 0 \\ 0 & Q_{det} \end{bmatrix}$$

with

$$Q_w := \begin{bmatrix} 0 & 0 \\ 0 & \gamma_m \coth\left(\frac{\hbar\omega_m}{2k_BT}\right) \end{bmatrix}, \quad Q_w^\dagger := \begin{bmatrix} 0 & 0 \\ 0 & 0 \end{bmatrix}$$

and

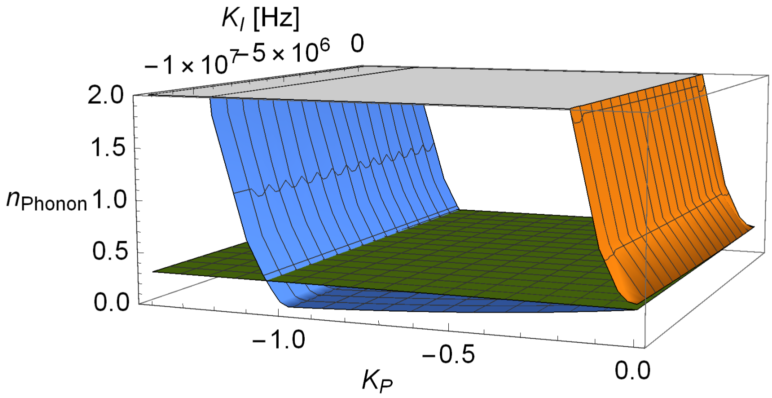

Figure 8.14: Steady State Phonon Number as a function of K_P and K_I. Phonon number without feedback control (green), with CP-controlled system (blue), and with CPI-controlled system ($s_{21}^{G,I} = 10$) (orange). We have used for the simulation: $\omega_m = 2\pi \times 10.56$ MHz, $g_m = 2\pi \times 32$ Hz, $g = 2\pi \times 20$ kHz, $\kappa = 2\pi \times 200$ kHz, and $T = 0.01$ K. Values adapted from [44].

$$
\begin{aligned}
Q_{det} &:= \begin{bmatrix} 2\kappa & 0 & -\sqrt{-2K_I\kappa} & 0 \\ 0 & 2\kappa & 0 & -\sqrt{-2K_I\kappa} \\ -\sqrt{-2K_I\kappa} & 0 & -K_I & 0 \\ 0 & -\sqrt{-2K_I\kappa} & 0 & -K_I \end{bmatrix} \\
&\quad \times \frac{(K_P^2-1)\left(\Theta(|K_P|-1)-\Theta(1-|K_P|)\right)+K_P^2({s_{21}^{G,I}}^2-1)}{2\left(\sqrt{2}-K_P\right)^2} \\
Q_{det}^{\dagger} &:= \begin{bmatrix} \kappa K_P & 0 & -\sqrt{-K_I\kappa} & 0 \\ 0 & \kappa K_P & 0 & -\sqrt{-K_I\kappa} \\ -\sqrt{-K_I\kappa} & 0 & 0 & 0 \\ 0 & -\sqrt{-K_I\kappa} & 0 & 0 \end{bmatrix} \frac{K_P}{2\left(\sqrt{2}-K_P\right)^2}.
\end{aligned}
$$

As one can find, the thermal bath contribution Q_w and the input contribution Q_{det} can be completely separated. Additionally, we can recognize the first term is the idler contribution and the second term is the "real" input contribution. Now, solving the Lyapunov equation, the steady state phonon number can be found as a function of K_P and K_I in Fig. 8.13. As expected, the influence of F_{PI} is quite large even for $s_{21}^{G,I} = 10$, and the minimal steady-state phonon number approximately increases by 60 phonons compared to CP controlled system. However, we can still manage to perform better than the no-feedback cooling by properly choosing the parameter $K_P \approx -0.6$ for $T = 4.4$ K. This can be roughly explained by saying the mechanical system is heated by the idler of coherent I controller, which adds $K_P^2({s_{21}^{G,I}}^2 - 1) \approx 36$ phonons to the CP-controlled optomechanical system. Indeed, the steady state particle number at $K_P = -0.6$ is about 60 phonons in CP case, while in CPI it is about 85. If we now compare their cooling performance at $T = 0.01$ K, we observe CPI controlled feedback system entirely fails to cool much better than the no-feedback one does (cf. Fig. 8.14). The reason is clear. At a cryogenic temperature near the ground state, the steady state phonon number is of the order of 1, while the idler contribution has not changed. Therefore, in contrast to $T = 4.4$ K case, the added noise effect is significant. However, this is not crucial because there is no point in using an I controller, which plays a role as steady-state error eliminator, in the first place for near-ground state operation since no steady-state error will appear. Thus, we can conclude, by properly choosing the amplifier gain CPI-controlled system can still be useful, if the effect of the idlers can be tolerated compared to the steady state mean value of the system variable or output signal, while for example for ground state operation CPI-controlled system is not useful with respect to the variance.

8.4 Coherent PD Feedback Control

Here, we want to utilize the coherent PD controller for cooling an optomechanical system. In contrast to previous *sideband-cooling* with coherent P controller, the *cold-damping* method is chosen, where the essence of this cooling is increasing the mechanical damping rate such that the vibration of the system is slowed down due to high "viscosity". We see the coherent PD feedback control system can reach the standard quantum limit even in the presence of idlers. In the last section, we also compare the performance with the homodyne-measurement-based feedback system, and we reach to the conclusion, the coherent one can in principle outperforms the measurement one, but under common experimental situations, the homodyne-measurement can cool better. The following calculations are very similar to that of Vitali et al.[38].

8.4.1 Coherent PD Controller

Same as in coherent PI controller case, we can exploit the directionality of the devices following to

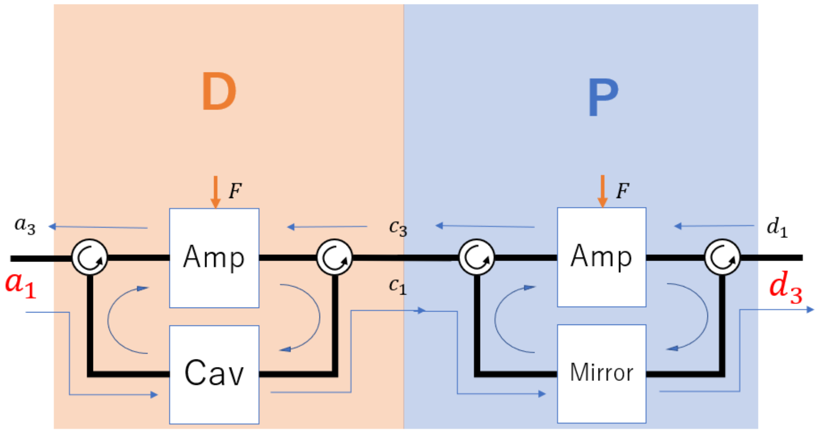

Figure 8.15: Coherent PD controller scheme. As in case of coherent PI controller (Fig. 8.9), a_1 is the input signal and d_3 is the output signal.

$$\begin{aligned}\begin{bmatrix} d_{out} \\ u \end{bmatrix} = \begin{bmatrix} 0 & 0 \\ s_{21}^D s_{21}^P & 0 \end{bmatrix} \begin{bmatrix} e \\ d_1 \end{bmatrix} \\ + \begin{bmatrix} s_{12}^P & 0 \\ 0 & 1 \end{bmatrix} \begin{bmatrix} F_1^P \\ F_2^P \end{bmatrix} \Theta(|s_{21}^P| - 1) \\ + \begin{bmatrix} 1 & 0 \\ 0 & s_{21}^P \end{bmatrix} \begin{bmatrix} F_1^D \\ F_2^D \end{bmatrix},\end{aligned} \tag{8.54}$$

where the matrix $s^{P,D}$ is the scattering matrix of the signal in coherent P and I controller, respectively (see Eqs. (6.3) and (7.3))[19]. The input e and outputs u and d_{out} correspond to a_1, d_3 and a_3, respectively. Then, the control input u is described in Laplace-s domain by

$$u[s] = s_{21}^D[s] s_{21}^P[s] e[s] + F_2^P[s]\Theta(|s_{21}^P| - 1) + s_{21}^P F_2^D[s] \tag{8.55}$$

$$= \left(1 + \frac{s}{\gamma_D/2}\right) s_{21}^P e[s] + F_2^P[s]\Theta(|s_{21}^P| - 1) + s_{21}^P F_2^D[s]$$

$$=: K_P e[s] + sK_D e[s] + F_2^P[s]\Theta(|K_P| - 1) + K_P F_2^D[s]. \tag{8.56}$$

Thus,

$$K_P := s_{21}^P, \qquad K_D := \frac{s_{21}^P}{\gamma_D/2}.$$

[19] For non-ideal case, see Appendix B.

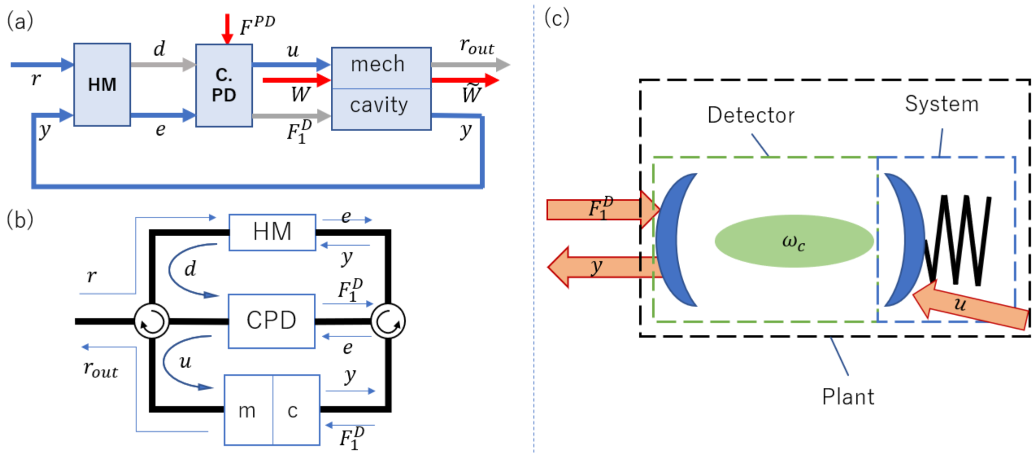

Figure 8.16: Coherent PD Feedback Control System depicted as (a) block diagram and (b) physical realization. "mech" and "cavity" refer to mechanical system and cavity, respectively. (c) Detailed plant configuration, where the converter is not needed due to the direct interaction between input and system.

8.4.2 Quantum Langevin Equation of PD controlled feedback system

In this subsection, we only focus on the optomechanical system. Its linearized quantum Langevin equation (classical contributions are omitted) without feedback is expressed in quadrature form as

$$\frac{d}{dt}\begin{bmatrix} Q \\ P \\ X \\ Y \end{bmatrix} = \begin{bmatrix} 0 & \omega_m & 0 & 0 \\ -\omega_m & -\gamma_m & 2G & 0 \\ 0 & 0 & -\frac{\gamma_c}{2} & 0 \\ 2G & 0 & 0 & -\frac{\gamma_c}{2} \end{bmatrix} \begin{bmatrix} Q \\ P \\ X \\ Y \end{bmatrix} - \begin{bmatrix} 0 & 0 & 0 \\ 1 & 0 & 0 \\ 0 & \frac{\sqrt{\gamma_c}}{2} & 0 \\ 0 & 0 & \frac{\sqrt{\gamma_c}}{2} \end{bmatrix} \begin{bmatrix} W \\ X_{in} \\ Y_{in} \end{bmatrix}$$

where ω_m and γ_m is the eigenfrequency and decay rate of the mechanical system, and G the coupling constant between by the quadratures (Q, P) described phonons and by (X, Y) characterized cavity photons, and γ_c is the cavity decay rate[20]. The detuning Δ is set to 0. (X_{in}, Y_{in}) are vacuum inputs, and W is thermal noise input with

[20]Note all system variables in quadrature form A and its canonical conjugate B are represented here in annihilation/creation operators $a^{(\dagger)}$ as: $A = (a^\dagger + a)/2$, $B = i(a^\dagger - a)/2$. However, all inputs and outputs are written: $A_{in/out} = (a^\dagger_{in/out} + a_{in/out})$, $B_{in/out} = i(a^\dagger_{in/out} - a_{in/out})$.

$$
\begin{aligned}
\left\langle W(t)W(t')^\dagger \right\rangle =&\frac{1}{2\pi}\frac{\gamma_m}{\omega_m}\left(F_r(t-t')+iF_i(t-t')\right),\\
F_r(t) =&\int_0^{\varpi} d\omega\omega\cos(\omega t)\coth\left(\frac{\hbar\omega}{2k_BT}\right),\\
F_i(t) =&-\int_0^{\varpi} d\omega\sin(\omega t),
\end{aligned}
$$

where ϖ is the frequency cutoff of the reservoir spectrum.
The associated input-output relation is

$$
\begin{aligned}
X_{out} =&2\sqrt{\gamma_c}X+X_{in}\\
Y_{out} =&2\sqrt{\gamma_c}Y+Y_{in}.
\end{aligned}
\tag{8.57}
$$

Now we consider the feedback effect, which feedback system is depicted in Fig. 8.16. The feedback flow is as follows: A vacuum input F_1^D is coming into the cavity and is reflected giving y. This output interferes with the reference signal r (vacuum) destructively and the error signal e is evaluated by the coherent PD controller, which gives the control input u. This control input u *directly acts as a radiation pressure* against the mechanical system and makes its motion viscous.
The control input u is given by

$$
u(t)=K_Pe(t)-K_D\dot{e}(t)+F_{PD}, \tag{8.58}
$$

where

$$
e(t)=\frac{1}{\sqrt{2}}\left(y(t)-r(t)\right) \tag{8.59}
$$

and

$$
\begin{aligned}
F_{PD}(t) :=& \underbrace{\sqrt{K_P^2-1}\Theta(|K_P|-1){d_P}^\dagger(t)+\sqrt{1-K_P^2}\Theta(1-|K_P|)d_P(t)}_{=:F_P}\\
&+\underbrace{K_D\dot{d}_D^\dagger(t)}_{=:\dot{F}_D}
\end{aligned}
\tag{8.60}
$$

in the ideal quantum amplifier limit[21]. This control input adds a feedback Hamiltonian term[37, 38].

[21] Some readers might concern about the CCR of the control input u. For its calculation see Appendix B

$$\mathcal{H}_{fb} = \left(\sqrt{\gamma_c}K_P Y_e(t) - K_D \dot{Y}_e(t)/\sqrt{\gamma_c} + \sqrt{\gamma_c}Y_F^{PD}\right) Q$$

with $Y_x := i(x^\dagger - x),\ x = e, F$.
On the other hand, we have to determine the signal coming from the other port of coherent PD controller. We will see the fed-back signal contribution is so small such that only the idler F_1^D is going into the cavity: The constructively interfered signal d is changed after going through the controller to

$$-\frac{1}{K_P + s_{12}^{G,P}}\frac{1}{1+s_{21}^{G,D}}d + F_1^D + \frac{1}{1+s_{21}^{G,D}}F_1^P,$$

where $s_{21}^{G,(P,D)}$ is the amplifier gain of the quantum amplifier in the proportional and derivative controller, respectively, and $F_1^{P,D}$ is the idler of the P and D controller, which is the same as that of the amplifier, $F_1^{G,(P,D)}$. Therefore, for a high gain limit, d and F_1^P vanish, and only F_1^D remains, which is equivalent to vacuum noise. In the following, we define

$$\begin{aligned} X_{in} :=& F_1^{D\dagger} + F_1^D \\ Y_{in} :=& i\left(F_1^{D\dagger} - F_1^D\right). \end{aligned}$$

After adiabatic elimination (by assuming very low quality factor of the cavity) the quantum Langevin equation is modified to

$$\begin{aligned} \frac{d}{dt}\left[\begin{array}{c} Q \\ P \end{array}\right] =& \left[\begin{array}{cc} 0 & \omega_m \\ -\omega_m' & -\gamma_m' \end{array}\right]\left[\begin{array}{c} Q \\ P \end{array}\right] \\ & - \left[\begin{array}{cccccc} 0 & 0 & 0 & 0 & 0 & 0 \\ 1 & 2G/\sqrt{\gamma_c} & -\frac{K_P}{\sqrt{2}}\frac{\sqrt{\gamma_c}}{2} & \frac{K_D}{2\sqrt{2}\sqrt{\gamma_c}} & \frac{\sqrt{\gamma_c}}{2} & \frac{1}{2\sqrt{\gamma_c}} \end{array}\right]\left[\begin{array}{c} W \\ X_{in} \\ Y_{in}+Y_r \\ \dot{Y}_{in}+\dot{Y}_r \\ Y_{F_P} \\ \dot{Y}_{F_D} \end{array}\right], \end{aligned} \tag{8.61}$$

where

$$
\begin{aligned}
\omega_m' :=& \omega_m + \frac{K_P}{\sqrt{2}}4G, \quad \gamma_m' := \gamma_m - 2\sqrt{2}K_D G\frac{\omega_m}{\gamma_c}, \\
Y_P :=& i(d_P - d_P^\dagger), \qquad Y_{F_P} := \left(\sqrt{K_P^2-1}\Theta(|K_P|-1) - \sqrt{1-K_P^2}\Theta(1-|K_P|)\right) Y_P, \\
Y_D :=& i(d_D - d_D^\dagger), \qquad Y_{F_D} := K_D Y_D. \\
&.
\end{aligned}
$$

Note that we have

$$
\left\langle \dot{Y}_{in}(t)\dot{Y}_{in}(t')\right\rangle = \left\langle \dot{Y}_r(t)\dot{Y}_r(t')\right\rangle = \left\langle \dot{Y}_D(t)\dot{Y}_D(t')\right\rangle = -\ddot{\delta}(t-t').
$$

8.4.3 Steady-State Covariance of Q and P

The previous quantum Langevin equation (8.61) can be solved as follows:

$$
Q(t) = K(t)Q(0) + \chi(t)P(0) + \int_0^t dt' \chi(t-t')\xi(t') \tag{8.62}
$$

with

$$
\begin{aligned}
\xi(t) :=& -W(t) - \frac{2G}{\sqrt{\gamma_c}}X_{in}(t) + \frac{K_P}{\sqrt{2}}\frac{\sqrt{\gamma_c}}{2}(Y_{in}(t) + Y_r(t)) \\
&- \frac{K_D}{2\sqrt{2}\sqrt{\gamma_c}}(\dot{Y}_{in}(t) + \dot{Y}_r(t)) - \frac{\sqrt{\gamma_c}}{2}Y_F^{PD}(t) \\
\chi(t) :=& \frac{\omega_m}{\sqrt{\omega_m\omega_m' - \gamma_m^2\left(\frac{1+g_2}{2}\right)^2}} e^{-(1+g_2)\gamma_m t/2} \sin\left(\sqrt{\omega_m\omega_m' - \gamma_m^2\left(\frac{1+g_2}{2}\right)^2}\, t\right) \\
K(t) :=& 1 - \omega_m \int_0^t dt'\chi(t'), \qquad g_2 := -\sqrt{\frac{\zeta}{\gamma_m\gamma_c}}\omega_m\frac{K_D}{\sqrt{2}}, \qquad \zeta := \frac{16G^2}{\gamma_m\gamma_c}.
\end{aligned}
$$

So, ξ is the total noise/input operator, g_2 is the rescaled feedback derivative gain and ζ the rescaled input power.

Thus, the steady state of its variance can be calculated as

$$
\left\langle Q^2\right\rangle_{ss} := \lim_{t\to\infty}\left\langle Q(t)^2\right\rangle = \frac{1}{4}\left(1 - \frac{\omega_m}{\omega_m'}\right)^2 + \int_0^\infty dt' \int_0^\infty dt'' \chi(t')\chi(t'')c(t'-t''),
$$

where we have defined c for the stationary symmetric correlation function of the noise term $\xi(t)$. That is, the term $F_i(t)$ of the thermal noise term vanishes. Considering the commonly met condition $\hbar\omega_m \ll k_B T$, we then obtain

$$\begin{aligned}\left\langle Q^2\right\rangle_{ss} =& \frac{1}{4}\left(1-\frac{\omega_m}{\omega_m'}\right)^2 + \frac{\omega_m}{\omega_m'}\frac{1}{1+g_2}\left(\frac{\zeta}{8}+\frac{\gamma_c}{8\gamma_m}\left(K_P^2+2\left|K_P^2-1\right|\right)\right)\\ &+\frac{g_2^2}{4\zeta}\frac{1}{1+g_2}+\frac{\omega_m}{2\omega_m'}\frac{1}{1+g_2}\frac{k_B T}{\hbar\omega_m}.\end{aligned} \tag{8.63}$$

The first and second term is the input contribution, the third the feedback and the last the thermal noise contribution.

In case of P, in the narrow feedback frequency cut-off limit, we have to make a logarithmic correction regarding to the thermal contribution, namely,

$$\left\langle P^2\right\rangle_{ss,th} = \frac{\omega_m\gamma_m}{4\omega_m'\gamma_m}\frac{1}{1+g_2}\left(\frac{k_B T}{\hbar\omega_m}+\frac{\gamma_m}{\pi\omega_m}\ln\left(\frac{\hbar\varpi}{2\pi k_B T}\right)\right).$$

However, in the common experimental situation, $\gamma_m \ll \omega_m$ is given such that we can neglect the correction. Hence, we obtain $\langle Q^2\rangle_{ss} \approx \langle P^2\rangle_{ss}$.

Let us also calculate the optimal feedback derivative gain $g_{2,opt}$, which reads

$$g_{2,opt} = \sqrt{1+\frac{\omega_m}{\omega_m'}\left(\frac{\zeta^2}{2}+\frac{\zeta}{2}\frac{\gamma_c}{\gamma_m}\left(K_P^2+2\left|K_P^2-1\right|\right)+2\frac{k_B T\zeta}{\hbar\omega_m}\right)}-1. \tag{8.64}$$

The remarkable point is the optimal feedback gain is now dependent on temperature and on γ_c/γ_m. That is, due to $g_2 \propto \sqrt{\zeta}K_D$ we have to choose a high input power ζ and/or parameter $K_D = K_P/(\gamma_D/2)$ for $\hbar\omega_m \ll k_B T$ and $\gamma_m \ll \gamma_c$, respectively. This results to

$$\left\langle Q^2\right\rangle_{ss,opt} \xrightarrow{\hbar\omega_m \ll k_B T} \frac{1}{2}\sqrt{\frac{\omega_m}{\omega_m'}}\sqrt{\frac{2k_B T}{\hbar\omega_m\zeta}} \tag{8.65}$$

and

$$\left\langle Q^2\right\rangle_{ss,opt} \xrightarrow{\gamma_m \ll \gamma_c} \frac{1}{8}\sqrt{\frac{\omega_m}{\omega_m'}}\sqrt{\frac{2\gamma_c}{\gamma_m\zeta}\left(K_P^2+2|K_P^2-1|\right)} \geq \frac{1}{8}\sqrt{\frac{\omega_m}{\omega_m'}}\sqrt{\frac{2\gamma_c}{\gamma_m\zeta}}. \tag{8.66}$$

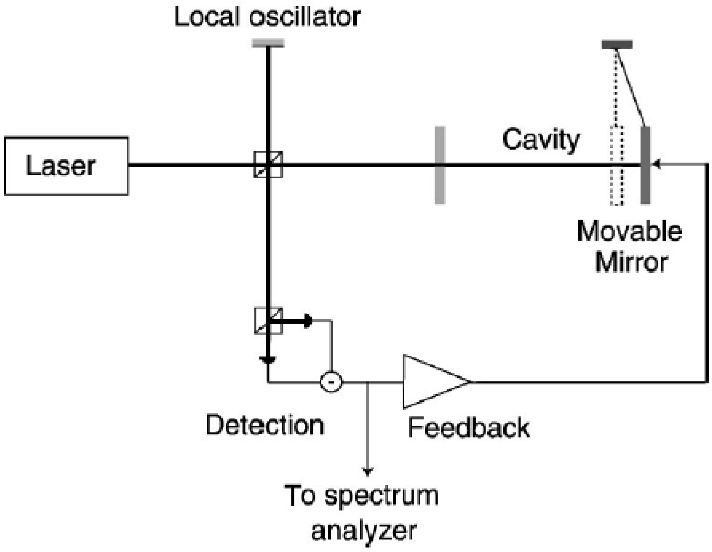

Figure 8.17: Schematic description of of the system using homodyne measurement. Figure adapted from [38].

Furthermore, by choosing the optimal feedback gain, we can indeed reach the standard quantum limit $\langle Q^2 \rangle_{ss} = 1/4$ for $\zeta \to \infty$, since only the first term in Eq. (8.63) remains. We remind the readers $\omega'_m = \omega_m + K_P \sqrt{\gamma_m \gamma_c \zeta / 2}$.

8.4.4 Coherent PD Controller vs. Homodyne Detected Controller

Now, we want to compare the performance of coherent feedback and measurement feedback system. In case of measurement feedback, we use homodyne detected feedback system as shown in Fig. 8.17.
The steady-state covariance of Q is obtained by[38][22]

$$\left\langle Q_{hd}^2 \right\rangle_{ss} = \frac{1}{1 + g_2\sqrt{\eta}} \left(\frac{g_2^2}{4\zeta} + \frac{\gamma_c}{8\gamma_m} + \frac{\zeta}{8} + \frac{k_B T}{2\hbar\omega_m} \right), \tag{8.67}$$

where η is the quantum/detection efficiency of the homodyne measurement. As in the coherent controller case, $\langle P_{hd}^2 \rangle_{ss} = \langle Q_{hd}^2 \rangle_{ss}$ for $\gamma_m \ll \omega_m$. The optimal rescaled feedback gain $g_{2,hd,opt}$ is obtained by

[22] Here, we have additionally considered the CCR of outputs such that we have changed two points to their calculations: 1. Modeling the imperfect detection with an ideal detector intercepted by a beam splitter with transmissivity $\sqrt{\eta}$, so mixing the incident field with a vacuum field[47]. 2. Adding the added noise coming out from the derivative controller.

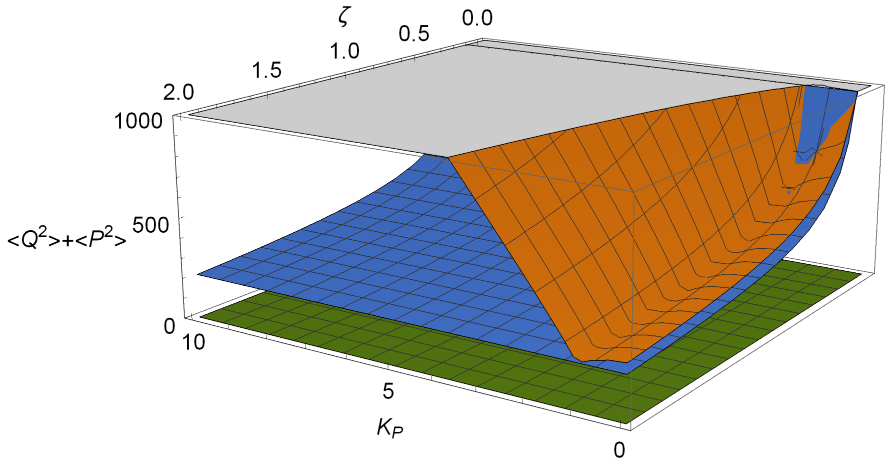

Figure 8.18: Comparison between coherent PD feedback controlled system (orange) and homodyne measurement feedback controlled system (blue) for $\eta = 1$. For both systems, optimal rescaled feedback derivative gain is chosen. For any input power ζ, the coherent PD controller cannot outperform the measurement-based controller. We have used for the simulation: $\omega_m = 2\pi \times 4.3$ MHz, $g_m = 2\pi \times 5.7$ Hz, $g = 2\pi \times 10.1$ MHz, $\gamma_c = 2\pi \times 9.1$ MHz, and $T = 1.0$ K. Values are adapted from [35].

$$g_{2,hd,opt} = \sqrt{1 + \frac{\gamma_c}{2\gamma_m}\zeta + \frac{\zeta^2}{2} + 2\frac{k_B T}{\hbar\omega_m}\zeta} - \frac{1}{\sqrt{\eta}}. \tag{8.68}$$

The optimal $\langle Q_{hd}^2 \rangle_{ss}$ then gives for $\hbar\omega_m \ll k_B T$

$$\left\langle Q_{hd}^2 \right\rangle_{ss,opt} \xrightarrow{\hbar\omega_m \ll k_B T} \frac{1}{2}\sqrt{\frac{1}{\eta}}\sqrt{\frac{2k_B T}{\hbar\omega_m\zeta}} \tag{8.69}$$

$$\left\langle Q^2 \right\rangle_{ss,opt} \xrightarrow{\gamma_m \ll \gamma_c} \frac{1}{8}\sqrt{\frac{1}{\eta}}\sqrt{\frac{2\gamma_c}{\gamma_m\zeta}}. \tag{8.70}$$

This means, the better the quantum efficiency η the better the cooling performance.
Comparing both systems at optimal values in Eqs. (8.65) and (8.69) for $\hbar\omega_m \ll k_B T$ and Eqs.(8.66) and (8.70) for $\gamma_m \ll \gamma_c$, its cooling supremacy depends on the effective mechanical frequency ω_m' and quantum detection η with

$$\frac{\langle Q^2 \rangle_{ss,opt}}{\langle Q_{hd}^2 \rangle_{ss,opt}} \geq \sqrt{\frac{\omega_m}{\omega_m'}\eta}. \tag{8.71}$$

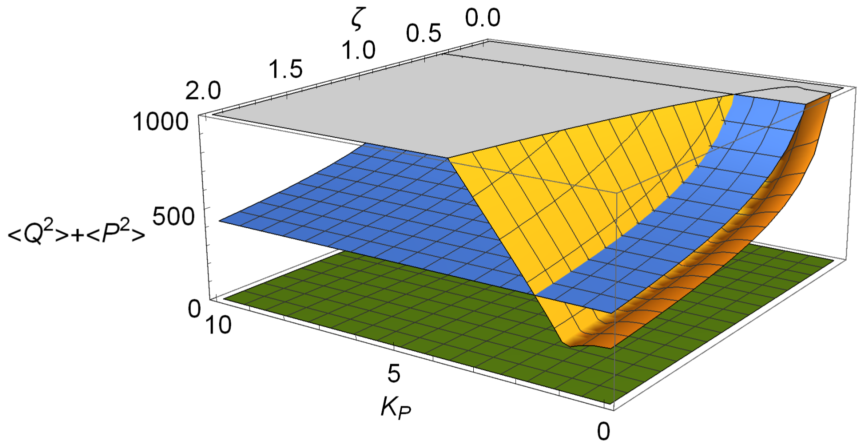

Figure 8.19: Comparison between coherent PD feedback controlled system (orange) and homodyne measurement feedback controlled system (blue) for $\eta = 0.5$. For both systems, optimal rescaled feedback derivative gain is chosen. For relatively small K_P, the coherent PD controller can outperform the measurement-based controller. We have used for the simulation: $\omega_m = 2\pi \times 4.3$ MHz, $g_m = 2\pi \times 5.7$ Hz, $g = 2\pi \times 10.1$ MHz, $\gamma_c = 2\pi \times 9.1$ MHz, and $T = 1.0$ K. Values are adapted from [35].

If we consider typical experimental values $\sqrt{\gamma_c \gamma_m} \ll \omega_m$, we have

$$\frac{\langle Q^2 \rangle_{ss,opt}}{\langle Q^2_{hd} \rangle_{ss,opt}} \geq \sqrt{\eta}. \tag{8.72}$$

That is for perfect detection, CPD feedback control system cannot cool the optomechanical system better than the measurement-based one. The numerical simulation of both feedback systems is demonstrated in Fig. 8.18 and 8.19. The reason why we have a minimum at $K_P = 1$ can be explained that $K_P \neq 1$ is equivalent to have a superposition with another state, which produces a new zero point energy and therefore added noises.

8.5 Coherent PID Feedback Control

Because we now have all necessary components for the CPID controller, we design it, and then embark on a strategy towards its feedback system.

As the reader might have already noticed, the transfer function of the coherent P, I, and D controller is similar to that of the analog electrical circuit using feedback amplifier (see section 2.2.3). Thus, due to its directional properties, we can straightforwardly adapt the series PID controller scheme as shown in Fig. 8.20. In the ideal limit, we have the transfer function for $|K_P| > 1$

$$\begin{bmatrix} a_3 \\ u \end{bmatrix} = \begin{bmatrix} 0 & 0 \\ \frac{1}{\beta}\left(\frac{\gamma_I/2}{s}+1\right)\left(\frac{s}{\gamma_D/2}+1\right) & 0 \end{bmatrix} \begin{bmatrix} e \\ d_1 \end{bmatrix} + \begin{bmatrix} 0 & 0 \\ 0 & \frac{\alpha}{\beta}\frac{1}{s_{21}^{G,P}} \end{bmatrix} \begin{bmatrix} F_1^P \\ F_2^P \end{bmatrix}$$
$$+ \begin{bmatrix} 0 & 0 \\ 0 & \frac{\gamma_I/2}{s}\frac{\beta}{}\frac{1}{s_{21}^{G,I}} \end{bmatrix} \begin{bmatrix} F_1^I \\ F_2^I \end{bmatrix} + \begin{bmatrix} 1 & 0 \\ 0 & \frac{s+\gamma_I/2}{\beta\gamma_D/2}\frac{1}{s_{21}^{G,D}} \end{bmatrix} \begin{bmatrix} F_1^D \\ F_2^D \end{bmatrix}, \tag{8.73}$$

where $e = a_1$ is the error signal and $u = d_3$ the control input, and $\Delta = 0$ is set. Here, we remind the readers that $F_1^{P,I,D}$ are scaling by $\mathcal{O}(1)$ and $F_2^{P,I,D}$ by $\mathcal{O}(s_{21}^G)$. Hence, $F_2^{P,I,D}$ in u do not diverge, but remain by $\mathcal{O}(1)$.
If we pick up the 21 element of CPID matrix and define the PID factors as

$$\begin{aligned} G_{21}^{PID}[s] &= \frac{1}{\beta}\left(\frac{\gamma_I/2}{s}+1\right)\left(\frac{s}{\gamma_D/2}+1\right) \\ &= \frac{1}{\beta}\left(\frac{\gamma_I}{\gamma_D}+1\right) + \left(\frac{\gamma_I/2}{s\ \beta}\right) + \left(\frac{s}{\beta\gamma_D/2}\right) \\ &=: K_P + \frac{K_I}{s} + K_D s, \end{aligned} \tag{8.74}$$

as already formulated in Eq. (3.7) in section 3, we then choose the parameters β, γ_I, and γ_D as a function of K_P, K_I, and K_D as follows

$$\frac{1}{\beta} = \frac{K_P}{2K_I K_D} \pm \sqrt{(\frac{K_P}{2K_I K_D})^2 - \frac{1}{K_I K_D}} \tag{8.75a}$$
$$\gamma_I = \frac{K_P}{2K_D} \pm \sqrt{(\frac{K_P}{2K_D})^2 - \frac{K_I}{K_D}} \tag{8.75b}$$
$$\frac{1}{\gamma_D} = \frac{K_P}{2K_I} \pm \sqrt{(\frac{K_P}{2K_I})^2 - \frac{1}{K_D K_I}}. \tag{8.75c}$$

In case of $|K_P| < 1$ with the scattering matrix

$$\begin{bmatrix} \alpha & -\beta \\ \beta & \alpha \end{bmatrix}$$

the transfer function of the CPID controller changes to

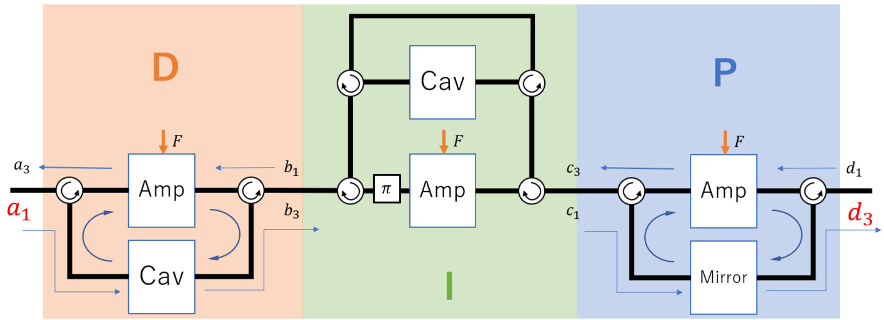

Figure 8.20: Coherent PID controller scheme. a_1 is the input signal and d_3 is the output signal. When implemented in the feedback scheme, the input is an error signal and the output a control input of the plant.

$$
\begin{aligned}
\begin{bmatrix} a_3 \\ u \end{bmatrix} &= \begin{bmatrix} 0 & 0 \\ \beta\left(\frac{\gamma_I/2}{s}+1\right)\left(\frac{s}{\gamma_D/2}+1\right) & -\alpha \end{bmatrix} \begin{bmatrix} e \\ d_1 \end{bmatrix} \\
&+ \begin{bmatrix} 0 & 0 \\ 0 & \beta\frac{1}{s_{21}^{G,I}} \end{bmatrix} \begin{bmatrix} F_1^I \\ F_2^I \end{bmatrix} + \begin{bmatrix} 1 & 0 \\ 0 & \beta\left(\frac{\gamma_I/2}{s}+1\right)\frac{1}{s_{21}^{G,D}} \end{bmatrix} \begin{bmatrix} F_1^D \\ F_2^D \end{bmatrix},
\end{aligned}
\tag{8.76}
$$

Expressing the parameters in K_P, K_I and K_D we just replace $1/\beta \to \beta$ in Eq. (8.75). We also remind the readers

$$
\begin{aligned}
F_2^P[s] =& \sqrt{K_P^2 - 1} d^{P\dagger} \\
F_2^I[s] =& -\frac{\gamma_I}{2}\frac{1}{s} d^{I\dagger} \\
F_2^D[s] =& -s\frac{1}{\gamma_D/2} d^{D\dagger}
\end{aligned}
$$

in the ideal quantum amplifier limit.

For the realization of the feedback structure of the CPID in Fig. 8.2, we use a half mirror or a half beam splitter with

$$
\begin{bmatrix} e \\ d_1 \end{bmatrix} = \begin{bmatrix} 1/\sqrt{2} & 1/\sqrt{2} \\ -1/\sqrt{2} & 1/\sqrt{2} \end{bmatrix} \begin{bmatrix} r \\ y \end{bmatrix},
$$

to obtain an error signal e and exploit the property of the directionality such that the error signal goes as a control input u to the plant.

Assuming the converter-system-detector configuration and using the description in Eq. (8.9), the augmented state-space representation is expressed by

$$\begin{bmatrix} \dot{x} \\ \dot{e}_I \end{bmatrix} = \begin{bmatrix} A + BC(K_P + K_D A) & K_I B \\ C & 0 \end{bmatrix} \begin{bmatrix} x \\ e_I \end{bmatrix} + \begin{bmatrix} K_P BD + K_D BCB_{add} & -K_P B & K_D BD & -K_D B & B \\ D & -1 & 0 & 0 & 0 \end{bmatrix} \begin{bmatrix} \xi \\ r \\ \dot{\xi} \\ \dot{r} \\ F_{PID} \end{bmatrix}. \tag{8.77}$$

9 Summary and Conclusion

In this thesis, we have suggested the quantum feedback amplification scheme based on 2-input-2-output quantum amplifier and found the quantum amplifier can indeed be feedback-controlled. Depending on which element of the controller we want to have in the feedback gain, we have to choose the appropriate feedback scheme. In the feedback gain analysis, we see the sensitivity of gain fluctuations dramatically reduces by applying the feedback scheme in contrast to the no-feedback case. Thus, robustness against fluctuations is achieved. Furthermore, a broad gain bandwidth can be obtained. While these results are similar to classical ones, its quantum-noise limit and added noises are quantum. A remarkable result is the quantum feedback amplifier can reach its quantum-noise limit despite noisy feedback system.

We have applied this feedback scheme to construct an active directional coherent differentiator and integrator. In both controllers, the condition for minimum noise is the same for achieving a high gain. For a coherent D controller, a bad cavity limit is required, while for a coherent I controller a good cavity limit is demanded. In addition to that, using detuning the coherent D controller can work as a band-pass filter in that detuning frequency, while the coherent I controller can act as a band-pass rejector.

Finally, combining the previous results we have suggested a coherent PID controller and its basic coherent PID feedback control system based on converter-system-detector concept. Since the main difference between the classical PID controller and this coherent PID controller lies on the existence of idlers coming from that controller, we have analyzed the effect of those added noises by investigating the steady-state covariance matrix of the system operators. Applying the coherent P feedback control, we could modify the decay rate in order to get the optimal mechanical-frequency-to-cavity-decay-rate-ratio for enhanced sideband-cooling of an optomechanical system. In the coherent PI controller case, the divergence problem of $\left\langle F_{PI}^{\dagger}F_{PI}\right\rangle$ in the gain limit has been found yielding to an immense variance in the steady-state covariance matrix. But the proper choice of the amplifier gain still opens the way to use the CPI-controlled system for semi-classical system, where a trade-off problem occurs. For near ground-state control, CPI-control might not be useful, which is not a crucial problem, because I controller acts to eliminate the steady-state error and the ground-state control does not require additional supply. In the coherent PD feedback control section, we have compared its cooling performance with that of the homodyne-detected measurement-based feedback control system by applying them to cold-damping of the optomechanical system. As a result, we have found if the quantum efficiency is

1, then the coherent PD controller can never outperform the measurement-based one.

As a conclusion, this new suggested no measurement- and no system-based coherent PID controller enables now to fully operate the system on the quantum level for achieving steady-state system. For an outlook, we can generalize the analysis of idler more abstractly to gain more deep insights. Additionally, we can extend this coherent PID controller to a coherent lock-in amplifier to coherently lock the oscillation frequency such as Rabi oscillation in the system.

A Conversion List of Network Parameters

	S	Z	Y	G	H
s_{11}	s_{11}	$\frac{(Z_{11}-Z_0)(Z_{22}+Z_0)-Z_{12}Z_{21}}{(Z_{11}+Z_0)(Z_{22}+Z_0)-Z_{12}Z_{21}}$	$\frac{(Y_0-Y_{11})(Y_0+Y_{22})+Y_{12}Y_{21}}{(Y_{11}+Y_0)(Y_{22}+Y_0)-Y_{12}Y_{21}}$	$\frac{(G_{12}/Z_0+1)(G_{21}Z_0-1)-G_{12}G_{21}}{-(1+G_{21}Z_0)(1+G_{12}/Z_0)-G_{11}G_{22}}$	$\frac{(H_{12}/Z_0-1)(H_{21}Z_0+1)-H_{12}H_{11}}{(H_{22}/Z_0+1)(H_{21}Z_0+1)-H_{11}H_{22}}$
s_{12}	s_{12}	$\frac{2Z_{12}Z_0}{(Z_{11}+Z_0)(Z_{22}+Z_0)-Z_{12}Z_{21}}$	$\frac{-2Y_{12}Y_0}{(Y_{11}+Y_0)(Y_{22}+Y_0)-Y_{12}Y_{21}}$	$\frac{2G_{22}}{-(1+G_{21}Z_0)(1+G_{12}/Z_0)-G_{11}G_{22}}$	$\frac{2H_{11}}{(H_{22}/Z_0+1)(H_{21}Z_0+1)-H_{11}H_{22}}$
s_{21}	s_{21}	$\frac{2Z_{21}Z_0}{(Z_{11}+Z_0)(Z_{22}+Z_0)-Z_{12}Z_{21}}$	$\frac{-2Y_{21}Y_0}{(Y_{11}+Y_0)(Y_{22}+Y_0)-Y_{12}Y_{21}}$	$\frac{-2G_{11}}{-(1+G_{21}Z_0)(1+G_{12}/Z_0)-G_{11}G_{22}}$	$\frac{-2H_{22}}{(H_{22}/Z_0+1)(H_{21}Z_0+1)-H_{11}H_{22}}$
s_{22}	s_{22}	$\frac{(Z_{11}+Z_0)(Z_{22}-Z_0)-Z_{12}Z_{21}}{(Z_{11}+Z_0)(Z_{22}+Z_0)-Z_{12}Z_{21}}$	$\frac{(Y_0+Y_{11})(Y_0-Y_{22})+Y_{12}Y_{21}}{(Y_{11}+Y_0)(Y_{22}+Y_0)-Y_{12}Y_{21}}$	$\frac{(1-G_{12}/Z_0)(1+G_{21}Z_0)+G_{12}G_{21}}{-(1+G_{21}Z_0)(1+G_{12}/Z_0)-G_{11}G_{22}}$	$\frac{(1+H_{12}/Z_0)(1-H_{21}Z_0)-H_{12}H_{11}}{(H_{22}/Z_0+1)(H_{21}Z_0+1)-H_{11}H_{22}}$
Z_{11}	$Z_0\frac{(1+s_{11})(1-s_{22})+s_{12}s_{21}}{(1-s_{11})(1-s_{22})-s_{12}s_{21}}$	Z_{11}	$\frac{Y_{22}}{\lvert Y\rvert}$	$\frac{1}{G_{21}}$	$\frac{-\lvert H\rvert}{H_{21}}$
Z_{12}	$Z_0\frac{2s_{12}}{(1-s_{11})(1-s_{22})-s_{12}s_{21}}$	Z_{12}	$\frac{-Y_{12}}{\lvert Y\rvert}$	$\frac{-G_{22}}{G_{21}}$	$\frac{H_{11}}{H_{21}}$
Z_{21}	$Z_0\frac{2s_{21}}{(1-s_{11})(1-s_{22})-s_{12}s_{21}}$	Z_{21}	$\frac{-Y_{21}}{\lvert Y\rvert}$	$\frac{G_{11}}{G_{21}}$	$\frac{-H_{11}}{H_{21}}$
Z_{22}	$Z_0\frac{(1-s_{11})(1+s_{22})+s_{12}s_{21}}{(1-s_{11})(1-s_{22})-s_{12}s_{21}}$	Z_{22}	$\frac{Y_{11}}{\lvert Y\rvert}$	$\frac{-\lvert G\rvert}{G_{21}}$	$\frac{1}{H_{21}}$
Y_{11}	$\frac{1}{Z_0}\frac{(1-s_{11})(1+s_{22})+s_{12}s_{21}}{(1+s_{11})(1+s_{22})-s_{12}s_{21}}$	$\frac{Z_{22}}{\lvert Z\rvert}$	Y_{11}	$\frac{-\lvert G\rvert}{G_{12}}$	$\frac{1}{H_{12}}$
Y_{12}	$\frac{1}{Z_0}\frac{-2s_{12}}{(1+s_{11})(1+s_{22})-s_{12}s_{21}}$	$\frac{-Z_{12}}{\lvert Z\rvert}$	Y_{12}	$\frac{G_{22}}{G_{12}}$	$\frac{-H_{22}}{H_{12}}$
Y_{21}	$\frac{1}{Z_0}\frac{-2s_{21}}{(1+s_{11})(1+s_{22})-s_{12}s_{21}}$	$\frac{-Z_{21}}{\lvert Z\rvert}$	Y_{21}	$\frac{-G_{11}}{G_{12}}$	$\frac{H_{22}}{H_{11}}$
Y_{22}	$\frac{1}{Z_0}\frac{(1+s_{11})(1-s_{22})+s_{12}s_{21}}{(1+s_{11})(1+s_{22})-s_{12}s_{21}}$	$\frac{Z_{11}}{\lvert Z\rvert}$	Y_{22}	$\frac{1}{G_{12}}$	$\frac{-\lvert H\rvert}{H_{12}}$

	$ABCD$
s_{11}	$\frac{A+B/Z_0-CZ_0-D}{A+B/Z_0+CZ_0+D}$
s_{12}	$\frac{2(AD-BC)}{A+B/Z_0+CZ_0+D}$
s_{21}	$\frac{2}{A+B/Z_0+CZ_0+D}$
s_{22}	$\frac{-A+B/Z_0-CZ_0+D}{A+B/Z_0+CZ_0+D}$
Z_{11}	$\frac{A}{C}$
Z_{12}	$\frac{AD-BC}{C}$
Z_{21}	$\frac{1}{C}$
Z_{22}	$\frac{D}{C}$
Y_{11}	$\frac{D}{B}$
Y_{12}	$\frac{-(AD-BC)}{B}$
Y_{21}	$\frac{-1}{B}$
Y_{22}	$\frac{A}{B}$

	S	Z	Y	G	H	$ABCD$
G_{11}	$\frac{2s_{21}}{(1+s_{11})(1-s_{22})+s_{12}s_{21}}$	$\frac{Z_{21}}{Z_{11}}$	$\frac{-Y_{21}}{Y_{22}}$	G_{11}	$\frac{H_{22}}{\|H\|}$	$\frac{1}{A}$
G_{12}	$Z_0\frac{(1+s_{11})(1+s_{22})-s_{12}s_{21}}{(1+s_{11})(1-s_{22})+s_{12}s_{21}}$	$\frac{\|Z\|}{Z_{11}}$	$\frac{1}{Y_{22}}$	G_{12}	$\frac{-H_{12}}{\|H\|}$	$\frac{-B}{A}$
G_{21}	$\frac{1}{Z_0}\frac{(1-s_{11})(1-s_{22})-s_{12}s_{21}}{(1+s_{11})(1-s_{22})+s_{12}s_{21}}$	$\frac{1}{Z_{11}}$	$\frac{\|Y\|}{Y_{22}}$	G_{21}	$\frac{-H_{21}}{\|H\|}$	$\frac{C}{A}$
G_{22}	$\frac{-2s_{12}}{(1+s_{11})(1-s_{22})+s_{12}s_{21}}$	$\frac{-Z_{12}}{Z_{11}}$	$\frac{Y_{12}}{Y_{22}}$	G_{22}	$\frac{H_{11}}{\|H\|}$	$\frac{AD-BC}{A}$
H_{11}	$\frac{2s_{12}}{(1-s_{11})(1+s_{22})+s_{12}s_{21}}$	$\frac{Z_{12}}{Z_{22}}$	$\frac{-Y_{12}}{Y_{11}}$	$\frac{G_{22}}{\|G\|}$	H_{11}	$\frac{AD-BC}{D}$
H_{12}	$Z_0\frac{(1+s_{11})(1+s_{22})-s_{12}s_{21}}{(1-s_{11})(1+s_{22})+s_{12}s_{21}}$	$\frac{\|Z\|}{Z_{22}}$	$\frac{1}{Y_{11}}$	$\frac{-G_{12}}{\|G\|}$	H_{12}	$\frac{B}{D}$
H_{21}	$\frac{1}{Z_0}\frac{(1-s_{11})(1-s_{22})-s_{12}s_{21}}{(1-s_{11})(1+s_{22})+s_{12}s_{21}}$	$\frac{1}{Z_{22}}$	$\frac{\|Y\|}{Y_{11}}$	$\frac{-G_{21}}{\|G\|}$	H_{21}	$\frac{C}{D}$
H_{22}	$\frac{-2s_{21}}{(1-s_{11})(1+s_{22})+s_{12}s_{21}}$	$\frac{-Z_{11}}{Z_{22}}$	$\frac{Y_{21}}{Y_{11}}$	$\frac{G_{11}}{\|G\|}$	H_{22}	$\frac{-1}{D}$
A	$\frac{(1+s_{11})(1-s_{22})+s_{12}s_{21}}{2s_{21}}$	$\frac{Z_{11}}{Z_{21}}$	$\frac{-Y_{22}}{Y_{21}}$	$\frac{1}{G_{11}}$	$\frac{\|H\|}{H_{22}}$	A
B	$Z_0\frac{(1+s_{11})(1+s_{22})-s_{12}s_{21}}{2s_{21}}$	$\frac{\|Z\|}{Z_{21}}$	$\frac{-1}{Y_{21}}$	$\frac{-G_{12}}{G_{11}}$	$Z_0\frac{-H_{12}}{H_{22}}$	B
C	$\frac{1}{Z_0}\frac{(1-s_{11})(1-s_{22})-s_{12}s_{21}}{2s_{21}}$	$\frac{1}{Z_{21}}$	$\frac{-\|Y\|}{Y_{21}}$	$\frac{G_{21}}{G_{11}}$	$\frac{1}{Z_0}\frac{-H_{21}}{H_{22}}$	C
D	$\frac{(1-s_{11})(1+s_{22})+s_{12}s_{21}}{2s_{21}}$	$\frac{Z_{22}}{Z_{21}}$	$\frac{-Y_{11}}{Y_{21}}$	$\frac{\|G\|}{G_{11}}$	$\frac{-1}{H_{22}}$	D

B Proof of Equations and Detailed Formulations

In this section, all proofs and detailed formulations are written. Each subsection is categorized in sections of the main text in order to find them easily.

B.1 2-Input-2-Output Quantum Feedback Amplifier

B.1.1 Lower Bound of the Added Noise $\mathcal{A}$ in Eq. (6.11)

Here, we substantiate that the added noise is lower bounded by 1/2. The key point of this fundamental limit is the canonical commutation relation (CCR), which restricts the degree of freedom of added noises with

$$\left[b_j, b_j^\dagger\right] = 1 = \left|s_{j1}^G\right|^2 + \left|s_{j2}^G\right|^2 - \left|s_{j4}^G\right|^2 + \sum_{k\neq 1,2,4}^{N} \left|s_{jk}^G\right|^2. \tag{B.1}$$

From here on, w.l.o.g., we set $j = 2$, in order to be able to directly compare with the result in section 6. From Eq. (B.1), we obtain the lower bound of $\left|s_{24}^G\right|^2$ being responsible for permitting values $\left|s_{21}^G\right|^2 > 1$

$$\begin{aligned}\left|\frac{s_{24}^G}{s_{21}^G}\right|^2 &= \frac{\left|s_{21}^G\right|^2 + \left|s_{22}^G\right|^2 - 1 + \sum_{k\neq 1,2,4}^{N} \left|s_{2k}^G\right|^2}{\left|s_{21}^G\right|^2} \\ &\geq 1 - \frac{1 - \left|s_{22}^G\right|^2}{\left|s_{21}^G\right|^2}.\end{aligned} \tag{B.2}$$

Further, by combining the CCR (B.1) with Eq. (6.11), we find the fundamental limit of the added noise

$$\begin{aligned}\mathcal{A}_2^{(0)} =& \frac{1}{2|s_{21}^G|^2} \sum_{k=3}^{N} |s_{2k}^G|^2 \\ =& \left|\frac{s_{24}^G}{s_{21}^G}\right|^2 - \frac{1}{2} + \frac{1 - \left|s_{22}^G\right|^2}{2\left|s_{21}^G\right|^2} \\ \geq& \frac{1}{2} - \frac{1 - \left|s_{22}^G\right|^2}{2\left|s_{21}^G\right|^2}.\end{aligned} \tag{B.3}$$

For $\left|s_{21}^G\right| \to \infty$, we obtain the celebrated quantum noise limit $\mathcal{A}_2^{(0)} \geq 1/2$ [48, 30].

B.1.2 Detailed Formulation of Feedback Noises under Added Noise Environment in Eqs. (6.17) and (6.18)

First, Eq. (6.17) is described by

$$\begin{aligned}\begin{bmatrix}\tilde{F}_1^G\\ \tilde{F}_2^G\end{bmatrix} =& \frac{1}{1-\alpha_1\alpha_2 s_{12}^K s_{21}^G}\begin{bmatrix}1-\alpha_1\alpha_2 s_{12}^K s_{21}^G & \alpha_1\alpha_2 s_{12}^K s_{11}^G\\ 0 & \alpha_1 s_{22}^K\end{bmatrix}\\ &\times\left(\begin{bmatrix}s_{13}^G & s_{14}^G & s_{15}^G\\ s_{23}^G & s_{24}^G & s_{25}^G\end{bmatrix}\begin{bmatrix}d_1\\ d_2^\dagger\\ d_3\end{bmatrix}+\alpha_2\delta_2\begin{bmatrix}s_{11}^G\\ s_{21}^G\end{bmatrix}d_6\right)\\ =&\begin{bmatrix}s_{13}^{G,fb} & s_{14}^{G,fb} & s_{15}^{G,fb} & s_{16}^{G,fb}\\ s_{23}^{G,fb} & s_{24}^{G,fb} & s_{25}^{G,fb} & s_{26}^{G,fb}\end{bmatrix}\begin{bmatrix}d_1\\ d_2^\dagger\\ d_3\\ d_6\end{bmatrix}\end{aligned}\tag{B.4}$$

and the Eq. (6.18) by

$$\begin{aligned}\begin{bmatrix}F_1^K\\ F_2^K\end{bmatrix} =& \frac{1}{1-\alpha_1\alpha_2 s_{12}^K s_{21}^G}\begin{bmatrix}\alpha_2 s_{11}^G & 0\\ \alpha_1\alpha_2 s_{22}^K s_{21}^G & 1-\alpha_1\alpha_2 s_{12}^K s_{21}^G\end{bmatrix}\\ &\times\left(\begin{bmatrix}s_{13}^K\\ s_{23}^K\end{bmatrix}d_4+\begin{bmatrix}s_{12}^K\\ s_{22}^K\end{bmatrix}\alpha_1\delta_1 d_5\right)\\ =&\begin{bmatrix}s_{13}^{K,fb} & s_{14}^{K,fb}\\ s_{23}^{K,fb} & s_{24}^{K,fb}\end{bmatrix}\begin{bmatrix}d_4\\ d_5\end{bmatrix}.\end{aligned}\tag{B.5}$$

B.2 Coherent PID Controller

B.2.1 Input-Output Formalism of Coherent PI Controller in Non-Ideal Quantum Amplifier Case

The detailed formulation of coherent PI controller is provided. According to Fig. 8.9, we have the following input-output relation

$$\begin{aligned}\begin{bmatrix}r_{out}\\ u\end{bmatrix} =& \frac{1}{1-s_{22}^I s_{11}^P}\begin{bmatrix}s_{11}^I-|s^I|s_{11}^P & s_{12}^I s_{12}^P\\ s_{21}^I s_{21}^P & s_{22}^P-|s^P|s_{22}^I\end{bmatrix}\begin{bmatrix}e\\ d_1\end{bmatrix}\\ &+\frac{1}{1-s_{22}^I s_{11}^P}\begin{bmatrix}s_{12}^P & 0\\ s_{22}^I s_{21}^P & 1-s_{22}^I s_{11}^P\end{bmatrix}\begin{bmatrix}F_1^P\\ F_2^P\end{bmatrix}\Theta(|s_{21}^P|-1)\\ &+\frac{1}{1-s_{22}^I s_{11}^P}\begin{bmatrix}1-s_{22}^I s_{11}^P & s_{12}^I s_{11}^P\\ 0 & s_{21}^P\end{bmatrix}\begin{bmatrix}F_1^I\\ F_2^I\end{bmatrix}\end{aligned}\tag{B.6}$$

with

$$\begin{bmatrix} F_1^P \\ F_2^P \end{bmatrix} = \frac{1}{1 - s_{21}^{G,P} s_{12}^{K,P}} \begin{bmatrix} 1 - s_{21}^{G,P} s_{12}^{K,P} & s_{12}^{G,P} s_{11}^{K,P} \\ 0 & s_{22}^{K,P} \end{bmatrix} \begin{bmatrix} F_1^{G,P} \\ F_2^{G,P} \end{bmatrix} \tag{B.7}$$

and

$$\begin{bmatrix} F_1^I \\ F_2^I \end{bmatrix} = \frac{1}{1 + s_{21}^{G,I} s_{11}^{K,I}} \begin{bmatrix} -(1 + s_{21}^{G,I} s_{11}^{K,I}) & s_{11}^{G,I} s_{11}^{K,I} \\ 0 & s_{21}^{K,I} \end{bmatrix} \begin{bmatrix} F_1^{G,I} \\ F_2^{G,I} \end{bmatrix}. \tag{B.8}$$

B.2.2 Calculation of CCR of Control Input u in Coherent PI Control Feedback System

In this subsection, we assume $|K_P| > 1$ for simplicity. The $|K_P| < 1$ case goes analogously.

frequency domain

The control input $u[\omega]$ in frequency domain is expressed as

$$\begin{aligned} u[\omega] =& K_P e[\omega] + K_I \frac{e[\omega]}{-i\omega} + \sqrt{K_P^2 - 1} d^{P\dagger}[\omega] \Theta(|K_P| - 1) \\ &+ \sqrt{1 - K_P^2} d^P[\omega] \Theta(1 - |K_P|) + K_I \frac{d^{I\dagger}[\omega]}{-i\omega}, \end{aligned} \tag{B.9}$$

where

$$\begin{aligned} \left[e[\omega], e^\dagger[\omega']\right] =& \frac{1}{2} \left[y[\omega], y^\dagger[\omega']\right] + \frac{1}{2} \left[r[\omega], r^\dagger[\omega']\right] \\ =& \delta(\omega - \omega') \end{aligned}$$

with $e[\omega] = (y[\omega] - r[\omega])/\sqrt{2}$. Hence the CCR becomes

$$\begin{aligned} \left[u[\omega], u^\dagger[\omega']\right] =& \left| K_P + \frac{K_I}{-i\omega} \right|^2 \delta(\omega - \omega') + \left(1 - K_P^2\right) \delta(\omega - \omega') \\ & - \left| \frac{K_I}{-i\omega} \right|^2 \delta(\omega - \omega') \qquad \text{(B.10)} \\ =& \delta(\omega - \omega'). \qquad \text{(B.11)} \end{aligned}$$

time domain

In the time domain, the control input $u(t)$ is described by

$$u(t) = K_P e(t) + K_I \int_0^t d\tau e(\tau) + \sqrt{K_P^2 - 1} d^{P\dagger}(t)\Theta(|K_P| - 1) + \sqrt{1 - K_P^2} d^P(t)\Theta(1 - |K_P|) + K_I \int_0^t d\tau d^{I\dagger}(\tau). \tag{B.12}$$

Thus,

$$\begin{aligned}\left[u(t), u^\dagger(t')\right] =& K_P^2 \delta(t - t') + K_I^2 \int_0^t d\tau_1 \int_0^{t'} d\tau_2 \delta(\tau_1 - \tau_2) \\ &+ \left(1 - K_P^2\right) \delta(t - t') - K_I^2 \int_0^t d\tau_1 \int_0^{t'} d\tau_2 \delta(\tau_1 - \tau_2) \qquad \text{(B.13)} \\ =& \delta(t - t'), \qquad \text{(B.14)}\end{aligned}$$

which satisfies the CCR.

B.2.3 Calculation of CCR of Control Input u in Coherent PD Control Feedback System

frequency domain

The control input $u[\omega]$ in frequency domain is expressed as

$$u[\omega] = K_P e[\omega] - i\omega K_D e[\omega] + \sqrt{K_P^2 - 1} d^{P\dagger}[\omega]\Theta(|K_P| - 1) + \sqrt{1 - K_P^2} d^P[\omega]\Theta(1 - |K_P|) - i\omega K_D d^{D\dagger}[\omega], \tag{B.15}$$

where

$$\begin{aligned}\left[e[\omega], e^\dagger[\omega']\right] =& \frac{1}{2}\left[y[\omega], y^\dagger[\omega']\right] + \frac{1}{2}\left[r[\omega], r^\dagger[\omega']\right] \\ =& \delta(\omega - \omega')\end{aligned}$$

with $e[\omega] = (y[\omega] - r[\omega])/\sqrt{2}$. Hence the CCR becomes

$$\begin{aligned}\left[u[\omega], u^\dagger[\omega']\right] =& \left|K_P - i\omega K_D\right|^2 \delta(\omega - \omega') + \left(1 - K_P^2\right) \delta(\omega - \omega') \\ &- \left|-i\omega K_D\right|^2 \delta(\omega - \omega') \qquad \text{(B.16)} \\ =& \delta(\omega - \omega'). \qquad \text{(B.17)}\end{aligned}$$

time domain

In the time domain, the control input $u(t)$ is described by

$$\begin{aligned} u(t) =& K_P e(t) - K_D \frac{d}{dt} e(t) + \sqrt{K_P^2 - 1} d^{P\dagger}(t) \Theta(|K_P| - 1) \\ &+ \sqrt{1 - K_P^2} d^P(t) \Theta(1 - |K_P|) + K_D \frac{d}{dt} d^{D\dagger}(t). \end{aligned} \tag{B.18}$$

Note the CCR between derivatives gives

$$\begin{aligned} \left[\frac{d}{dt} x(t), \frac{d}{dt'} x^\dagger(t')\right] &= \int \frac{d\omega}{2\pi} \int \frac{d\omega'}{2\pi} (-i\omega)(i\omega') \left[x[\omega], x^\dagger[\omega']\right] e^{i\omega' t - i\omega t} \\ &= \int \frac{d\omega}{2\pi} \omega^2 e^{-i\omega(t-t')} \\ &= -\frac{d^2}{dt^2} \delta(t - t'). \end{aligned}$$

Thus,

$$\begin{aligned} \left[u(t), u^\dagger(t')\right] =& K_P^2 \delta(t - t') - K_D^2 \frac{d^2}{dt^2} \delta(t - t') \\ &+ \left(1 - K_P^2\right) \delta(t - t') + K_D^2 \frac{d^2}{dt^2} \delta(t - t') \qquad \text{(B.19)} \\ =& \delta(t - t'), \qquad \text{(B.20)} \end{aligned}$$

which satisfies the CCR.

B.2.4 Corrected Calculation of Homodyne-Detected Cold-Damping Method

We revise the result of the paper [38].

Output Homodyne Photocurrent

In Eq. (12) of [38] the output homodyne photocurrent is written as

$$Y_{out}(t) = 2\eta\sqrt{\gamma_c} Y(t) - \sqrt{\eta} Y_{in}^\eta(t),$$

where η is the detection/quantum efficiency of the detector and Y_{in}^η is a generalized phase input noise. But because this output does not satisfy the CCR we have to add a vacuum noise Y_{in}^ν [47] yielding to

$$Y_{out}(t) = 2\sqrt{\eta}\sqrt{\gamma_c} Y(t) - \sqrt{\eta} Y_{in}^\eta(t) + \sqrt{1 - \eta} Y_{in}^\nu(t). \tag{B.21}$$

Idler of Derivative Controller

As can be seen from Eq. (21) of [38], the output after time derivation is expressed as

$$\tilde{Y}_{out}(t) = -K_D \frac{d}{dt} Y_{out}(t),$$

where $K_D = g_{cd}$ in their notation. Since this does not fulfill the CCR requirement, we add a vacuum noise $F(t)$ with

$$F(t) = d^{\mu}(t) + K_D \frac{d}{dt} d^{\xi\dagger}(t) \tag{B.22}$$

as an annihilation operator expression with the vacuum noises d^{μ} and d^{ξ}. In the phase quadrature formalism, we write

$$Y_F(t) = Y^{\mu}(t) + Y^{\xi}(t) \tag{B.23}$$

with

$$Y^{\mu}(t) = i(d^{\mu\dagger}(t) - d^{\mu}(t)), \qquad Y^{\xi}(t) = i(d^{\xi}(t) - d^{\xi\dagger}(t)). \tag{B.24}$$

Quantum Langevin Equation

Eq. (22) in [38] then becomes

$$\frac{d}{dt} Q(t) = \omega_m P(t) \tag{B.25}$$

$$\begin{aligned}\frac{d}{dt} P(t) =& -\omega_m Q(t) - \gamma_m P(t) + 2G X(t) - K_D \sqrt{\eta} \frac{d}{dt} Y(t) \\ & - \frac{K_D \sqrt{\eta}}{2\sqrt{\gamma_c}} \frac{d}{dt} Y_{in}^{\eta}(t) - \frac{K_D \sqrt{1-\eta}}{2\sqrt{\gamma_c}} \frac{d}{dt} Y_{in}^{\nu}(t) - \frac{\sqrt{\gamma_c}}{2} Y^{\mu}(t) \\ & - \frac{K_D}{2\sqrt{\gamma_c}} \frac{d}{dt} Y^{\xi}(t) - W(t) - f(t)\end{aligned} \tag{B.26}$$

$$\frac{d}{dt} Y(t) = -\frac{\gamma_c}{2} Y(t) + 2G Q(t) - \frac{\sqrt{\gamma_c}}{2} Y_{in}(t) \tag{B.27}$$

$$\frac{d}{dt} X(t) = -\frac{\gamma_c}{2} X(t) - \frac{\sqrt{\gamma_c}}{2} X_{in}(t), \tag{B.28}$$

where we have used different input definition leading to $+ \rightarrow -$ in all inputs. Adiabatic elimination of the cavity mode gives us

$$
\begin{aligned}
\frac{d}{dt}Q(t) =&\omega_m P(t) \qquad\qquad (B.29) \\
\frac{d}{dt}P(t) =& -\omega_m Q(t) - \gamma_m P(t) + \frac{2G}{\sqrt{\gamma_c}}X_{in}(t) - W(t) - f(t) \\
&- \frac{4GK_D}{\gamma_c}\sqrt{\eta}\frac{d}{dt}Q(t) + \frac{K_D\sqrt{\eta}}{2\sqrt{\gamma_c}}\frac{d}{dt}Y_{in}(t) - \frac{K_D\sqrt{\eta}}{2\sqrt{\gamma_c}}\frac{d}{dt}Y_{in}^{\eta}(t) \\
&- \frac{K_D\sqrt{1-\eta}}{2\sqrt{\gamma_c}}\frac{d}{dt}Y_{in}^{\nu}(t) - \frac{\sqrt{\gamma_c}}{2}Y^{\mu}(t) - \frac{K_D}{2\sqrt{\gamma_c}}\frac{d}{dt}Y^{\xi}(t). \qquad (B.30)
\end{aligned}
$$

After some calculations, we then obtain Eq. (8.67).

B.2.5 Input-Output Formalism of Coherent PID Controller in Non-Ideal Quantum Amplifier Case

Since in reality there is no ideal quantum amplifier, it is useful to have written down as a formula e.g. for numerical simulations, although no clarity may be present. Thus, the input-output relation of CPID for non-ideal quantum amplifier is expressed as

$$
\begin{aligned}
\begin{bmatrix} r_{out} \\ u \end{bmatrix} =& \frac{1}{1 - s_{22}^D s_{11}^I - s_{22}^D \left|s^I\right| s_{11}^P - s_{22}^I s_{11}^P} \\
\times (& \begin{bmatrix} s_{11}^D + \left|s^D\right| (\left|s^I\right| s_{11}^P - s_{11}^I) - s_{11}^D s_{22}^I s_{11}^P & s_{12}^D s_{12}^I s_{12}^P \\ s_{21}^D s_{21}^I s_{21}^P & s_{22}^P + \left|s^P\right| (s_{22}^D \left|s^I\right| - s_{22}^I) - s_{22}^D s_{11}^I s_{22}^P \end{bmatrix} \begin{bmatrix} e \\ d_1 \end{bmatrix} \\
+& \begin{bmatrix} s_{12}^D s_{12}^I & 0 \\ s_{22}^I s_{21}^P - s_{22}^D \left|s^I\right| s_{21}^P & 1 - s_{22}^D s_{11}^I - s_{22}^D \left|s^I\right| s_{11}^P - s_{22}^I s_{11}^P \end{bmatrix} \begin{bmatrix} F_1^P \\ F_2^P \end{bmatrix} \\
+& \begin{bmatrix} s_{12}^D (1 - s_{22}^I s_{11}^P) & s_{12}^D s_{12}^I s_{11}^P \\ s_{22}^D s_{21}^I s_{21}^P & s_{21}^P (1 - s_{22}^D s_{11}^I) \end{bmatrix} \begin{bmatrix} F_1^I \\ F_2^I \end{bmatrix} \\
+& \begin{bmatrix} 1 - s_{22}^D s_{11}^I - s_{22}^D \left|s^I\right| s_{11}^P - s_{22}^I s_{11}^P & s_{12}^D s_{11}^I - s_{12}^D \left|s^I\right| s_{11}^P \\ 0 & s_{21}^I s_{21}^P \end{bmatrix} \begin{bmatrix} F_1^D \\ F_2^D \end{bmatrix})
\end{aligned} \qquad (B.31)
$$

with

$$
\begin{bmatrix} F_1^{P/D} \\ F_2^{P/D} \end{bmatrix} = \frac{1}{1 - s_{21}^{G,P/D} s_{12}^{K,P/D}} \begin{bmatrix} 1 - s_{21}^{G,P/D} s_{12}^{K,P/D} & s_{12}^{G,P/D} s_{11}^{K,P/D} \\ 0 & s_{22}^{K,P/D} \end{bmatrix} \begin{bmatrix} F_1^{G,P/D} \\ F_2^{G,P/D} \end{bmatrix} \qquad (B.32)
$$

and

$$\begin{bmatrix} F_1^I \\ F_2^I \end{bmatrix} = \frac{1}{1+s_{21}^{G,I}s_{11}^{K,I}} \begin{bmatrix} -(1+s_{21}^{G,I}s_{11}^{K,I}) & s_{11}^{G,I}s_{11}^{K,I} \\ 0 & s_{21}^{K,I} \end{bmatrix} \begin{bmatrix} F_1^{G,I} \\ F_2^{G,I} \end{bmatrix}. \tag{B.33}$$

Now the matrix elements $s_{ij}^{P/I/D}$ represent the transfer function of the P, I, D (feedback) system, $s_{ij}^{G,x}$ and $s_{ij}^{K,x}$ $(x = P, I, D)$ are the quantum amplifier and the controller scattering matrix elements in the P, I, and D system, respectively. Analogously, $F_i^{P/I/D}$ are effective noises of the P, I, and D system, and $F_i^{G,x}$ are idler noises of the quantum amplifier in the P, I, and D system. To have an overlook, each input-output-relations (referring to Fig. 7.2 and 7.6) are described as

$$\begin{aligned}
\begin{bmatrix} a_3 \\ b_3 \end{bmatrix} =& s^{P/D} \begin{bmatrix} a_1 \\ b_1 \end{bmatrix} + \begin{bmatrix} F_1^{P/D} \\ F_2^{P/D} \end{bmatrix} \\
=& \frac{1}{1-s_{21}^{G,P/D}s_{12}^{K,P/D}} \begin{bmatrix} s_{11}^{G,P/D}s_{11}^{K,P/D} & s_{12}^{G,P/D}+s_{12}^{K,P/D}|s^{G,P/D}| \\ s_{21}^{K,P/D}+s_{21}^{G,P/D}|s^{K,P/D}| & s_{22}^{G,P/D}s_{22}^{K,P/D} \end{bmatrix} \begin{bmatrix} a_1 \\ b_1 \end{bmatrix} \\
&+ \frac{1}{1-s_{21}^{G,P/D}s_{12}^{K,P/D}} \begin{bmatrix} 1-s_{21}^{G,P/D}s_{12}^{K,P/D} & s_{12}^{G,P/D}s_{11}^{K,P/D} \\ 0 & s_{22}^{K,P/D} \end{bmatrix} \begin{bmatrix} F_1^{G,P/D} \\ F_2^{G,P/D} \end{bmatrix}
\end{aligned}$$

$$\begin{aligned}
\begin{bmatrix} a_3 \\ b_3 \end{bmatrix} =& s^{I} \begin{bmatrix} a_1 \\ b_1 \end{bmatrix} + \begin{bmatrix} F_1^{I} \\ F_2^{I} \end{bmatrix} \\
=& \frac{1}{1+s_{21}^{G,I}s_{11}^{K,I}} \begin{bmatrix} s_{11}^{G,I}s_{12}^{K,I} & s_{12}^{G,I}+s_{11}^{K,I}|s^{G,I}| \\ s_{22}^{K,I}-s_{21}^{G,I}|s^{K,I}| & s_{22}^{G,I}s_{21}^{K,I} \end{bmatrix} \begin{bmatrix} a_1 \\ b_1 \end{bmatrix} \\
&+ \frac{1}{1+s_{21}^{G,I}s_{11}^{K,I}} \begin{bmatrix} 1-s_{21}^{G,I}s_{11}^{K,I} & s_{11}^{G,I}s_{11}^{K,I} \\ 0 & s_{21}^{K,I} \end{bmatrix} \begin{bmatrix} F_1^{G,I} \\ F_2^{G,I} \end{bmatrix}
\end{aligned}$$

References

[1] Thomas H. Lee. *The Design of CMOS Radio-Frequency Integrated Circuits.* Cambridge University Press, Cambridge, 1998.

[2] Richard C. Jaeger and Travis N. Blalock. *Microelectronic Circuit Design.* McGraw-Hill, New York, 2011.

[3] David M. Pozar. *Microwave Engineering.* John Wiley and Sons, Inc., Hoboken, NJ, 4 edition, 2012.

[4] Adel S. Sedra and Kenneth C. Smith. *Microelectronic Circuits.* Oxford University Press, New York, 2009.

[5] H. S. Black. *Inventing the negative feedback amplifier*. IEEE Spectrum, **14**, 55, 1977.

[6] H. S. Black. *Stabilized feed-back amplifiers*. Proceedings of the IEEE, **72**, 6, 1984.

[7] B. E. Kane. *A silicon-based nuclear spin quantum computer.* Nature, **393**, 133, 1998.

[8] J. I. Cirac and P. Zoller. *Quantum computations with cold trapped ions.* Physical Review Letters, **74**, 4091, 1995.

[9] L. Childress and R. Hanson. *Diamond NV centers for quantum computing and quantum networks.* MRS Bulletin, **38**, 134, 2013.

[10] Lilian Childress, Ronald Walsworth, and Mikhail Lukin. *Atom-like crystal defects: From quantum computers to biological sensors.* Physics Today, **67**, 38, 2014.

[11] D. F. Walls and Gerald J. Milburn. *Quantum Optics.* Springer-Verlag, Berlin Heidelberg, 2008.

[12] I. Siddiqi, R. Vijay, F. Pierre, C. M. Wilson, M. Metcalfe, C. Rigetti, L. Frunzio, and M. H. Devoret. *RF-Driven Josephson Bifurcation Amplifier for Quantum Measurement.* Physical Review Letters, **93**, 20, 2004.

[13] Baleegh Abdo, Flavius Schackert, Michael Hatridge, Chad Rigetti, and Michel Devoret. *Josephson amplifier for qubit readout.* Applied Physics Letters, **99**, 16, 2011.

[14] N. Bergeal, F. Schackert, M. Metcalfe, R. Vijay, V. E. Manucharyan, L. Frunzio, D. E. Prober, R. J. Schoelkopf, S. M. Girvin, and M. H. Devoret. *Phase-preserving amplification near the quantum limit with a Josephson ring modulator.* Nature, **465**, 64, 2010.

[15] Archana Kamal, John Clarke, and Michel H. Devoret. *Gain, directionality, and noise in microwave SQUID amplifiers: Input-output approach.* Physical Review B, **86**, 14, 2012.

[16] A. A. Clerk, M. H. Devoret, S. M. Girvin, Florian Marquardt, and R. J. Schoelkopf. *Introduction to quantum noise, measurement, and amplification.* Reviews of Modern Physics, **82**, 2, 2010.

[17] H. Nyquist. *Regeneration Theory.* Bell System Technical Journal, **11**, 126, 1932.

[18] Michael A. Johnson and Mohammed H. Moradi. *PID Control.* Springer-Verlag London, London, 2005.

[19] Katsuhiko Ogata. *Modern Control Engineering.* Pearson Education, New Jersey, 2010.

[20] John Clarke and Alex I. Braginski (Eds.). *The SQUID Handbook. Vol. I Fundamentals and Technology of SQUIDs and SQUID System.* WILEY-VCH Verlag GmbH and Co. KGaA, Weinheim, 2004.

[21] Archana Kamal, Ananda Roy, John Clarke, and Michel H. Devoret. *Asymmetric frequency conversion in nonlinear systems driven by a biharmonic pump.* Physical Review Letters, **113**, 24, 2014.

[22] Uri Vool and Michel H. Devoret. *Introduction to Quantum Electromagnetic Circuits*. International Journal of Circuit Theory and Applications, pages **45**, 897, 2017.

[23] Baleegh Abdo, Katrina Sliwa, Luigi Frunzio, and Michel Devoret. *Directional amplification with a Josephson circuit.* Physical Review X, **3**, 3, 2014.

[24] Leonardo Ranzani and José Aumentado. *Graph-based analysis of nonreciprocity in coupled-mode systems.* New Journal of Physics, **17** 023024, 2015.

[25] A. Metelmann and A. A. Clerk. *Non-reciprocal quantum interactions and devices via autonomous feed-forward.* Physical Review A, **95**, 1, 2016.

[26] Archana Kamal. *Nonreciprocity In Active Josephson Junction Circuits.* PhD Thesis, Yale University, 2012.

[27] Stephen A. Maas. *Nonlinear Micorwave and RF Circuits.* Artech House, Inc., Norwood, MA 02062, 2003.

[28] Michael Tinkham. *Introduction to Superconductivity.* Dover Publications, inc., Mineola, New York, 1996.

[29] A. O. Caldeira and A. J. Leggett. *Quantum tunneling in a dissipative system.* Annals of Physics, **149**, 374, 1983.

[30] Naoki Yamamoto. *Quantum feedback amplification.* Physical Review Applied, **5**, 044012, 2016.

[31] J. M. Geremia. *Deterministic and nondestructively verifiable preparation of photon number states.* Physical Review Letters, **97**, 073601, 2006.

[32] Takashi Nakajima, Matthieu R. Delbecq, Tomohiro Otsuka, Peter Stano, Shinichi Amaha, Jun Yoneda, Akito Noiri, Kento Kawasaki, Kenta Takeda, Giles Allison, Arne Ludwig, Andreas D. Wieck, Daniel Loss, and Seigo Tarucha. *Robust Single-Shot Spin Measurement with 99.5% Fidelity in a Quantum Dot Array.* Physical Review Letters, **119**, 017701, 2017.

[33] Naoki Yamamoto. *Robust observer for uncertain linear quantum systems. Physical Review A*, **74**,032107, 2006.

[34] Hendra I. Nurdin and Naoki Yamamoto. *Linear Dynamical Quantum Systems.* Springer Nature, 6330 Cham, Switzerland, 2017.

[35] D. J. Wilson, V. Sudhir, N. Piro, R. Schilling, A. Ghadimi, and T. J. Kippenberg. *Measurement-based control of a mechanical oscillator at its thermal decoherence rate.* Nature, **524**,325, 2015.

[36] R. Vijay, C. MacKlin, D. H. Slichter, S. J. Weber, K. W. Murch, R. Naik, A. N. Korotkov, and I. Siddiqi. *Stabilizing Rabi oscillations in a superconducting qubit using quantum feedback.* Nature, **490**, 77, 2012.

[37] V. Giovannetti, P. Tombesi, and D. Vitali. *Non-Markovian quantum feedback from homodyne measurements: The effect of a nonzero feedback delay time.* Physical Review A, **60**, 2, 1999.

[38] David Vitali, Stefano Mancini, Luciano Ribichini, and Paolo Tombesi. *Mirror quiescence and high-sensitivity position measurements with feedback*. Physical Review A, **65**, 063803, 2002.

[39] C. Genes, D. Vitali, P. Tombesi, S. Gigan, and M. Aspelmeyer. *Ground-state cooling of a micromechanical oscillator: Comparing cold damping and cavity-assisted cooling schemes.* Physical Review A, **77**, 033804, 2008.

[40] Yoshiki Kashiwamura and Naoki Yamamoto. *Dispersive-dissipative control strategy for quantum coherent feedback*. IFAC-PapersOnLine, **50**, 1, 2017.

[41] Ryan Hamerly and Hideo Mabuchi. *Advantages of coherent feedback for cooling quantum oscillators.* Physical Review Letters, **109**, 173602, 2012.

[42] S. Iida, M. Yukawa, H. Yonezawa, N. Yamamoto, and A. Furusawa. *Experimental demonstration of coherent feedback control on optical field squeezing*. IEEE Trans. Automat. Contr., **57** (8), 2045, 2017.

[43] I. Wilson-Rae, N. Nooshi, W. Zwerger, and T. J. Kippenberg. *Theory of ground state cooling of a mechanical oscillator using dynamical backaction*. Physical Review Letters, **99**, 093901, 2007.

[44] D. Li J.W. Harlow M.S. Allman K. Cicak A.J. Sirois J.D. Whittaker K.W. Lehnert J.D. Teufel, T. Donner and R.W. Simmonds. *Sideband cooling of micromechanical mo- tion to the quantum ground state*. Nature, **475**, 359, 2011.

[45] R. Patel and M. Toda. *On norm bounds for algebraic Riccati and Lyapunov equations*. IEEE Trans. Automatic Control, **23**, 87, 1978.

[46] Z. Gajic and M. T. J. Qureshi. *Lyapunov Matrix Equation in System Stability and Control.* Dover Publications, Inc., Mineola, NY, 1 edition, 1995.

[47] C. W. Gardiner and P. Zoller. *Quantum Noise.* Springer-Verlag, Berlin Heidelberg, 2004.

[48] Carlton M. Caves. *Quantum limits on noise in linear amplifiers*. Physical Review D, **26**, 1817, 1982.

Acknowledgements

Finally, I would like to thank everyone who has supported me to the success of completing this master thesis. When I look back, it was quite a tough (like sailing through the storms), but an exciting and especially a fruitful journey. The credits definitely go to

Associated Prof. Naoki Yamamoto I would like to express my deepest gratitude to my supervisor Naoki Yamamoto for kindly accepting me in his laboratory team and for providing me the excellent working environment. He further invited me into the deep, wide and exciting world of quantum engineering, and offered me this great interesting research topic and for the long, deep, and critical discussions and advices. His comprehensive knowledge and his deep understanding amazed me, and he additionally recommended and gave me the opportunity to get lost in the maze of quantum (engineering) world. These significantly changed me the behavior towards science and engineering, helped me a lot to find the essence of each topic and the process of my research.

Dr. Frank Deppe from Walther-Meißner Institute. I also would like to express my deepest gratitude to my supervisor Frank Deppe for being able to write my master thesis in TUM, for taking time for the long and deep discussions and advice (they last for hours every time!), and for taking me into the world of physics, especially of experimental physics. The repeating questions how we can physically interpret the results, took me always back from engineering mindset to physical one and lead me to a deep physical understanding. I also would like to apologize for causing all the troubles regarding bureaucratic things.

Yu Yokotera I also would like to thank my senpai Yu Yokotera. The starting point of everything between us was always the lunch time. When I revealed my problems with my research, he discussed with me while eating. If we could not finish our discussions, he took time for me, and we continued our discussions in the lab, which helped me a lot. But the trigger did not only caused discussions about the research, but also conservations about our hobbies, which yielded to meeting in private in other days!

Kensuke Yoshimura-Gallock I further would like to thank my colleague Kensuke Yoshimura-Gallock. All the discussions and conservations from the research, physics to unimportant topics were really inspiring and funny. All the trials to connect anything to physics, and your interesting comments and view definitely made me always laugh and made the atmosphere in lab bright. I also wish luck for getting into the university in the USA and for the long and undoubtedly exotic journey to the world of entanglement and quantum gravity.

Masashi Misa I additionally would like to thank my colleague Masashi Misa for the discussions and conservation about physics (quantum field theory, infinite dimensions, and thermodynamics) and hobbies. And I want to hear more about the charming points of insects!

Rion Shimazu I furthermore would like to thank my colleague Rion Shimazu for the discussions and conservation about engineering and hobbies. The time in Hiroshima, especially in Miyajima, was surely amazing. Next time, I want to play tennis with you, although I'm not so good at it.

Masaki Tanaka I moreover would like to thank my colleague Masaki Tanaka for participating in many events I have organized and hence providing us, lab members, a really cheerful place.

Yukihira Kobayashi, Kaiki Yo (Maki lab), Yuzuru Kato, Masahide Okada, Jun Oomura, Yuri Tanaka, Kentaro Tamura, Sho Sasaki, Yoshiki Kashiwamura, Ryosuke Kuroyanagi, Tomoaki Mikami, Yuji Tanaka, Kenta Usui, Akane Takashima, and **Yoshiki Ohashi** In addition, I would like to thank them for the very comfortable atmosphere in and outside the lab.

My parents, Naoki Nojiri and Hiromi Nojiri Finally, I would like to express my deepest gratitude to my parents for supporting me entirely through my study in TUM and Keio financially and mentally, without which my study was not possible.